REVIEW

Electrically Rechargeable Zinc–Air Batteries: Progress, Challenges, and Perspectives

*Jing Fu, Zachary Paul Cano, Moon Gyu Park, Aiping Yu, Michael Fowler, and Zhongwei Chen**

Zinc–air batteries have attracted much attention and received revived research efforts recently due to their high energy density, which makes them a promising candidate for emerging mobile and electronic applications. Besides their high energy density, they also demonstrate other desirable characteristics, such as abundant raw materials, environmental friendliness, safety, and low cost. Here, the reaction mechanism of electrically rechargeable zinc–air batteries is discussed, different battery configurations are compared, and an in depth discussion is offered of the major issues that affect individual cellular components, along with respective strategies to alleviate these issues to enhance battery performance. Additionally, a section dedicated to battery-testing techniques and corresponding recommendations for best practices are included. Finally, a general perspective on the current limitations, recent application-targeted developments, and recommended future research directions to prolong the lifespan of electrically rechargeable zinc–air batteries is provided.

1. Introduction

Ever-increasing demands in energy and awareness of climate change has propelled and accelerated the inevitable transition from fossil fuels to clean renewable energy. Given the limited fossil-fuel resources on Earth, it is reasonable to expect a more volatile energy economy in the near future. Even with the levelized energy cost for renewable energy sources approaching or headed below that of fossil fuels, their intermittent nature remains a challenge to widespread adoption in the global energy mix.[1] With this in mind, the task of developing new energy-storage systems is more urgent than ever.

For centuries, batteries have been known for their excellence in converting and storing chemical energy. One of their biggest advantages over traditional forms of energy storage is the ability to be scaled down to small sizes, which has made them indispensable for portable electronic devices. Electric vehicles (EVs), which are expected to replace internal combustion engine vehicles in the coming years, are another industry where batteries have the potential to be the dominant form of energy storage. However, many believe that widespread consumer adoption of EVs could still be decades away due to the issues of range anxiety and high upfront cost.[2] Most EVs today use lithium-ion batteries, which have dominated the rechargeable battery market since their advent in the late 1990s. Going forward, the main disadvantages of lithium-ion batteries are their high cost and concerns regarding both their safety and the supply of lithium and cobalt (the latter of which is most commonly used in the positive electrode). Their energy density is also limited by the capacity of the electrode materials. These factors have led to intense research activity involving alternative rechargeable battery technologies.

Metal–air batteries display considerably high energy densities, because oxygen is used as the reactant at the positive electrode and is stored outside of the battery until it is discharged. Primary and secondary metal–air batteries, with metals such as zinc, aluminum, iron, lithium, potassium, sodium, and magnesium have attracted much attention.[3,4] The theoretical specific energies (i.e., gravimetric energy densities), volumetric energy densities, and nominal cell voltages of various metal anodes in metal–air batteries are shown in **Figure 1**. For secondary metal–air batteries, lithium metal is considered to be a strong anode candidate since it has the highest theoretical specific energy (5928 W h kg^{-1}) and a high cell voltage (nominally 2.96 V). However, lithium in the metallic form is plagued by its inherent instability when exposed to air and aqueous electrolytes.[5] Magnesium and aluminum–air batteries are both compatible with aqueous electrolytes and have energy densities comparable to lithium–air; however, their low reduction potentials typically lead to rapid self-discharge and poor Coulombic charging efficiency.[3] Zinc and iron are more stable and can be charged more efficiently in aqueous electrolytes; out of these two, zinc has received far more attention due to its greater energy and cell voltage within an aqueous metal–air battery. Compared with lithium, zinc is inexpensive and more abundant in the earth's crust. More importantly, zinc metal within a metal–air battery has a relatively high specific energy (1218 W h kg^{-1}) and a volumetric energy density (6136 W h L^{-1}) comparable to that of lithium–air. A high volumetric energy density is particularly desirable for mobile and portable devices

J. Fu, Z. P. Cano, M. G. Park, Prof. A. Yu, Prof. M. Fowler, Prof. Z. Chen
Department of Chemical Engineering
Waterloo Institute for Nanotechnology
Waterloo Institute for Sustainable Energy
University of Waterloo
200 University Avenue West, Waterloo, ON N2L 3G1, Canada
E-mail: zhwchen@uwaterloo.ca

DOI: 10.1002/adma.201604685

(e.g., EVs and personal electronics) because there is a limited volume for mounting the batteries in these applications.[6] Moreover, the inherent safety of zinc means that zinc–air batteries can be placed in the front hood of an automobile, where provision for air access is already well established in today's vehicles.

Zinc, due to its low cost and high capacity, is the most common anode material in primary metal–air batteries. Primary zinc–air batteries are most notable for being the predominant energy source for hearing aids, where they provide an impressive volumetric energy density of 1300–1400 W h L^{-1}.[7] Rechargeable zinc–air batteries for EVs were heavily investigated between ca. 1975 and 2000.[8–10] Mechanically rechargeable and electrically rechargeable forms of the battery were both proposed. In mechanically recharged zinc–air batteries (also referred to as zinc–air fuel cells), the battery was charged by removing spent zinc and re-supplying a fresh zinc anode. This avoided the issues of poor zinc electrode reversibility and unstable bifunctional air electrodes. However, this concept was never widely adopted due to the high costs of setting up a network of zinc recharging and supplying stations. The most successful electrically rechargeable zinc–air batteries employed a flowing electrolyte design, which greatly improved the durability of the zinc electrode.[8,11] However, their power performance has traditionally been a drawback due mainly to fundamental challenges in catalyzing reactions involving oxygen gas at the air electrode. Moreover, corrosion of the air electrode during the charging reaction was another critical issue, which, along with the advent of lithium ion batteries, slowed down zinc–air battery development at the end of the 20th century.

Notwithstanding these problems, advances in materials science and nanotechnology have brought about renewed interest in electrically rechargeable zinc–air batteries in this decade. Several companies have developed unique zinc–air systems; the most prominent ones are EOS Energy Storage, Fluidic Energy, and ZincNyx Energy Solutions. EOS Energy Storage's Aurora product is a 1 MW/4 MW h zinc–air battery for utility scale grid storage, offered for as low as 160 US$ $(kW\ h)^{-1}$.[12] Fluidic Energy has partnered with Caterpillar and Indonesia's public utility to provide over 250 MW h of its zinc–air batteries to store photovoltaic solar energy in 500 remote communities.[13] ZincNyx Energy Solutions has developed a 5 kW/40 kW h zinc–air backup system that is undergoing a field test at a subsidiary of Teck Resources.[14] The 160 US$ $(kW\ h)^{-1}$ price offered by EOS Energy Storage is remarkable given that manufacturing of rechargeable zinc–air batteries is far from mature; for comparison, average lithium-ion battery prices are not expected to approach 160 US$ $(kW\ h)^{-1}$ until at least 2025.[15] A recent economic analysis also found that zinc–air batteries were the most economically feasible battery technology for smart-grid energy storage.[16] Therefore, the combination of high energy density, low cost, safe operation, and market-ready solutions leads us to believe that the recent enthusiasm for zinc–air batteries is particularly well-deserved among many other types of emerging batteries.

The zinc–air battery is typically composed of four main components: an air electrode comprising a catalyst-painted gas diffusion layer (GDL), an alkaline electrolyte, a separator, and a zinc electrode. A schematic of a rechargeable zinc–air battery is shown in **Figure 2**. During discharge, the zinc–air battery functions as a power generator through the electrochemical

Jing Fu received her Master's degree (2011) under the supervision of Prof. Jinli Qiao and Prof. Jianxin Ma at East China University of Science and Technology, Shanghai, China, where she specialized in alkaline fuel cells. After graduation, she worked with Volvo Cars Corporation as a chassis design engineer (2011–2014). She is now pursuing her Ph.D. in chemical engineering under the supervision of Prof. Zhongwei Chen at the University of Waterloo, Waterloo, Canada. Her current research interests include the development of advanced nanostructured electrode materials and solid-state electrolytes for flexible rechargeable metal–air batteries.

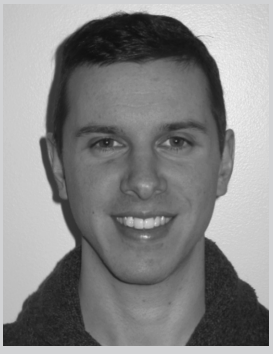

Zachary Paul Cano received his bachelor's degree (2012) and master's degree (2015) in materials science and engineering from McMaster University, Hamilton, Canada, where he specialized in corrosion science. He is now pursuing his Ph.D. in chemical engineering (nanotechnology) under the supervision of Prof. Zhongwei Chen and Prof. Michael Fowler at the University of Waterloo, Waterloo, Canada. His research is currently focused on the development of novel cathode structures and cell designs for long–lasting rechargeable metal–air batteries.

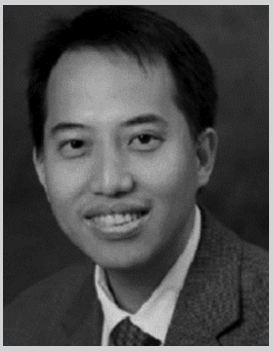

Zhongwei Chen is Canada Research Chair Professor in Advanced Materials for Clean Energy at University of Waterloo, Waterloo, Canada. He is also the Director of Collaborative Graduate Program in Nanotechnology at University of Waterloo. He received his Ph.D. (2008) in Chemical and Environmental Engineering from University of California Riverside. His expertise is advanced energy materials for zinc–air/lithium-ion/lithium–sulfur batteries and fuel cells.

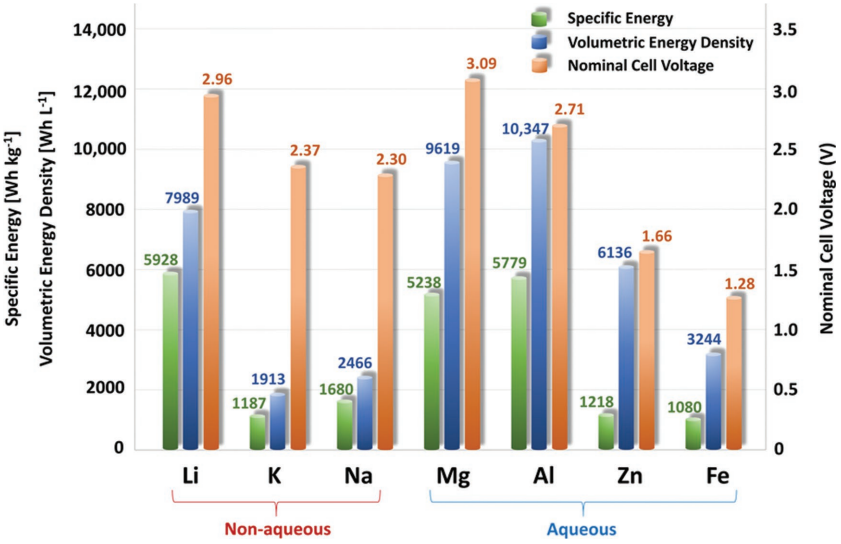

Figure 1. Theoretical specific energies, volumetric energy densities, and nominal cell voltages for various metal anodes in aqueous and non-aqueous metal–air batteries. Specific energy values account for oxygen uptake in the battery by numeric integration between the fully charged and fully discharged states. Volumetric energy densities were calculated using the density of the anode in the fully discharged state. Refer to the Supporting Information for calculations and further explanations.

coupling of the zinc metal to the air electrode in the presence of an alkaline electrolyte with an inexhaustible cathode reactant (oxygen) from the atmosphere. The electrons liberated at the zinc travel through an external load to the air electrode, while zinc cations are produced at the zinc electrode. At the same time, atmospheric oxygen diffuses into the porous air electrode and is ready to be reduced to hydroxide ions via the oxygen reduction reaction (ORR) (forward Reaction (1)) at a three-phase reaction site, which is the interface of oxygen (gas), electrolyte (liquid), and electrocatalysts (solid). The generated hydroxide ions then migrate from the reaction site to the zinc electrode, forming zincate ($Zn(OH)_4^{2-}$) ions, which then further decompose to insoluble zinc oxide (ZnO) at supersaturated $Zn(OH)_4^{2-}$ concentrations. Reaction (2) shows the overall zinc redox reaction. During charging, the zinc–air battery is capable of storing electric energy through the oxygen-evolution reaction (OER) (backward Reaction (1)), occurring at the electrode–electrolyte interface, whereas zinc is deposited at the cathode surface (backward Reaction (2)). The overall reaction (Reaction (3)) can be simply shown as Zn combining with O_2 to form ZnO.

The air electrode reaction:

$$O_2 + 2H_2O + 4e^- \Leftrightarrow 4OH^-, \quad E = 0.40\text{V vs SHE} \tag{1}$$

The zinc electrode reaction:

$$Zn + 2OH^- \Leftrightarrow ZnO + H_2O + 2e^-, \quad E = -1.26\text{ V vs SHE} \tag{2}$$

The overall reaction:

$$2Zn + O_2 \Leftrightarrow 2ZnO, \quad E = 1.66\text{ V vs SHE} \tag{3}$$

Thermodynamically, both reactions are spontaneous and produce a theoretical voltage of 1.66 V. However, the redox reactions of oxygen during the charging and discharging cycles are kinetically slow; thus, electrocatalysts are often used to accelerate the process. For the electrically rechargeable zinc–air battery, each main structural component faces its own challenges. For the air electrode, it is difficult to find a catalyst that facilitates both redox reactions, thereby limiting the power density of zinc–air batteries. Further, carbon dioxide (CO_2) in the air can undergo a carbonation reaction with the alkaline electrolyte, thus changing the reaction environment inside the cell. The carbonate by-product can potentially block the pores of the GDL, which limits access to air. For the separator, it is challenging to find a material that is robust in a basic environment, yet also allows the flow of hydroxide ions exclusively while blocking the zinc ions. For the zinc-metal electrode, it is difficult to control the non-uniform dissolution and deposition of zinc, which is the main cause of dendrite formation and shape change.

Recent reviews on zinc–air batteries[17,18] have provided basic overviews of the components and mechanisms governing the performance and durability of electrically rechargeable zinc–air batteries. They also reviewed the major developments leading to improvements of each of the components, with the most attention being paid to the capacity density of the zinc electrode and the type of catalysts for the bifunctional air electrode. Here, we begin by differentiating between the various possible configurations of zinc–air batteries and identify their advantages and disadvantages. Then, the key components influencing the performance of rechargeable zinc–air batteries will be thoroughly discussed, including the reversible zinc electrode, bifunctional air electrode, electrolytes, and separators. Particularly, we will address and offer a state-of-art understanding of the problematic issues that impede the efficiency, durability, and cycle-life of zinc–air batteries. We also pay major attention to areas that previous articles have not extensively reviewed, including a critical analysis of different methods of extending the cycle life of the zinc electrode and novel strategies for integrating oxygen catalysts into a free-standing air electrode assembly. We further include a section dedicated to performance evaluation of zinc–air batteries and offer recommendations for best practices. Finally, the current status, remaining technical challenges, and a perspective of rechargeable zinc–air batteries is provided. Overall, this review should serve as a comprehensive reference that will aid new and existing researchers in carrying out impactful research on electrically rechargeable zinc–air batteries.

2. Battery Configuration

Electrically rechargeable zinc–air batteries can currently be divided into three main configuration types. The conventional

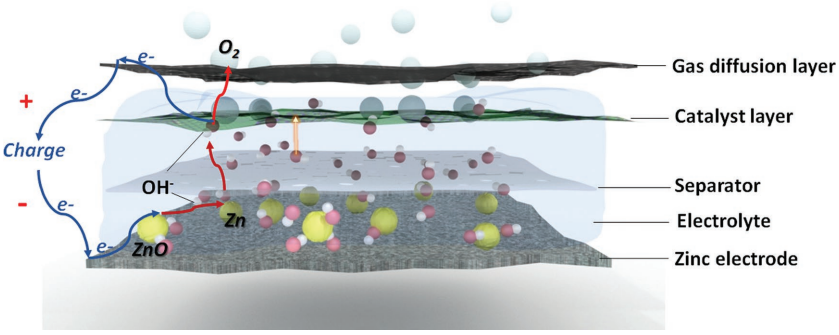

Figure 2. Schematic of an aqueous rechargeable zinc–air battery at charging status.

planar configuration was originally designed for primary zinc–air batteries and prioritizes a high energy density, while zinc–air flow batteries prioritize high cycle numbers and operational lifetimes. Flexible zinc–air batteries are an emerging technology that is particularly promising for the advanced electronics industry, due to the need for energy-dense power sources that are compatible with flexible electronics.

2.1. Conventional Planar Batteries

Conventional zinc–air batteries are constructed in a planar arrangement; in fact, most other configurations discussed in Section 2.2–2.4 also employ this general arrangement. This configuration is favored over a spiral-wound design in order to maximize open air access, although the latter design has received some consideration.[19] In small primary button cells employed for hearing aids, the zinc-electrode compartment is composed of atomized zinc powder intermixed with a gelled KOH electrolyte. This compartment is separated from the air electrode by an electrically isolating and ionically conducting separator layer. In order to maximize the energy density, the button cell's casing and cap also act as the current collectors.[7] Larger and multi-cell primary zinc–air batteries (historically used for railroad signaling, underwater navigation, and electric fencing) employ a prismatic configuration,[7] as shown in Figure 3. Besides the shape, this configuration differs from the button cell by including conductive current collectors within a plastic casing, in addition to external tabs from the positive and negative electrodes. The prismatic design is also the most common configuration used in electrically rechargeable zinc–air-battery research. Many research groups use a combination of plastic plates and gaskets fastened together with bolts and nuts, which allows quick assembly and disassembly of the electrodes and electrolytes being investigated.[20–23]

Planar zinc–air batteries can either be positioned horizontally (i.e., electrode surfaces parallel to the ground, as depicted in Figure 2, 3) or vertically. Horizontally positioned zinc–air batteries, with the air electrode facing upward, are claimed to offer better current distribution in the zinc electrode and easier oxygen removal from the air electrode during charging.[22] However, substantial loss of liquid electrolyte due to evaporation could lead to a complete loss of ionic connectivity between the zinc electrode and air electrode in a horizontal configuration; therefore, most research groups employ a vertical configuration in their investigations.[21,23,24] Electrically rechargeable zinc–air batteries with a conventional planar configuration have not yet penetrated the commercial market. However, they are good candidates for EVs and other energy-storage applications requiring low weights and volumes due to their simple design, which prioritizes a high energy density.

2.2. Flow Batteries

Several zinc–air batteries have been designed with a circulating electrolyte that flows past the electrodes in a planar configuration, as shown in **Figure 4**. This configuration is similar to that of hybrid flow cells such as zinc–bromine batteries,[25] with the main difference being that the zinc–air flow battery uses only a single electrolyte channel. The flowing-electrolyte design helps to alleviate performance and degradation issues concerning both the zinc electrode and the air electrode. For the zinc electrode, the large volume of circulating electrolyte avoids the problems of dendrite formation, shape change, and passivation (refer to Section 3.1) by improving current distribution and reducing concentration gradients.[9,26] On the air-electrode side, precipitated carbonates (refer to Section 5.1) or other unwanted solids can be rinsed away by the flowing electrolyte and removed by an external filter.[9] Circulating electrolytes are also commonly employed in alkaline fuel cells in order to combat carbonate precipitation within the air electrode,[27] which operates identically to the air electrode of zinc–air batteries in discharge mode. For these reasons, rechargeable zinc–air flow batteries should provide higher operational and cycling lifetimes in comparison to conventional configurations with a static electrolyte.

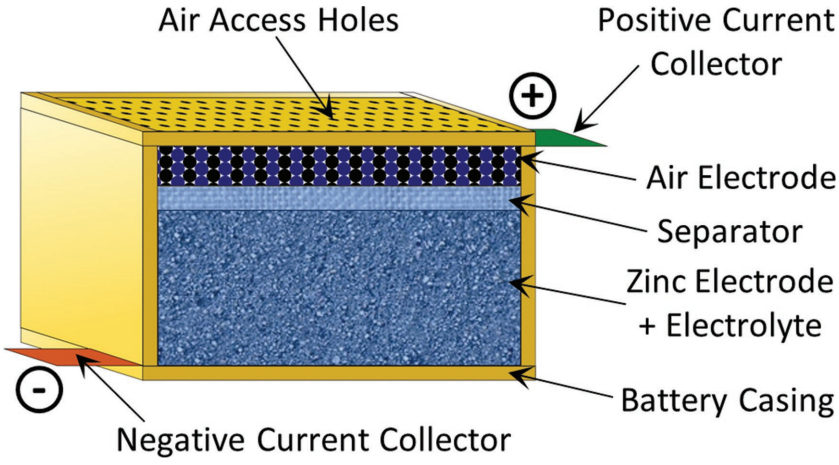

Figure 3. Schematic representation of prismatic zinc–air battery configuration.

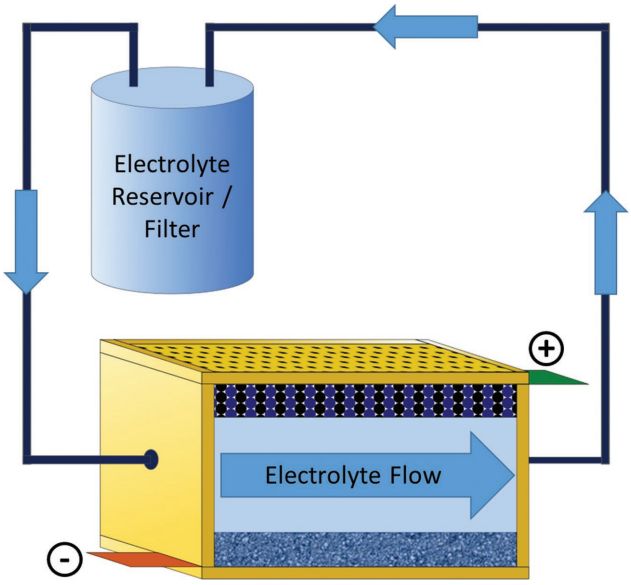

Figure 4. Schematic representation of zinc–air flow battery configuration.

Negative aspects of zinc–air flow batteries include the increased complexity and the decreased energy efficiency, due to the requirement of pumping and circulating the electrolyte through the cells. The tubing, pumps, and excess electrolyte volume also results in reduced specific and volumetric energy density. Nevertheless, the three most prominent commercial developers of electrically rechargeable zinc–air batteries have all chosen to employ flowing electrolytes (according to their patents or patent applications);[28,29] EOS Energy Storage uses a near-neutral-pH chloride-based electrolyte,[29] while Fluidic Energy uses a sulfonate-containing ionic liquid.[30] Zinc-Nyx Energy Solutions utilizes a flowing electrolyte suspension of zinc particles, which allows discharging and charging in separate compartments (each with their own air electrodes).[31] Therefore, the flow configuration appears to be the most successful type of electrically rechargeable zinc–air battery to date. However, the bulky nature of this technology likely limits it to large-scale grid storage applications where weight and space requirements are not critical.

2.3. Flexible Batteries

Flexible batteries have become a major area of research due to the development of a wide variety of flexible electronics over the past 15 years.[32] Zinc–air batteries are an excellent candidate to be designed into flexible power sources due to their low cost, high energy density, and inherent safety, the latter of which negates the requirement for a rigid protective casing. Therefore, research groups have begun investigating materials and methods for producing flexible zinc–air batteries such as the thin-film "wearable" design shown in **Figure 5**.[33–35] A cylindrical cable-type flexible battery[36] and a biocompatible flexible battery[37] have also been demonstrated. Since zinc–air batteries are open to the air, it is not desirable to use liquid electrolytes, which can evaporate or leak onto sensitive electronic equipment. Therefore, the major focus of current flexible zinc–air battery research is on developing a solid-state electrolyte that is mechanically flexible and durable while maintaining sufficient ionic conductivity. The electrodes and support materials must also be able to withstand and maintain operation at a high degree of bending.[33–36]

2.4. Multi-Cell Configuration

Several zinc–air cells can be stacked in series in order to raise the battery voltage to a required level for its application. The cells can be stacked using two possible arrangements, referred to as monopolar and bipolar. In the monopolar arrangement (**Figure 6**a), the zinc electrode is sandwiched in between two externally connected air electrodes and this basic unit is repeated over multiple cells. To connect the cells in series, external connections are made between the zinc electrode of one cell and the air electrode of the adjacent cell. In the bipolar arrangement (Figure 6b), each zinc electrode is paired with a single air electrode on only one of its sides. A series connection is made between the air electrode and the zinc electrode of an adjacent cell through an electrically conductive bipolar plate with air-flow channels rather than through an external connection.[38]

A large advantage of the bipolar arrangement is that cells can be packaged more efficiently due to the absence of external wiring. In addition, the current distribution is more even across the electrodes of a bipolar arrangement versus a monopolar arrangement, since the latter uses external connections to collect current from the electrode edges. However, it is known that edge current collection can generally be employed without significant current-distribution effects in alkaline fuel cells with electrode areas less than 400 cm^2.[39] Therefore, this advantage for the bipolar arrangement is likely to be minimal in zinc–air batteries, which typically operate at lower current densities than fuel cells. A disadvantage of the bipolar arrangement is that the air electrode must be electrically conductive across its entire thickness. This means that the air-facing side of the air electrode

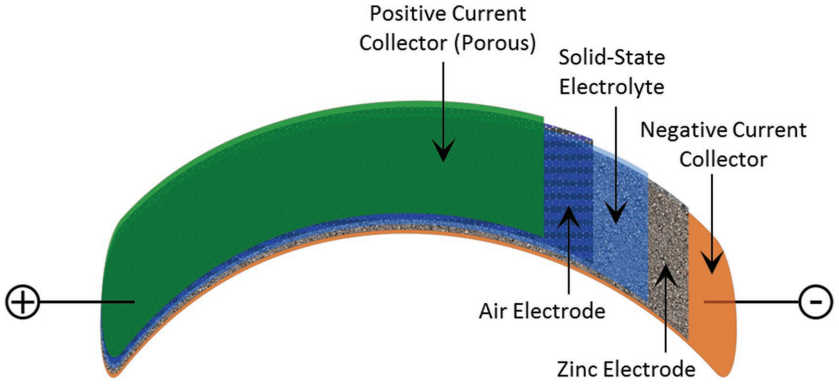

Figure 5. Schematic representation of a flexible zinc–air battery configuration.

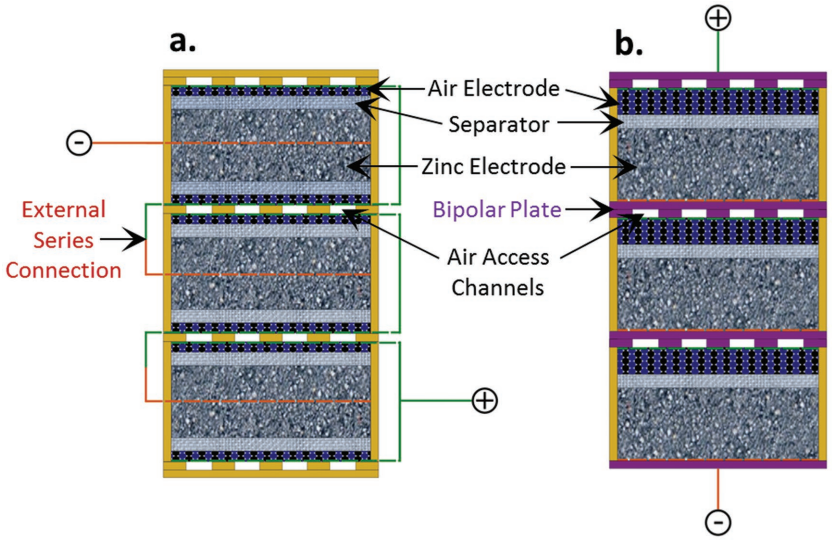

Figure 6. Multi-cell zinc–air battery configuration with: a) monopolar arrangement, and b) bipolar arrangement. Air access channels are depicted as going into the page.

cannot be composed of a pure poly(tetrafluoroethylene) (PTFE) layer, which is often preferred in order to maximize the hydrophobicity and minimize flooding or leakage of the liquid electrolyte from the cell. The bipolar arrangement also requires that a certain pressure be maintained in order to provide sufficient interfacial contact between the electrodes and bipolar plates.[39]

3. Reversible Zinc Electrodes

Given that zinc–air batteries are supplied with an unlimited source of oxygen, the zinc electrode is solely responsible for the battery's capacity. A successful zinc electrode should have a high proportion of utilizable active material, be capable of high-efficiency recharging, and sustain its capacity over long time periods and several hundred charge and discharge cycles. The following two sub-sections detail the scientific phenomena that constrain the achievement of these goals and the strategies that battery developers have used to battle and overcome these constraints.

3.1. Performance-Limiting Phenomena

The performance of a zinc electrode is limited by four major phenomena that occur during operation in a zinc–air battery: i) dendrite growth (**Figure 7**a), ii) shape change (Figure 7b), iii) passivation and internal resistance (Figure 7c), and iv) hydrogen evolution (Figure 7d). Each of these phenomena is discussed in the following four sections.

3.1.1. Dendrite Growth

Zinc dendrites, which are defined as sharp, needle-like metallic protrusions, are well known to form under certain conditions during electrodeposition.[40–43] In secondary alkaline zinc-based batteries, zinc dendrites may form during the charging process and can fracture and disconnect from the electrode (resulting in capacity losses), or more critically, can puncture the separator and make contact with the positive electrode (resulting in a short circuit). Dendritic morphologies arise as a result of concentration-controlled zinc electrodeposition, whereby a positively sloped concentration gradient of $Zn(OH)_4^{2-}$ ions is established as a function of distance from the zinc-electrode surface. Under this condition, $Zn(OH)_4^{2-}$ ions are deposited preferentially at raised surface heterogeneities, such as screw dislocations, which are higher up the concentration gradient.[44] Upon continued deposition, these deposits grow past the boundary of the diffusion-limited region, giving rise to dendrites rapidly growing under nearly pure activation control.[45]

Several studies of zinc electrodeposition in alkaline solutions have identified the zinc reduction overpotential as the key parameter dictating the formation of zinc dendrites.[41,44,45] For instance, Diggle et al.[44] identified a critical overpotential of 75–85 mV, above which zinc dendrites were initiated in 2 M KOH containing 0.01–0.2 M dissolved ZnO. Electrodeposition at lower overpotentials tends to produce epitaxial, boulder or sponge morphologies.[42,43,46] However, it is important to note that, given a relatively long time for initiation, dendrites can also form at lower deposition overpotentials.[41] Therefore, even at relatively low overpotentials, multiple dissolution and deposition cycles under concentration control can result in the progressive amplification of surface heterogeneities on zinc electrodes, eventually leading to dendritic growth.

3.1.2. Shape Change

Another issue related to zinc-electrode failure is referred to as shape change. This phenomenon is observed in zinc–air and

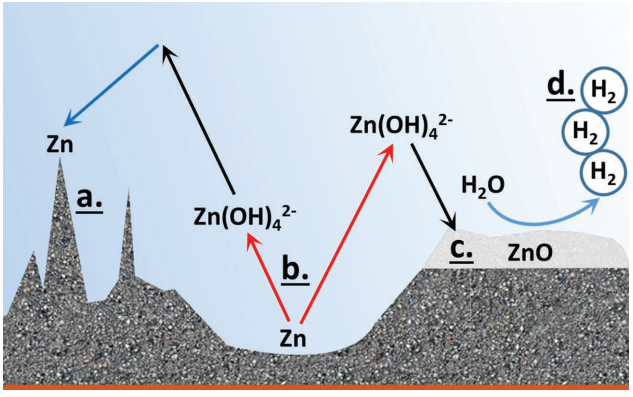

Figure 7. Schematic representation of performance-limiting phenomena that may occur on the zinc electrode: a) dendrite growth, b) shape change, c) passivation, and d) hydrogen evolution.

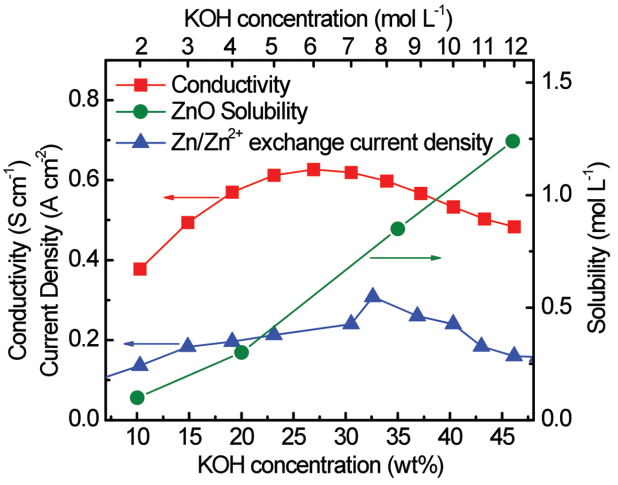

Figure 8. Electrolyte conductivity, Zn/Zn^{2+} exchange current density, and ZnO solubility as a function of KOH concentration (data from ref. [52,53]).

other alkaline–zinc batteries when the zinc is dissolved in the electrolyte during the discharge reaction and then deposits at a different locations on the zinc electrode during charging. Over many charge–discharge cycles, this leads to densification of the electrode and a loss of usable capacity.[47–49] In general, modeling and mechanistic investigations have attributed shape change to uneven current distribution within the zinc electrode, uneven reaction zones, and convective flows caused by electro-osmotic forces across the battery.[20,47,48,50,51]

It can be observed in **Figure 8** that this problem is exacerbated by the properties of the conventional KOH electrolyte that is most typically used in alkaline–zinc batteries. A high concentration of approximately 6–7 M or 25–30 wt% KOH is typically chosen due to the maximum electrolyte conductivity achieved. However, it can also be seen that zinc redox kinetics (indicated by the Zn/Zn^{2+} exchange current density) is near its maximum at this concentration, and the solubility of the ZnO discharge product increases with increasing concentration. Therefore, during battery operation a large amount of zinc is expected to dissolve, migrate, and re-deposit under non-uniform conditions caused by the reasons described above.

3.1.3. Passivation and Internal Resistance

Passivation is the term used to describe an electrode that cannot be further discharged due to the formation of an insulating film on its surface that blocks migration of the discharge product and/or OH^- ions. When a zinc electrode is discharged and the $Zn(OH)_4^{2-}$ discharge product has reached its solubility limit, ZnO is precipitated on the electrode surface. In the case of a porous zinc electrode, passivation is preceded by the reduction of the pore size due to precipitation of ZnO (which takes up more volume than zinc) and finally occurs when freshly discharged $Zn(OH)_4^{2-}$ is far above the solubility limit, causing it to immediately precipitate and fully plug the remaining pore volume.[51,54] This helps to explain why rechargeable zinc electrodes typically require a porosity of 60–75% (in the metallic or charged form),[48,55,56] while the theoretical porosity required to physically accommodate the volume expansion from zinc to ZnO is only 37%. Increasing the electrode thickness is also known to cause earlier onset of passivation, since increased diffusive resistance of hydroxide ions through the electrode pores favors the formation of ZnO over $Zn(OH)_4^{2-}$.[54] The nonconductive property of ZnO also increases the internal resistance of the zinc electrode, which naturally leads to voltage losses during discharging and voltage increases during charging.

Zinc utilization is a common metric that is reported for zinc electrodes. It is defined as the percentage of the theoretical capacity of the zinc mass that is actually used when the electrode is fully discharged. This percentage is limited by the point at which the zinc electrode becomes completely passivated or its internal resistance becomes too high to maintain a sufficient operating voltage. The zinc utilization for conventional powder-based electrodes can range from 60–80%,[55,57,58] while novel developments that will be discussed below can push this value up to 90% or above.

3.1.4. Hydrogen Evolution

The Zn/ZnO standard reduction potential (–1.26 V vs standard hydrogen electrode (SHE)) at pH 14) is below that of the hydrogen-evolution reaction (HER) (Reaction (4), –0.83 V vs SHE at pH 14). Therefore, hydrogen evolution is thermodynamically favored and a zinc electrode at rest will be corroded (Reaction (5), referred to as self-discharge in a battery context) over time. This also means that a zinc electrode cannot be charged with 100% Coulombic efficiency, since the HER will consume some of the electrons provided to the zinc electrode during charging. However, the actual rate of hydrogen evolution is defined by its exchange current density and Tafel slope on a zinc electrode surface, which has been measured at 8.5×10^{-7} mA cm^{-2} and 0.124 V decade^{-1}, respectively in 6 M KOH.[59] Therefore, at the Zn/ZnO standard reduction potential, the hydrogen-evolution current on a zinc surface is on the order of 1×10^{-5} mA cm^{-2}.[59] However, the hydrogen-evolution overpotential is significantly reduced on a ZnO surface,[60] which means that the self-discharge rate should increase as ZnO forms on the discharging zinc electrode. Strategies to decrease the rate of hydrogen evolution (i.e., increase the overpotential for significant hydrogen evolution to occur) are thus needed to improve the charging efficiency and reduce the rate of self-discharge of the zinc electrode.

$$H_2O + 2e^- \Leftrightarrow 2OH^- + H_2 \quad (4)$$

$$Zn + 2H_2O \rightarrow ZnO + H_2 \quad (5)$$

3.1.5. Interaction of these Phenomena

The four issues discussed above can often have significant interaction with each other. For example, shape change can lead to densification, which reduces the active surface area of the zinc electrode. This causes an increase in overpotential (when current is kept constant) during charging, which in turn increases the likelihood of dendritic growth. Zinc passivation also reduces

the active surface area, leading to dendritic growth and increased shape change due to worsening of the current distribution.[47,48,51] A further example is the convective electrolyte flow caused by hydrogen evolution, which speeds up the rate of shape change.[47] Therefore, it can be seen that solutions aimed at mitigating one of the above phenomena can often indirectly mitigate one or more of the others. However, there are also some cases where mitigating one of these problems can make another one worse. For example, reducing the solubility of $Zn(OH)_4^{2-}$ can reduce the rate of shape change, but this can also lead to quicker onset of passivation due the larger amount of precipitated ZnO. The strategies for improving zinc-electrode performance should be implemented with a specific battery design in mind, as different properties, such as electrolyte volume, electrode thickness, and porosity, and many others can dictate the most appropriate solutions.

3.2. Strategies for Improving Performance

A multitude of strategies have been investigated to increase the performance of zinc electrodes, in terms of cycle life (measured by capacity retention as a function of cycle number), capacity (determined by zinc utilization, among other factors), and Coulombic efficiency (determined by extent of hydrogen evolution). These strategies have been organized into seven methods and are summarized in **Table 1**. It should be noted that these strategies are mostly aimed at improving the performance of zinc electrodes employed with a static electrolyte. As noted in Section 2.2, excess circulating electrolyte in a zinc–air flow battery greatly alleviates dendrite formation, shape change, and passivation of the zinc electrode.

3.2.1. High Surface Area/3D Electrode Structure

The geometry of the zinc electrode and the current collector is an important consideration in efforts to improve its performance. Increasing the surface area of the electrode and current collector allows a lower zinc-deposition overpotential, therefore minimizing the likelihood of dendrite formation upon charging. Additionally, designing the electrode and current collector such that current and electrolyte is well distributed throughout all three dimensions of the zinc minimizes the potential for the zinc's passivation.[61] Open-cell metal foams (most commonly copper foam) are a common choice as a current collector, since they possess a high surface area and mechanical rigidity in addition to a high porosity (typically 95% or higher) into which the active zinc species can be loaded. Most investigators typically use electrodeposition to load the zinc into the metal foam; however, the volumetric capacity density reported in these cases is several times lower than the theoretical value for zinc electrodes.[9,62,63] This is likely due to difficulties in achieving a thick, uniform metal electrodeposition throughout the entire thickness of metal foams.[64]

Chamoun et al.[65] reported a 3D hyperdendritic zinc electrode electrodeposited at a high overpotential (≈600 mV vs zinc equilibrium potential) without the use of a metal-foam support. However, they could only cycle to 40% depth-of-discharge (DOD) due to the fragility of the 3D electrode structure. Another issue with pure-zinc electrodeposited electrodes is that they contain no additives such as binders or hydrogen-evolution suppressors that are often necessary for long-term lifetimes, and it would likely require extensive investigation to develop the methods necessary to co-deposit these additives in the desired quantities. Parker et al.[61] developed a novel casting and heat-treatment procedure in order to produce a 3D zinc-sponge electrode (**Figure 9**) with a high specific and volumetric capacity density. This electrode was capable of up to 89% zinc utilization and over 80 charge–discharge cycles at high currents without visible dendrite growth. However, while this electrode included a binder and hydrogen-evolution-suppressing additives, the fact that it did not contain a separate, rigid supporting layer meant that a long cycle life could only be demonstrated when discharging to 23% DOD. Presumably, the foam

Table 1. Strategies for improving zinc electrode performance.

Strategy	Direct influence on:			
	Dendritic growth	Shape change	Passivation and internal resistance	Hydrogen evolution
(1) High Surface Area/3D electrode structure	Minimized (Decreases charging overpotential)	Minimized (3D Structure improves current distribution)	Minimized (High surface area minimizes ZnO film thicknesses)	Increased (Higher surface area causes higher hydrogen evolution rate)
(2) Polymeric binders	–	Minimized (Improves mechanical strength)	Increased (Increases electrode resistance)	–
(3) Carbon-based electrode additives	–	Minimized (Improves current distribution)	Minimized (Improves electrode conductivity)	–
(4) Heavy-metal electrode additives	Minimized ("Substrate effect" promotes denser deposits)	Minimized (Improves current distribution)	Minimized (Improves electrode conductivity)	Minimized (Increases hydrogen overpotential)
(5) Discharge-trapping electrode additives	Minimized ($Zn(OH)_4^{2-}$ concentration gradient is reduced)	Minimized (Discharge product migration is reduced)	Possibly minimized (If trapped discharge product is more conductive than ZnO)	–
(6) Electrolyte additives	Minimized (If additive adsorption onto active hydrogen evolution sites occurs)	Minimized (Reduces $Zn(OH)_4^{2-}$ solubility)	Possibly increased (If early ZnO precipitation is induced)	Possibly minimized (If additive adsorption onto active hydrogen evolution sites occurs)
(7) Electrode coatings	Minimized ($Zn(OH)_4^{2-}$ concentration gradient is reduced)	Minimized (Discharge product migration is reduced)	–	–

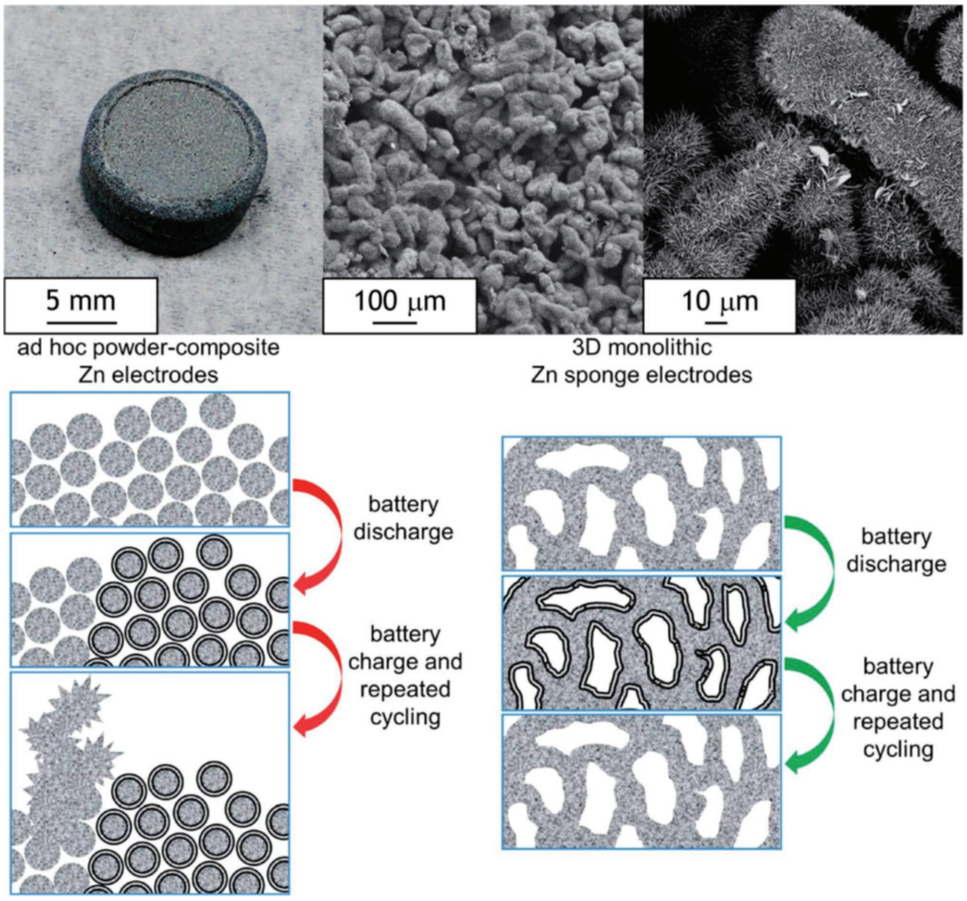

Figure 9. Photograph and SEM images of a 3D zinc-sponge electrode, with schematic image exhibiting its cycle-life advantage over a traditional zinc-powder-based electrode. Reproduced with permission.[61] Copyright 2014, The Royal Society of Chemistry.

structure could collapse at deeper discharge depths, leading to a densified structure upon recharging.

It should be noted that one disadvantage of using a high-surface-area zinc electrode is that the rate of hydrogen evolution increases with exposed surface area. This leads to increased self-discharge when the battery is not operating, and also worse Coulombic efficiency when charging the battery. Hydrogen-evolution reduction methods therefore require increased attention as investigators develop zinc electrodes with increasingly larger surface areas.

3.2.2. Polymeric Binders

As alluded to above, polymeric binders are usually added to electrodes composed of zinc and/or ZnO powders in order to provide mechanical stability by binding the active powders to each other and to the current collector. PTFE is the most common choice as a binder material, likely due to its relatively low cost, ease of dispersion, and good chemical compatibility with alkaline electrolytes.[38,48,66] Other, more hydrophilic binders such as carboxymethyl cellulose (CMC),[61,66] agar,[67–69] and poly(vinylidene fluoride) (PVDF)[33,70] have also been employed. Although there does not appear to be any comprehensive studies in the literature on the effects of binders on zinc-electrode performance, it has generally been claimed that the increased mechanical strength imparted to the zinc electrode helps to avoid shape change.[47,71] In addition, binders can improve the dispersion of Zn/ZnO powders in the electrode,[68] which increases the effective surface area and thus reduces the likelihood for dendrite growth. However, polymeric binders are generally nonconductive and thus increase the internal resistance of the zinc electrode.

3.2.3. Carbon-Based Electrode Additives

Polymeric binders, along with nonconductive ZnO that forms during discharge, increase the internal resistance of a zinc electrode; this can lead to lower zinc utilization. Carbon-based additives (most often carbon black) are sometimes used to lower the resistance of zinc electrodes due to their conductivity and good chemical resistance to alkaline environments.[33,67,69,72–76] This helps to avoid passivation and thus improves zinc utilization. For example, Masri and Mohamad[69] demonstrated that the addition of 2 wt% Super P carbon black improved the zinc utilization of a zinc/agar paste electrode from 68% to 95%. Carbon nanofibers have also been used in conjunction with carbon black, not only to enhance the electrical conductivity by acting as conductive bridges, but also to

provide mechanical stability to zinc electrodes in flexible zinc–air batteries.[33,34,76]

3.2.4. Heavy-Metal Electrode Additives

Another common additive in zinc electrodes is heavy metals or heavy-metal oxides/hydroxides/nitrides possessing more positive reduction potentials compared to zinc. Bi,[43,61,72,74,77–84] In,[61,77,79,85–91] and Pb[56,66,77,79,85,92–98] appear to be the most commonly used elements in this regard, while others, including Cd,[72,77–79,85,86,99] Ti,[72,83,96,100,101] and Sn[72,85,102,103] have also received attention in the literature. These additives improve the conductivity and current distribution within zinc electrodes, owing to the fact that they stay in metallic form while the active zinc mass is discharged and transformed to relatively insulating ZnO.[72,79,80,83] In some cases, these additives have also been reported to impart a beneficial "substrate effect" to the zinc electrode, whereby, upon charging, the additives promote the formation of compact zinc structures.[80,86,104] Many of these additives are also reported to have a higher overpotential for hydrogen evolution than zinc and ZnO.[48,105] Therefore, shape change, dendritic growth, zinc passivation, and hydrogen evolution can all be reduced with appropriate heavy-metal additions. Synergistic beneficial effects have also been claimed for binary mixtures of different heavy-metal additive combinations,[77,85] although the mechanism behind this synergy has not been explained.

Typically, investigators have physically mixed heavy-metal additives in the form of oxide or hydroxide powders together with ZnO powders when fabricating the electrode. However, this brings up a concern regarding adequate dispersion of the additives in the electrode, such that their beneficial effects are fully realized. Poor dispersion can lead to the requirement of a larger proportion of additives in the electrode mixture, which would then reduce the proportion of active zinc material and thus lead to a loss of overall capacity. For instance, Zhang et al.[81] found that the addition of 10 wt% of 500 mesh bismuth powder to a zinc electrode was required in order to reach a maximum in zinc utilization of 63%. Several investigations have addressed this problem by employing zinc electrodes with chemically doped heavy metals.[84,88,90,91,103] For example, Zeng et al.[88] showed that ZnO powder doped with 2.5 wt% In_2O_3 using the co-precipitation method could achieve better zinc utilization (92%) and less capacity fading after charge–discharge cycling than a physical mixture of ZnO and In_2O_3 powders in the same proportions (84% zinc utilization).

3.2.5. Discharge-Trapping Electrode Additives

Preventing migration of the $Zn(OH)_4^{2-}$ discharge product is a key to preventing shape change of zinc electrodes, as discussed earlier. While physical blocking of $Zn(OH)_4^{2-}$ through coatings on the zinc electrode is one possible solution, another is to use additives that chemically bond to the $Zn(OH)_4^{2-}$ ion.[48] This leads to saturation and precipitation of the discharge products, and thus they are effectively "trapped" close to or nearby their original location during discharge. Upon charging, the distance the $Zn(OH)_4^{2-}$ ions need to diffuse in order to be reduced is decreased. This minimizes the concentration gradients of $Zn(OH)_4^{2-}$ ions that would normally be established during charging, which creates another benefit of reducing the likelihood of dendrite formation.

Calcium (Ca) is a commonly used "discharge-trapping" additive,[58,75,78,81,87,93,94,97,98,106,107] since it forms a solid compound with $Zn(OH)_4^{2-}$ that can be written as $Ca(OH)_2 \cdot 2Zn(OH)_2 \cdot 2H_2O$.[108,109] In a KOH electrolyte, the solubility of this structure is lower than ZnO by a factor of 1.5 to 2.5, depending on the KOH concentration.[109] Therefore, capacity losses due to shape change are minimized through the addition of Ca to zinc electrodes. Several reports have demonstrated 100 to 550 charge–discharge cycles with at least 80% capacity retention using this strategy.[58,75,78,94,97,98,107] Zinc utilization is also increased with the addition of Ca,[94] perhaps because precipitated calcium zincate facilitates OH^- transfer better than precipitated ZnO on a Ca-free electrode, which would therefore delay the onset of passivation. Unfortunately, substantial Ca addition is required in order to meaningfully increase the cycle life of a zinc electrode. Jain et al.[94] found it necessary to use a $Ca(OH)_2$/ZnO molar ratio of 0.25, which decreases the theoretical capacity of the zinc electrode from 658 A h kg^{-1} to 505 A h kg^{-1} in the discharged form, or from 820 A h kg^{-1} to 595 A h kg^{-1} in the charged form (neglecting other electrode additives). Other authors used chemically synthesized calcium zincate powders in their electrodes, which has an even lower theoretical capacity of 347 A h kg^{-1} (discharged form) or 523 A h kg^{-1} (charged form).[75,98,107]

Huang et al.[110] demonstrated a zinc electrode using a Zn–Al layered double-oxide powder, which was derived through calcination of ZnAl-CO_3 layered double hydroxides[111] with a 3:1 Zn:Al ratio (**Figure 10**). Assuming the layered double oxide has the structure $(Zn_{0.75}Al_{0.25})O_{1.125}$, this material has a theoretical capacity of 545 A h kg^{-1}, which is significantly larger than that of calcium zincate. Upon immersion in the electrolyte, it is transformed back into a double-layered hydroxide with OH^- as the charge-compensating anion in the interlayers,[112] with a structure that can be written as $[Zn_{0.75}Al_{0.25}(OH)_2](OH)_{0.25} \cdot nH_2O$. This structure has a high surface area and allows efficient transfer of OH^- ions during charging and discharging of the zinc electrode, thus delaying passivation and providing a maximum zinc utilization of 87%. Minimal capacity fading of the electrode based on this material was also demonstrated over an impressive 1000 charge–discharge cycles. Presumably, the bonding of the charge-compensating layers helped to lock in the position of the active zinc during charging and discharging, effectively preventing shape change of the structure.

3.2.6. Electrolyte Additives

Many investigators use a KOH electrolyte that is pre-saturated with $Zn(OH)_4^{2-}$ ions (usually by dissolving ZnO powder).[56,63,66,87,88,94,98,110] This is intended to minimize shape change by inducing the formation of a solid ZnO discharge product at the zinc electrode at an earlier point during discharge. However, the precipitation of ZnO from anodically discharged $Zn(OH)_4^{2-}$ can occur slowly even in

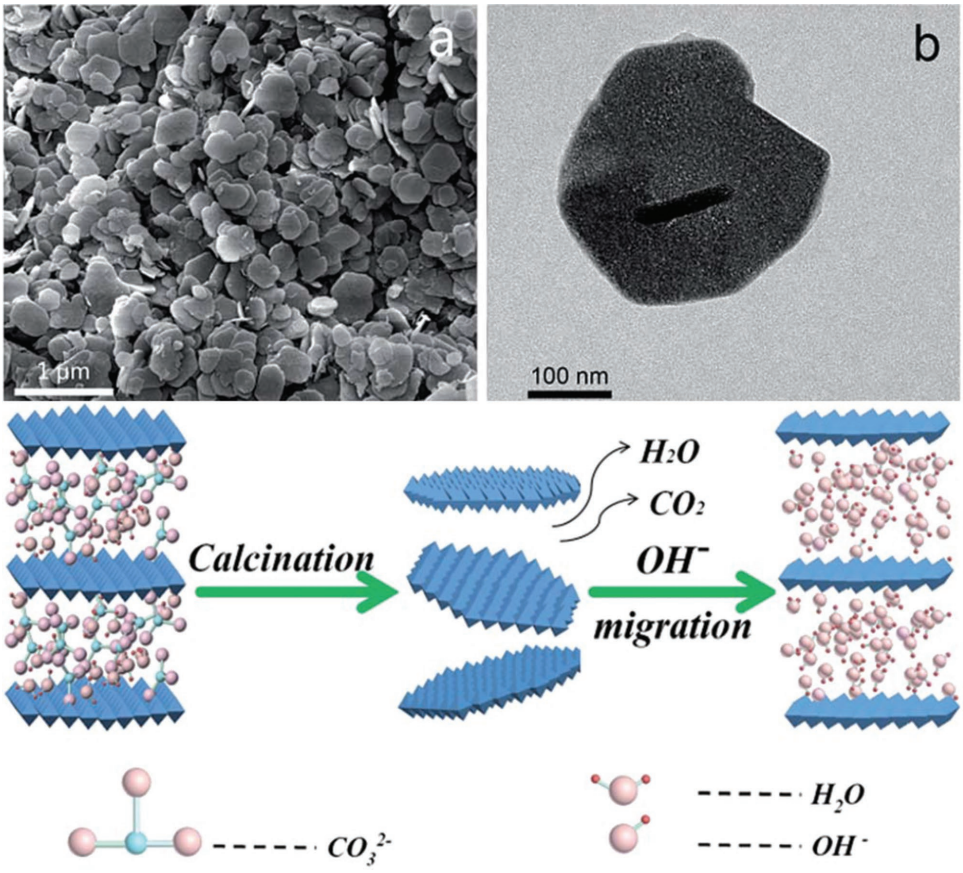

Figure 10. Zn–Al layered double hydroxides with schematic of their formation and OH^--migration property in an alkaline electrolyte. Reproduced with permission.[110] Copyright 2015, The Royal Society of Chemistry.

$Zn(OH)_4^{2-}$-saturated KOH solutions.[113,114] In terms of the Zn/Zn^{2+} exchange current density, the addition of $Zn(OH)_4^{2-}$ ions to KOH solutions only lowers it by a small amount.[52] Also, recent work by Parker et al.[115] revealed a potential problem with using ZnO-saturated electrolyte. Scanning electron microscopy (SEM) analysis of a porous zinc electrode after cycling revealed that the pores became blocked with additional zinc that was plated from the $Zn(OH)_4^{2-}$ originally present in the electrolyte. During charging, the "extra" $Zn(OH)_4^{2-}$ ions from the electrolyte and the "original" ZnO discharged from the zinc electrode were both reduced to zinc at the same time. The resulting densification of the zinc electrode would likely lead to, upon continued cycling, poorer current distribution, earlier passivation, and eventually dendrite growth due to rising deposition overpotentials.

The solubility of the $Zn(OH)_4^{2-}$ discharge product can also be reduced by altering the composition of the alkaline electrolyte. As shown in Figure 8, the solubility of ZnO is reduced at KOH concentrations lower than approximately 6 M KOH, and thus choosing electrolytes with lower KOH concentrations will reduce the tendency for zinc-electrode shape change.[93] However, electrolytes with lower KOH composition also have lower conductivities, which reduces the power performance of zinc–air batteries due to Ohmic losses. Ni–Zn battery investigators have approached this problem by lowering the KOH concentration by as much as possible without substantially reducing the performance of the $NiOOH/Ni(OH)_2$ electrode, and then by adding other ionic compounds additives such as KF, K_2CO_3, K_3BO_3, and K_3PO_4 to restore the electrolyte conductivity.[48] With this strategy, the $Zn(OH)_4^{2-}$ solubility can be reduced to less than half of its original value (in 7 M KOH) while maintaining above 75% of the original electrolyte conductivity.[113] Adler et al.[56,116] found that an electrolyte composed of 3.2–4.5 M KOH, 2 M KF, 2 M K_2CO_3, saturated ZnO, and a suspension of 0.5 M LiF resulted in optimal performance and cycle life of a Ni–Zn battery (the Li^+ additive is beneficial to the $NiOOH/Ni(OH)_2$ electrode[48]). However, CO_3^- additives are not appropriate for aqueous electrolytes of zinc–air batteries, since this will lead to quicker saturation and precipitation of K_2CO_3 in the air-electrode pores as CO_2 enters from the outside environment. K_3BO_3 and K_3PO_4 additives, which have also shown promise for Ni–Zn batteries,[92] thus seem to be a better choice. In addition, the minimum OH^- concentration required for satisfactory performance of the OER at the air electrode might be substantially different from that required for the $NiOOH/Ni(OH)_2$ electrode during charging. The optimization of the aqueous electrolyte composition using the above approach is therefore an important research direction for zinc–air batteries.

Besides additives that reduce shape change, various organic additives, such as perfluorosurfactants,[117] tartaric/succinic/citric acid,[118] and tetra-alkyl ammonium hydroxides[119] have also been investigated in alkaline electrolytes for the

suppression of dendrite growth and hydrogen evolution. It was claimed that both of these phenomena were reduced through the adsorption of the additives onto the most electrochemically active sites of the zinc electrode during the charging process.

3.2.7. Electrode Coatings

Coatings applied to the surface of zinc electrodes or to the zinc powders comprising the zinc electrode have also been proposed as a strategy to improve cycle life. These coatings should allow sufficient migration of OH^- ions to facilitate the charge and discharge processes, while blocking or reducing the rate of $Zn(OH)_4^{2-}$ migration outward during the discharge process. The reduced $Zn(OH)_4^{2-}$ migration helps to mitigate shape change and also reduces concentration gradients during charging, which lowers the driving force for dendritic growth. If these coatings are designed to take up a smaller proportion of the whole zinc electrode than other zinc additives discussed above, they can allow a larger capacity by maximizing the proportion of active zinc material.

Zhu and Zhao developed an ionomer film that was dip-coated onto a conventional PTFE-bound zinc-powder electrode.[120] The coated zinc electrode showed improved discharge voltages and reduced dendritic growth after 50 charge–discharge cycles, although the capacity retention was not reported. Vatsalarani et al.[121] studied the effect of a polyaniline coating on a zinc electrode, and found that shape change and dendritic growth were minimized and stable cell capacity was achieved over 100 charge–discharge cycles.

ZnO powders coated with a thin layer of heavy-metal additives have also been investigated.[82,87,89,100,102] Yuan et al.[82] developed a ZnO powder with a Bi-based nanoparticle coating (5.1 wt% Bi overall), and demonstrated a maximum of 90% zinc utilization and very little capacity fading over 50 charge–discharge cycles. The authors attributed the capacity retention to the nanoporous Bi-based coating, which allowed passage of H_2O and OH^- ions to the inner Zn/ZnO cores while physically blocking discharged $Zn(OH)_4^{2-}$ ions from migrating outside the core.

3.3. Evaluation

Table 2 contains performance metrics of some zinc electrodes reported over the past five years, including capacity densities, zinc utilization, and the number of cycles with over 80% retained capacity. It should be noted that many authors only reported the specific capacity of the zinc electrode being investigated. Therefore, if it was not reported, a probable range of volumetric capacity densities was calculated from the available information in each reference. Also, it is important to note that some studies report the specific capacity relative to the mass of the charged electrode, while others report the mass of the discharged (i.e., oxidized) electrode. In addition, many authors report the specific capacity normalized to only the mass of the active material (i.e., zinc) in the electrode, rather than the mass of the entire electrode including additives. It is thus difficult to directly compare the capacity values of the large number of zinc electrodes across reports from many different research groups. Table 2 attempts to "standardize" the specific capacities by normalizing to the entire mass of the charged electrode (including additives). The specific capacities and volumetric capacity densities can be multiplied by a practical zinc–air cell voltage in order to calculate the specific energy and volumetric energy density (without taking into account the mass and thickness of additional battery components). Finally, it should be noted that the performance metrics in Table 2 cannot be perfectly compared to one another due to different electrolytes, electrode thicknesses, cell geometries, and cycling conditions that were used across the different studies.

As seen in Table 2, none of the zinc electrodes developed in recent years displays excellent performance across all the relevant metrics. Zinc-plated Cu foam displays a very high specific capacity and cycle life, but its volumetric capacity density is too low for applications with space constraints. 3D zinc-sponge electrodes display high specific and volumetric capacity densities, but their lack of mechanical robustness limits them to shallow depths of discharge and relatively low cycle life. Electrodes with discharge-trapping additives display good cycle life at deep discharge depths, but their capacity densities are relatively low due to the large proportion of non-active additives. Electrodes with chemically doped heavy metals and/or coatings appear to display the most promising combination of performance metrics. However, many of the zinc-electrode advancements discussed above need to be demonstrated at larger thicknesses (>1 mm) and longer testing periods to prove they are suitable for a wide range of battery applications.

4. Separators

In batteries, the basic function of a separator is to act as a physical barrier, allowing ionic flow while preventing physical contact of the two electrodes. Despite being an integral part of a zinc–air battery, the separator has not received its deserved attention in comparison to other parts of the battery. So far, most of the separators in use are not designed specifically for the zinc–air battery; they are commonly taken from lithium-based batteries.[122,123] The main function of the separator in rechargeable zinc–air batteries is to prevent short circuits from zinc dendrite penetration upon cycling. In addition to the dendritic inhibition, the separator should be electrochemically stable within a wide working potential window (≥2.5 V), remain intact in strong alkaline electrolytes (pH ≥ 13), and have a low electrical resistance and a high ionic conductivity. Ideally, the separator should also have a fine porous structure allowing OH^- ions to pass while blocking soluble $Zn(OH)_4^{2-}$ ions.[123,124] The transfer of $Zn(OH)_4^{2-}$ ions across the separator may have a detrimental effect on the polarization of the air electrode if ZnO precipitates on its active surface or due to the interference of $Zn(OH)_4^{2-}$ ions on the active sites of the catalysts. Polypropylene membranes such as commercial Celgard films with a laminated nonwoven structure (e.g., Celgard 5550 and Celgard 4560) are typically used as separators in most studies of zinc–air batteries, due to their superior mechanical strength to retard dendritic penetration and broad electrochemical stability window.[125,126] Despite these features, their pore size is

Table 2. Selected performance metrics of recent zinc electrodes disclosed in the literature.

Reference	Strategies (Table 1)	Electrode, electrolyte composition	Electrode thickness [mm]	Specific capacity[a] [A h kg^{-1}]	Volumetric capacity density[b] [Ah L^{-1}]	Zinc utilization [%]	Cycling conditions[c]	# Cycles with >80% retained capacity[d]
Theoretical		100% Zinc		820	5846			
		100% ZnO		658	3694			
[62]	1, 6	Zinc–electroplated Cu foam, 8 M KOH + 0.5 M ZnO	2	754	39	92	100 mA cm^{-2}	9000+
							100% DOD	
[65]	1	3D hyperdendritic zinc sponge electrodeposited onto Ni mesh, 8.9 M KOH	[e]	719	1282–2051	88	C/5 Rate	100+
							40% DOD	
[61]	1, 2, 4	3D zinc sponge + 300 ppm In + 300ppm Bi, 6 M KOH	1–4	728	928	89	5 mA cm^{-2} (discharge)	≈25
							3 mA cm^{-2} (charge)	
							20% DOD	
[75]	1, 2, 3, 5, 6	Calcium zincate powder + 5 wt% zinc + 10 wt% acetylene black + 5 wt% PTFE, 6 M KOH + Sat'd ZnO	0.2	385	338–540	98	2C Rate	250+
							100% DOD	
[110]	1, 2, 3, 5, 6	Zn–Al-layered double oxide powder + 10 wt% acetylene black + 5 wt% PTFE, 6 M KOH + Sat'd ZnO	0.2	469	552–883	87	1C Rate	1000+
							100% DOD	
[82]	1, 2, 4, 6, 7	Bi-based nanoparticle-coated ZnO powder + 4.8 wt% PTFE + 0.6 wt% CMC, 4.5 M KOH + 1.6 M K_2BO_3 + 0.9 M KF + 0.1 M LiOH	0.3	656	1025–1640	90	C/5 Rate	50+
							100% DOD	
[88]	1, 2, 3, 4, 6	In-doped ZnO powder + 8.3 wt% PTFE + 8.3 wt% graphite, 4.5 M KOH + 1.0 M NaOH + 0.5 M LiOH + Sat'd ZnO	0.28	586	727–1164	92	≈C/4 Rate	73+
							100% DOD	

[a]Includes mass of additives and based on mass of charged (non-oxidized) electrode with the exception of 100% solid ZnO; [b]If the necessary information to calculate volumetric capacity density was not reported, a range is calculated based on the electrode material densities and a typical charged electrode porosity of 60–75%;[48,55–57] [c]Depth of discharge is abbreviated as DOD; [d]"+" indicates that the electrode provided >80% of its initial capacity when cycling was terminated; [e]Not reported.

too large to limit the crossover of $Zn(OH)_4^{2-}$ ions, thus leading to increased polarization and decreased long-term durability of the batteries.[17]

Optimizing the ionic selectivity of the separators is of importance. For instance, the alkaline anion-exchange membranes applied in alkaline fuel cells can be feasible to be used in zinc–air batteries. Dewi et al.[127] developed a cationic polysulfonium membrane as the separator for a zinc–air battery. The membrane was highly effective in preventing the crossover of zinc cations, but simultaneously allowed a high OH^- permselectivity. This high ionic selectivity enabled the battery to have an increased discharge capacity almost six-fold larger than that of the commercial Celgard separator, presumably because it avoided the precipitation of ZnO on the air electrode. However, the insufficient chemical stability and high production cost of anion-exchange membranes remain to be resolved.[128] To avoid these issues, Kiros[129] adopted another approach by coating an insoluble inorganic barrier layer on a commercial microporous separator (Celgard 3401).Various inorganic compounds, including CaF_2, $Al(OH)_3$, $Mg(OH)_2$, and $Mn(OH)_2$, were tested for the separation of $Zn(OH)_4^{2-}$ ions ($Zn(OH)_4^{2-}$ permeability). Among them, the separator coated with $Mn(OH)_2$ was found to give the highest $Zn(OH)_4^{2-}$ ion-separation capacity due to the plugging of pores of the separator by the very fine colloidal particles. In addition to the ionic selectivity, the ionic conductivity of the separators must be sufficiently high to avoid large Ohmic polarization loss. Wu et al.[130] prepared a sulfonated separator based on a commercial microporous Celgard 2320 membrane. The sulfonation treatment improved the ionic conductivity of the membrane (3.52×10^{-2} S cm^{-1}) by 132% compared to that of the unsulfonated one. The solid-state zinc–air battery using a sulfonated microporous membrane exhibited a higher battery

power density of 38 mW cm^{-2} than that of the unsulfonated membrane (20 mW cm^{-2}).

5. Electrolytes

The role of electrolytes in zinc–air batteries is underestimated compared to electrode materials. Electrolytes can profoundly affect the battery performance in many aspects such as capacity retention, rate capability, and cycling efficiency. With the increasing interest in high-performance, durable, flexible, and rechargeable zinc–air batteries, the development of electrolytes is facing great challenges as well as opportunities. Up to now, aqueous alkaline electrolytes are still the most popular for zinc–air batteries, owing mainly to their excellent performance in terms of ionic conductivity and interfacial properties. However, the alkaline electrolyte is susceptible to the ambient atmosphere (e.g., CO_2 and relative humidity), causing undesirable electrolyte degradation and thereby inhibiting its use for prolonged battery operation. As alternatives to the aqueous electrolyte, special attention has been given to non-aqueous electrolytes, including solid-state ionic conducting mediums and room-temperature ionic liquids. However, up until now, the non-aqueous systems exhibit far less energy and lower power performance than that of their aqueous counterpart, due to their lower ionic conductivities. This section provides insight into the current status of aqueous alkaline electrolytes and non-aqueous systems for rechargeable zinc–air batteries.

5.1. Aqueous Electrolyte

Despite the fact that neutral and acidic electrolytes can minimize the formation of zinc dendrites and prevent carbonation, alkaline electrolytes are greatly favored for better zinc-corrosion resistance, higher oxygen reaction kinetics, and wider availability of electrocatalyst materials. For zinc–air batteries, potassium hydroxide (KOH), sodium hydroxide, and lithium hydroxide solutions are the most commonly used alkaline electrolytes.[131] Among these, concentrated KOH solutions demonstrate the highest ionic conductivity and the lowest viscosity, and thus are widely employed in zinc–air batteries for the sake of better electrochemical kinetics and mass transport.[132] For superior ionic conductivity and kinetic behavior, electrolytes with KOH concentrations of 20–40% are commonly used. At room temperature, a 30 wt% KOH solution has the maximum conductivity (around 640 mS cm^{-1}),[133] fast zinc reaction kinetics in terms of the highest exchange current, and solubility of zinc discharge products ($Zn(OH)_2$/$Zn(OH)_3^-$/$Zn(OH)_4^{2-}$/ZnO).[134] Although the high solubility could suppress the passivation of the zinc surface and consequently increase the capacity, it often yields supersaturated $Zn(OH)_4^{2-}$ species; as discussed in Section 3.1.1, $Zn(OH)_4^{2-}$ species are strongly associated with the formation of zinc dendrites and are deemed detrimental to the battery cycle life.[133] An efficient strategy to address these issues is optimizing the composition of the electrolytes together with the addition of additives (refer to Section 3.2) to reduce the zinc anodic polarization as well as increase the Faradaic efficiency of the anode reaction.

Another obstacle of batteries operated in air is that alkaline electrolytes are vulnerable to atmospheric CO_2, resulting in the formation of carbonates.[132] The carbonates precipitate inside the pores of the air electrode, which in turn reduces the conductivity and blocks the air-diffusion path in the air electrode, giving rise to an increased polarization and shortening longevity of the battery.[135] Although attempts to filter CO_2 by physico-chemical adsorption can reduce the carbonate formation, the cost in terms of materials and management could be high.[136,137] In addition to the effect of CO_2, electrolyte evaporation and/or moisture invasion (depending on the atmosphere's relative humidity and temperature) is unavoidable when the battery is exposed to a non-standard environment. Either situation can affect the viscosity and ionic conductivity of the electrolytes and therefore decrease battery performance over time. At room temperature, the 30 wt% KOH adjusts its level of hydration in accordance with the ambient humidity (60%).[7]

5.2. Solid-State Electrolyte

Solid-state electrolytes have drawn much attention for possessing both mechanical properties of solids and ion conduction of liquids. Due to this dual characteristic, zinc–air batteries with these electrolytes would sustain cell operation substantially longer than common aqueous alkaline electrolytes do; their extended applications include portable, flexible, and diversely shaped zinc–air batteries.[36,138] In the solid configuration, however, improving the interfacial properties between the solid electrolyte and a pair of electrodes (especially the high-surface-area air electrode) remains challenging.[139] For instance (**Figure 11**), in aqueous systems the high-surface-area catalysts at air electrodes have full access to the electrolyte, facilitating a three-phase reaction zone, consisting of solid (catalyst)–liquid (electrolyte)–gas (oxygen), for oxygen electrochemistry.[140,141] In contrast, in the solid configuration the three-phase interface reaction is severely restricted due to the poor wetting property of the "immobilized" electrolyte; thereby, interfacial resistance to hydroxide ions transporting over the catalyst surface is substantially higher than that of aqueous systems. The high interfacial resistance will lead to undesirable low current rates and high overpotentials during battery operation.

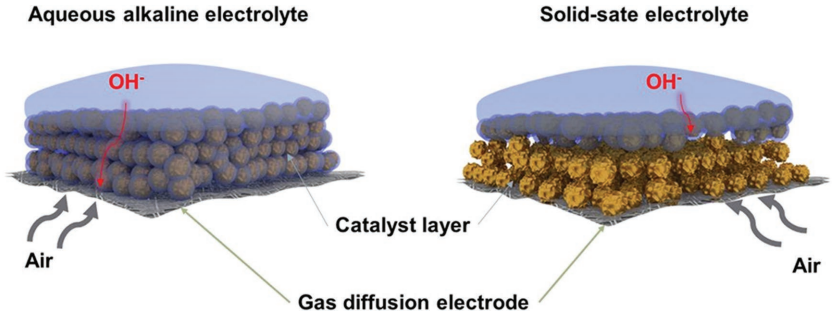

Figure 11. Illustration of the three-phase reaction zone in different electrolytes.

Alkaline gel electrolytes (AGEs), namely low–molecular–weight polymers gelled with alkaline solutions (e.g., KOH solutions), have been developed for primary zinc–air batteries.[142] These low–molecular–weight polymers, such as vinyl polymers and cellulose derivatives, are employed as mechanical matrices, and are swollen by essentially a large amount of alkaline electrolyte to ensure high ionic conductivity (thus low Ohmic resistance in batteries).[139] For instance, an AGE based on poly(vinyl alcohol)/poly(acrylic acid) exhibited a high ionic conductivity of 0.3 S cm^{-1}, which is of the same order of magnitude as that of aqueous electrolytes.[143] Also, the implementation of this gelled electrolyte in zinc–air batteries results in a high zinc utilization (82–90%) and, accordingly, high practical specific capacity close to the theoretical value. However, there is a trade-off between ionic conductivity and mechanical strength. The poor mechanical strength of AGEs results in unstable electrolyte–electrode contact and leads to high interfacial resistance.[144] Thus, solutions to improving simultaneously the ionic conductivity and the mechanical properties are critical to the success of AGEs in zinc–air batteries, especially when the batteries experience external (i.e., flexible devices) and internal deformation (i.e., volume change of the zinc electrode upon cycling).[145] Chen and co-workers[146] first reported a porous KOH-doped poly(vinyl alcohol) gelled electrolyte used in a flexible and rechargeable zinc–air battery, exhibiting an excellent cycle stability over 120 cycles at a rate of 50 A kg^{-1}. Peng and co-workers[147] reported a flexible and stretchable fiber-shaped zinc–air battery with a poly(vinyl alcohol)/poly(ethylene glycol)-based alkaline gel electrolyte, yielding an energy density of 5.7 W h L^{-1}. Recent advances made by Chen and co-workers[145,148] have shed further light on microporous-structured solid electrolytes with a high hydroxide-ion capacity and selectivity, as well as a strong mechanical property for flexible zinc–air batteries. For instance, they demonstrated a quaternary ammonia-functionalized cellulose electrolyte membrane, with a microporous structure, on a flexible rechargeable zinc–air battery device (**Figure 12**).[145] The interconnected porous structure based on cellulose nanofibers is of critical importance to retain a large degree of hydration for high ionic conductivity while maintaining dimensional stability in the water-swollen state of the membrane. Additionally, the uninhibited hydroxide-ion availability to the electrodes facilitates a superior reversibility of the zinc electrode and a charge-transfer process at the air electrode during repeated cycles. Despite the increasing interest in full flexibility, further improvements in ionic conductivity, interfacial properties, and mechanical robustness are still necessary for wide-scale integration of high-performance rechargeable zinc–air batteries.

5.3. Ionic Liquids

Room-temperature ionic liquids (RTILs) are molten salts in the liquid state below 100°C, composed of large organic cations and organic/inorganic anions; basically, RTILs can be considered as either protic or aprotic in character.[149] Due to their wide electrochemical window and nonflammability, RTILs have long attracted research attention as electrolytes for lithium–air batteries.[150] However, the application of RTILs as electrolytes in zinc–air batteries is still a relatively new area of study.[151] Conventional aqueous zinc–air batteries may greatly benefit from switching to low-volatility and water-/metal-free RTILs, because issues commonly faced by aqueous systems, such as electrolyte evaporation, zinc self-corrosion, and carbonation, can be avoided. Due to their high thermal stability, zinc–air batteries using RTILs have the potential to operate at moderate and high temperatures, enabling a lower thermodynamic barrier and better reaction kinetics. A reversible zinc electrochemistry has been proven to coordinate with zinc cations by selectively choosing anions in some aprotic RTILs.[152] With these aprotic RTILs, dendrite-free zinc deposition has also been demonstrated to be feasible.[153] However, aprotic RTILs generally do not work well with the current oxygen electrochemistry, which relies either on the presence of hydroxide ions or protons. In comparison, protic RTILs, which are able to dissociate protons, are more favorable in supporting the oxygen electrochemistry with a two-electron-transfer process (refer to Section 6.2), leading to the formation of hydrogen peroxide. Some researchers further investigated the effect of various protic additives (e.g., water and ethylene glycol) in RTILs as a means of combining the advantages of each liquid, and concluded that high proton availability helps to promote a four-electron oxygen-reduction process.[154] With regard to the mechanism for the reversible oxygen electrochemistry in protic RTILs, we refer readers to a specific review article in ref. [151]. Nevertheless, the electrochemical kinetics for both the zinc and oxygen redox reactions in RTILs are intrinsically slow because of their relatively high viscosity and low conductivity, which substantially restricts current rates. Thus the quest to find an RTIL that favors reversible oxygen electrochemistry while retaining high reaction kinetics remains a challenge for zinc–air batteries. To our knowledge, very few systematic investigations of RTILs as electrolytes in rechargeable zinc–air batteries have been conducted.[155] An ionic liquid containing sulfonate anions as the electrolyte was proposed for zinc–air batteries, and the reaction mechanism with a two-electron peroxide route (proposed Reaction (6)) was introduced by Wolfe and co-workers[30,155] for Fluidic Energy's zinc–air flow battery. However, the two-electron peroxide mechanism leads to a reduced energy density (compared to the four-electron ORR pathway) and radical peroxide species in the electrolyte, which can be detrimental to the catalysts and the air electrode. Overall, RTILs are relatively expensive compared to aqueous electrolytes, which also poses a challenge for their practical application in cost-competitive zinc–air batteries.

$$Zn^{2+} + O_2 + 2e^- \Leftrightarrow ZnO_2 \quad (6)$$

6. Bifunctional Air Electrodes

A bifunctional air electrode consumes oxygen during battery discharge and reversely evolves oxygen while charging. For the realization of high power-performance, electrically rechargeable zinc–air batteries rely significantly on air (oxygen) electrodes that are bifunctionally active and durable, such that they withstand the harsh conditions during repetitive discharge and charge in alkaline electrolytes. The development of a highly

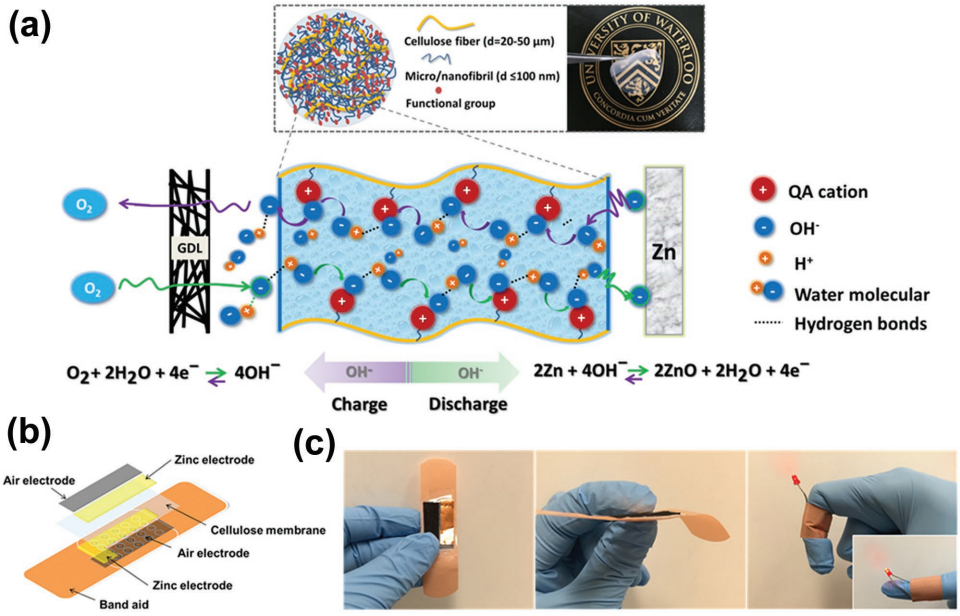

Figure 12. a) Schematic diagram of the solid-state rechargeable zinc–air battery using a functionalized nanocellulose membrane. (GDL: gas diffusion layer; QA: quaternary ammonium). b) Schematic diagram of a flexible zinc–air battery device integrated with a sticking plaster. c) A demonstration of the flexible device wrapped around an index finger to power a red LED under bending. Reproduced with permission.[145] Copyright 2016, The Royal Society of Chemistry.

bifunctionally active air electrode is quite challenging because both the ORR and the OER show considerably high overpotentials, and thereby significantly relies on a truly bifunctional electrocatalyst to efficiently promote both the ORR and the OER processes. The electrode materials must also be stable with respect to highly oxidative conditions upon oxygen evolution, as well as strong reducing conditions under oxygen reduction at high current rates; a wide working range of potentials spans from about 0.6 V (versus reversible hydrogen electrode (RHE), pH = 14) during discharge to about 2.0 V during charging. The use of decoupled air electrodes for respective ORR and OER has been reported to improve the battery cycling stability, but this configuration unavoidably complicates the cell design and incurs weight and volume penalties of power and energy density.[156] Typically, the bifunctional air electrode consists of a hydrophobic GDL and a moderately hydrophilic catalyst layer. The GDL provides a physical and conductive support for the catalysts, as well as a passage for oxygen diffusion in and out during discharging and charging, respectively. The ORR occurs at a three-phase interface (gaseous oxygen–liquid electrolyte–solid catalyst), while the OER takes place at a two-phase reaction zone (liquid electrolyte–solid catalyst). Thus, rational design of the air electrode in terms of an interfacial structure with optimal hydrophilicity is critical to optimize the catalytic activity and avoid flooding of the catalytic active sites. The search for bifunctional catalysts has mainly focused on nonprecious alternatives such as transition metal compounds (e.g., oxides, sulfides, nitrides, carbides, and macrocycles), carbon-based materials, and hybrids composed of the former two. In the following sections, the material and design aspects of the gas-diffusion layers and bifunctional catalysts are discussed; advanced bifunctional air electrodes that uniquely integrate the former two are also reviewed.

6.1. Gas-Diffusion Layer

The GDL plays a vital role in the performance of bifunctional catalysts at the air electrode. For zinc–air batteries, the GDL has the following essential functions: i) provides a physical support for the catalysts/catalyst layer, ii) allows a uniformly distributed transportation of air (oxygen) to/from the catalysts, iii) serves as a wet-proofing electrode backing that prevents electrolyte from leaking out, iv) possesses high electrical conductivity to provide an electrically conductive pathway for current collection. To facilitate air transport in zinc–air batteries, the GDL should be thin, highly porous, and hydrophobic in nature. The hydrophobicity can be realized by impregnating the GDL with hydrophobic agents such as PTFE,[157] PVDF,[158] and fluorinated ethylene propylene (FEP).[159] The degree of hydrophobicity in the GDL influences the battery polarization behavior in terms of electrical conductivity (Ohmic resistance) and gas permeability (mass transfer); to achieve optimal performance, it should possess the capability of alleviating electrolyte evaporation and resisting electrolyte flooding under extreme conditions.[160] Moreover, an ideal GDL should have properties such as fast air diffusion with high electrolyte repellency, high mechanical integrity (with optimum bending stiffness in the case of flexible designs), superior electrical conductivity, and reliable electrochemical-oxidation stability and chemical durability in strong alkaline electrolytes.

Two types of commercially available carbon-based GDLs that are commonly used in zinc–air batteries are nonwoven carbon paper (e.g., Toray, Freudenberg, and Sigracet) and woven carbon cloth (e.g., Zoltek, GDL-CT, and ELATTM). These carbon-based GDLs typically have a dual-layer design, consisting of a macroporous gas-diffusion backing and a thin microporous layer (MPL) (**Figure 13**a). The macroporous

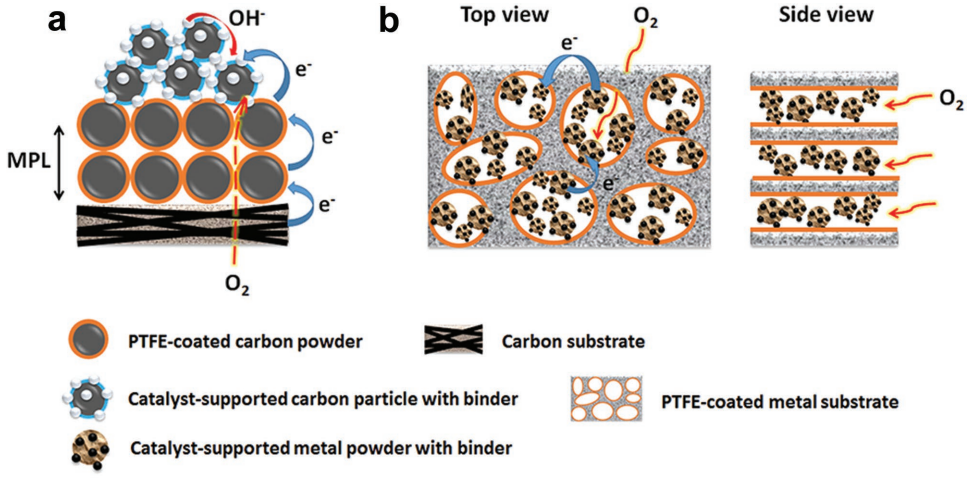

Figure 13. Schematic diagram of: a) carbon-based (cross-sectional view), and b) metal-based GDLs integrated with the catalysts.

backing layer is made up of a highly hydrophobic array of graphitized carbon fibers to provide large gas-diffusion pores, while the MPL is a thin, relatively hydrophilic carbon (e.g., carbon black) layer having fine porosity for supporting the catalytic active materials. The MPL helps to distribute air effectively throughout the catalyst layer and minimize the contact resistance between the macroporous layer and catalyst layer.[161] Thinner carbon-paper GDLs often tend to have a better battery performance, in terms of more favorable Ohmic resistance and mass transfer; however, they are quite brittle to handle. On the other hand, thicker carbon cloth GDLs are more mechanically flexible, and thereby can be employed as a robust catalyst layer support for small-scale, flexible zinc–air-battery applications. Although these state-of-the-art carbon-based GDLs have been successfully demonstrated in polymer-electrolyte-membrane fuel cells, their stability toward high oxidation potentials during oxygen evolution (charging), as well as exposure to highly alkaline electrolytes, is still an issue. These GDLs are highly susceptible to carbon corrosion, which consequently results in losses of active surface area for electrochemical oxygen reactions, uniform distribution of current throughout the air electrodes, and even severe leakage of electrolyte.[137,140] It is possible that alkaline electrolytes also can be negatively influenced by dissolved carbonate species resulting from carbon corrosion of the GDLs (refer to Section 5.1). For long-term operation, it is thus of utmost importance to prevent the corrosion of the GDLs either by the use of highly corrosion-resistant, graphitized carbon materials or by the use of metallic substrates. Typically, metal-based GDLs are fabricated by casting and pressing of a mixture of the catalysts, metal powders, and PTFE binder into a porous metallic substrate such as a metal foam (Figure 13b). In general, metal-based GDLs provide a higher electrical conductivity and a better electrochemically oxidative stability (either through a higher reduction potential or surface passivation via the formation of a thin oxide/hydroxide layer) over a wider potential range compared to carbon-based GDLs.[162] Metal substrates made of stainless-steel mesh, titanium mesh, nickel mesh, and nickel/copper foam have been employed as diffusion media, leading to comparable performance to carbon-based GDLs in zinc–air batteries.[20,163,164] Chen and Lee[162] reported an integrative air electrode, wherein the GDL and catalyst layer were combined in a single layer. The single-layer design with different porosities and hydrophobicities, made from sintered nickel powder as a base and Co_3O_4 as a bifunctional catalyst, was demonstrated in zinc–air batteries. The electrode was fabricated by casting and pressing of the mixture of Co_3O_4 catalyst, nickel macroparticles, and PTFE binder into a conductive nickel-foam substrate, with a thickness of 150–250 µm. The nickel macroparticles were used to provide a macroporous structure in the single layer, allowing efficient air diffusion to the active catalysts. In addition, the use of nickel macroparticles and nickel foam instead of carbon materials to form a hierarchical porous framework for air diffusion avoided the issue of carbon corrosion and subsequent mechanical failure and electrolyte leakage. Using this air electrode in zinc–air batteries led to a stable cycling performance of more than 100 cycles at a current rate of 17.6 mA cm^{-2}. Similarly, the active catalysts can be directly sintered on a corrosion-resistant, porous metallic substrate. Brost et al.[165] prepared a bifunctional air electrode consisting of a nickel-foam scaffold with perovskite $La_{0.6}Ca_{0.4}CoO_3$ catalysts chemically bonded to the conductive scaffold by a high-temperature thermal treatment. The porosity of the scaffold was controlled (≈80%) to facilitate the flow of air through the electrode. In this electrode, conductive additives such as metal fibers or particles were also used to provide additional current pathways between the catalysts and nickel-foam scaffold. This significantly improves the catalytic performance of the active catalysts and efficiency of the batteries due to an increase of surface area and electrical conductivity. It is worth mentioning that the use of plastic binders (e.g., PTFE) is unavoidable in both the cases of carbon- and metal-based GDLs. PTFE is gradually attacked by caustic and oxidizing conditions and consequently degraded over long operation times, resulting in collapse of the porous structure and mechanical failure of the GDLs. Both effects will lead not only to the increase of mass-transfer resistance at air electrodes but also to apparent reduction of long-term battery operation. With regard to the degradation of PTFE, making the distribution of the micropores in GDLs more uniform can alleviate the negative influence of the porous geometry change.[137]

6.2. Bifunctional Catalysts

6.2.1. Oxygen Electrochemistry

The kinetics for the electrochemical oxygen reactions are generally rather slow; therefore, bifunctional catalysts are needed in order to boost both the ORR and OER kinetics to practically usable levels in zinc–air batteries. Platinum (Pt) exhibits a superior activity for the ORR but rather poor performance for the OER due to the formation of a stable oxide layer with low electrical conductivity.[166] Noble-metal oxides such as ruthenium (Ru) and iridium (Ir) oxides, though being excellent OER catalysts, are less active for the ORR.[167] In particular, the durability of existing noble-metal-based catalysts is still far from being satisfied under rechargeable zinc–air-battery operation; their implementation in the zinc–air system is also plagued by the scarcity and resultant high cost of noble metals.[167,168] To be commercially viable, while achieving catalytic efficiency for both the ORR and OER at the same air electrode, bifunctional catalysts free of precious metals have been extensively sought for practical zinc–air batteries.[24,125,169–172] However, it is still quite challenging to find a stable catalyst material without significantly sacrificing bifunctional catalytic efficiency, due mainly to the wide operating range of the ORR/OER potential during the discharge and charge process.

Significant progress has been made in bifunctional-catalyst development including transition-metal-based materials (oxides, chalcogenides, nitrides, and carbides), heteroatom-doped carbon nanomaterials, and hybrid materials that consist of the former two.[173] Despite the progress, most catalyst research is still generally based on the trial-and-error method. This is because the mechanism and reaction kinetics of the ORR and OER vary between different catalyst materials and electrolytes, and thus are hard to predict.[174–176] In terms of the ORR, the reduction of oxygen in aqueous electrolytes may proceed by two overall pathways: a direct four-electron pathway (Reaction (7)) and a two-electron pathway (Reaction (8)).

$$O_2 + 2H_2O + 4e^- \Leftrightarrow 4OH^- \quad (7)$$

$$O_2 + H_2O + 2e^- \Leftrightarrow HO_2^- + OH^- \quad (8)$$

For practical battery applications, catalysts that can promote the ORR through the direct four-electron reduction pathway are highly preferred.[176] This is because the oxygen in this pathway is reduced to OH^- without producing peroxide in the solution phase. These catalysts are often noble-metal-based (e.g., Pt, Pd, Ag) materials,[177,178] some transition-metal macrocycles (e.g., iron phthalocyanine),[179] metal oxides (e.g., perovskites),[180] and some nitrogen-doped carbon materials.[171,181,182] In contrast, the two-electron reduction path involves peroxide species that are present in the electrolyte. The peroxide buildup not only reduces the efficiency of the ORR catalysis but also poisons the catalysts or carbon support materials because of its high oxidizability.[175]

Precise reaction pathways during the OER are relatively ambiguous and thus difficult to be determined. Generally accepted mechanisms for the metal-catalyzed OER involve the reverse process of the ORR through four sequential electron-transfer steps.[177,183] Noble-metal oxides (e.g., IrO_2 and RuO_2) are highly OER active and display metallic-like conductivity, but are fairly expensive.[184] The drive to replace these expensive noble-metal oxides has led to a class of catalysts consisting of earth-abundant transition-metal (e.g., Co, Ni, and Mn) oxides and (oxy)hydroxides.[185] Some transition-metal oxides, exhibiting semiconducting properties, have demonstrated good performance of oxygen evolution.[186] This is particularly the case in spinel- and perovskite-type metal oxides such as cobalt oxide,[187] nickel cobalt oxide,[188] and lanthanum nickel oxide.[189] In these materials, surface metal cations (M) are considered as the active sites for the OER, where the reaction proceeds via a series of metal-stabilized intermediates (i.e., M–OH, M–O, M–OOH, and M–OO) and changes the oxidation state of metal cations accordingly.[167] The relative stabilities of these intermediates at metallic surfaces, namely the binding strength of the M–O bonds and the activation barriers between the intermediates, determine the rate-determining step and therefore the overall OER rates.[167] A thorough understanding of the rate-determining steps could provide insight into how compositional, structural, geometric, and electronic properties of catalysts could be tuned to enhance the reaction rates of the OER. A number of activity trends have been presented, computationally and experimentally, in which the OER activities are relative to the number of d-electrons in the e_g orbital of the metal cations.[185] These trends are complex due to many factors, including electronic structure, electrochemically active surface area, surface composition and stoichiometry, electrical conductivity, and geometric structure (strain).[185]

Although recent advances in the computational analysis of catalysis enable us to predict and select potential candidates for the ORR and the OER, there is currently no exemplary benchmark performance for bifunctional catalysts to which all newly developed catalysts can be compared.[190] State-of-the-art carbon-supported Pt (i.e., Pt/C (carbon-black-supported platinum)) and RuO_2 or IrO_2 (i.e., RuO_2/C or IrO_2/C (carbon-black-supported iridium oxide)) catalysts are currently the most accepted benchmark electrocatalyst materials for the ORR and the OER, respectively.[173] A common approach to obtain high-performance bifunctional catalysts is to physically combine the above ORR catalysts (e.g., Pt/C) with efficient OER catalysts (e.g., IrO_2/C). Such an approach, however, is often neither effective nor reliable, due to poor material compatibility of these composite catalysts. It is thus challenging, but desirable, to find a general principle to achieve rational designs of bifunctional catalysts, yielding a strong bifunctional capability and high stability for the sake of long-term zinc–air battery rechargeability. The development of bifunctional catalysts is a topic of a large body of research, for which readers can refer to a recent review on bifunctional electrocatalysts for rechargeable zinc–air batteries.[173] There are three main characteristics that are important to an effective bifunctional catalyst: catalytic activity, selectivity, and stability.

Catalytic Activity: Catalytic activity should be considered to increase the number of active sites, to obtain suitable adsorption energy of the reaction intermediates on the catalysts' surface, and to reduce ionic and charge-transfer resistances.[191] Several volcano-like diagrams, which plot the catalyst activity

against adsorption energy of reaction intermediates for a given reaction, have been developed for the ORR (e.g., perovskite-based oxides,[192] and heteroatom-doped graphene[193]) and the OER (e.g., metal oxides,[194] and metal (oxy)hydroxides[185]). These volcano trends showed a clear activity peak at which there is an optimal binding energy.

Selectivity: Selectivity refers to the ability to minimize the production of peroxide radicals as intermediates in the solution phase and to obtain desired end-products of OH^- (for the ORR) and O_2 (for the OER). A bifunctional catalyst with a high selectivity can catalyze the oxygen reduction via the four-electron transfer pathway to produce the desired OH^- species, as well as the oxygen evolution by ruling out CO_2 evolution (due to carbon oxidation if the catalyst is carbon-based).[195]

Stability: Stability is required to withstand harsh conditions with respect to highly oxidative conditions upon oxygen evolution, as well as strong reducing conditions under oxygen reduction at high current rates. The stability loss of the catalysts could be due to many reasons, such as surface passivation, material corrosion/degradation, and phase change. For metal-based catalysts, Pourbaix diagrams are a useful tool to examine the thermodynamic stability of the various metals under different applied potentials and pH conditions.

The following sub-sections will discuss approaches to the rational design and improvement of bifunctional catalysts with respect to these characteristics.

6.2.2. Catalytic Activity and Selectivity

Activity and selectivity for the ORR and the OER depend highly on the intrinsic properties of the catalysts used, which can be affected by a variety of factors, such as crystallographic structure, composition/stoichiometry, size, and morphology as further discussed below.

Crystallographic Structure Control: The catalytic activity toward the ORR and the OER depends strongly on the surface structures of the catalyst in question. For the design of efficient bifunctional catalysts, precise control of surface properties with preferentially exposed crystal planes and appropriate surface energies is vital, and can lead to a high catalytic selectivity and activity. The importance of the exposed lattice facets on the bifunctionally catalytic activity was highlighted in a study of anisotropic MnO nanocrystals.[196] It was found that preferentially exposed (100) planes facilitated the adsorption of oxygen species (e.g., OH^- and O_2), which is known as one of the rate-determining steps for ORR/OER catalysis, and exhibited ORR and OER catalytic activities that were both superior to those of the (111) planes. Meng et al.[191] found that the catalytic performance of MnO_2 catalysts was highly dependent on their crystallographic structures (α-, β-, and δ-MnO_2, as well as amorphous MnO_2), with both ORR and OER activities following the order of α-MnO_2 > amorphous-MnO_2 > β-MnO_2 > δ- MnO_2. The kinetic studies utilizing Koutechy–Levich plots revealed the four-electron transfer mechanism of α-MnO_2 in the ORR compared to other phases that tend toward two-electron transfer. This indicated that α-MnO_2 had a higher selectivity for the fully reduced oxygen product (OH^-). Recently, Ling et al.[196] developed a high-performance bifunctional electrocatalyst through tuning the surface atomic structure of 1D single-crystal CoO nanorods (**Figure 14**). By creating oxygen-vacancy-rich pyramidal nanofacets of {111}, this surface structure engineering, in terms of electronic structure design, enabled great exposure of the active sites of the CoO to promote charge transfer, as well as optimal adsorption energies for ORR/OER intermediates. In particular, the vacancies on the {111}-O facets induced some new electronic states by hybridization of O-2p, Co-3d, and Co-3s in the bandgap, which were responsible for the high electronic conductivity of the CoO and the resulting superior electrocatalytic activity.

Composition Control: As promising nonprecious-metal-based electrocatalysts for both the ORR and the OER, transition-metal-based compounds, including oxides, sulfides, phosphates, nitrides, and macrocycles (these anions collectively referred to as A) are expected to serve as cost-effective substitutes for noble-metal-based catalysts in zinc–air batteries.[177] Transition metals (referred to as TM) such as Co, Ni, Mn, Fe, and Cu have been receiving increasing interest.[197] The catalytic activity of transition-metal compounds (TM_xA_y) toward the ORR/OER depends strongly on both the TM active center and TM/A composition. For instance, manganese oxides are generated with many stoichiometries, from a metal-rich phase (e.g., Mn_3O_4), which features extensive metal–metal bonding, to an oxide-rich phase (e.g., MnO_2, MnO), which exhibits extensive

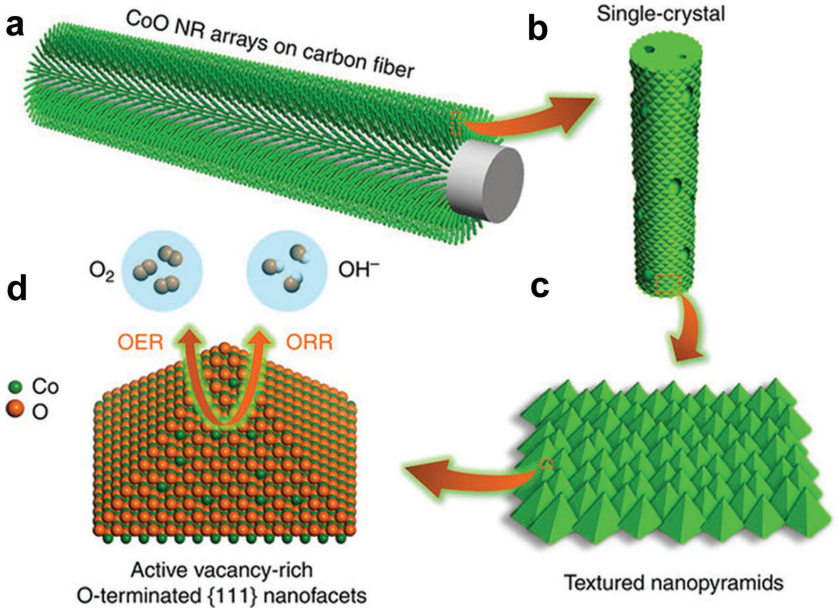

Figure 14. a) SC CoO NRs fabricated directly on carbon fiber substrate. b) Numerous nanopores present on the surface and across SC NRs. c) The surface of SC CoO NRs covered with textured nanopyramids. d) The dominant exposed facets of nanopyramids are electrochemically active-vacancy-rich O-terminated {111} facets. Reproduced with permission.[196] Copyright 2016, Nature Publishing Group.

oxide–oxide bonding. The bifunctional activity of manganese oxide catalysts is closely associated with the oxidation states of the Mn cations, which can be controlled by the Mn/O composition.[198] Similar to manganese oxides, rational control of the TM center and TM/A composition allows the ORR/OER catalysis to be tuned on other spinel- and perovskite-type transition-metal oxides. Such control, for instance, was well demonstrated in spinel-type metal oxides. Spinel-type oxides (single, binary, and ternary types) are capable of hosting various species of transition metals in their lattices. Menezes et al.[199] synthesized spinel tetragonal $CoMn_2O_4$ and cubic $MnCo_2O_4$ microspheres by controlling the ratio of the respective carbonate precursors. It was found that the octahedral sites of spinels (cubic $MnCo_2O_4$ phase) favor the OER and the tetrahedral sites of the tetragonal $CoMn_2O_4$ improve the ORR activity via the four-electron transfer path. Accordingly, engineering the composition of spinel oxides allows fine tuning of the properties, such as crystalline and electronic structure, which play vital roles in ORR/OER catalysis, affording an optimal catalytic activity and selectivity.

Size Control: For heterogeneous catalysis, the particle size of the catalysts usually has a significant interaction with their catalytic activities. When the catalyst size is reduced to the nanoscale, the physical and chemical properties of the catalysts change significantly from those at larger scales (bulk phase) due to quantum effects.[200] This size effect controls the behavior and properties of catalysts such as electrochemically catalytic reactivity, surface area, electrical conductivity, magnetic permeability, and structures. Unraveling the nanoscale particle-size effect on ORR/OER catalysis can provide important clues for the rational design of efficient electrocatalysts. A simple hypothesis is that, in the absence of size-induced strain (geometry) and electronic effects, the smaller the particle size, the greater the specific catalytic activity. Some scattered studies on the size dependency for respective ORR or OER have been reported; however, less insight has been given into bifunctional oxygen electrocatalysis.[201] Seo et al.[202] synthesized carbon-nanotube-supported cobalt oxide nanoparticles (CoO_x/CNTs) with sizes of 3–10 nm, and investigated their size dependency for bifunctional oxygen catalysis. The average particle sizes of the CoO_x were 4.3, 6.3, 7.5, and 9.5 nm (**Figure 15**a–d). High-resolution transmission electron microscopy (HRTEM) images of CoO_x/CNTs (Figure 15e–h) showed that the smallest CoO_x nanoparticles in the CoO_x(4.3)/CNTs were spinel-structured Co_3O_4, whereas the other three samples consisted of the cubic CoO phase. The particle-size-dependent catalytic activity was observed in the series of CoO_x/CNTs, where OER activities increased with decreasing CoO_x particle sizes. The OER enhancement was related to the increased oxidation state of the cobalt species and greater specific activity in smaller-sized CoO_x nanoparticles.

Morphology Control: Morphology control can influence a catalyst's properties, such as the specific surface area, which, in turn, tune the catalytic behavior. By fashioning bulk Co_3O_4 into a 3D ordered mesoporous structure (**Figure 16**a–c), for instance, Park et al.[24] boosted the catalytic activity for both the ORR and the OER, as well as the stability of spinel Co_3O_4. Compared to bulk shape (Figure 16d), the "honeycomb-like" 3D morphology (referred to as "3DOM") effectively increased the active surface area of the Co_3O_4; the microsized pores in the interconnected framework of the 3DOM Co_3O_4 significantly facilitated the OH^- and oxygen diffusion during the catalytic reactions. Furthermore, cyclic voltammetric (CV) measurements showed that the initial catalytic activities of the 3DOM Co_3O_4 were stably maintained after 1000 CV cycles in the range of 1.0–1.85 V (versus RHE), whereas the bulk Co_3O_4 exhibited larger polarization losses for both the ORR and the OER. Thus, the advanced 3DOM proved to be sufficiently stable to withstand harsh conditions with respect to highly oxidative conditions upon oxygen evolution, as well as strong reducing conditions under oxygen reduction. The enhanced stability can be attributed to the 3DOM framework, which prevented Co_3O_4 nanoparticles from aggregating.

In addition to the varying morphology of materials in the same composition, morphological control in hybrid nanocomposites (e.g., hybridizing ORR- and OER-active materials)

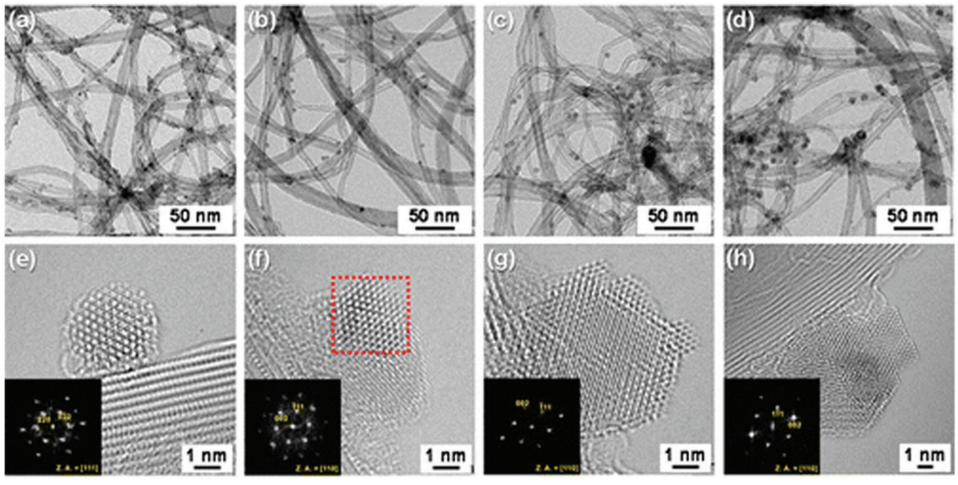

Figure 15. Characterizations of the CoO_x/CNTs. a–d) Bright-field TEM images of CoO_x (4.3)/CNTs (a), CoO_x (6.3)/CNTs (b), CoO_x (7.5)/CNTs (c), and CoO_x (9.5)/CNTs (d). e–h) Corresponding atomic-resolution TEM images and FFT patterns (insets). Reproduced with permission.[202] Copyright 2016, American Chemical Society.

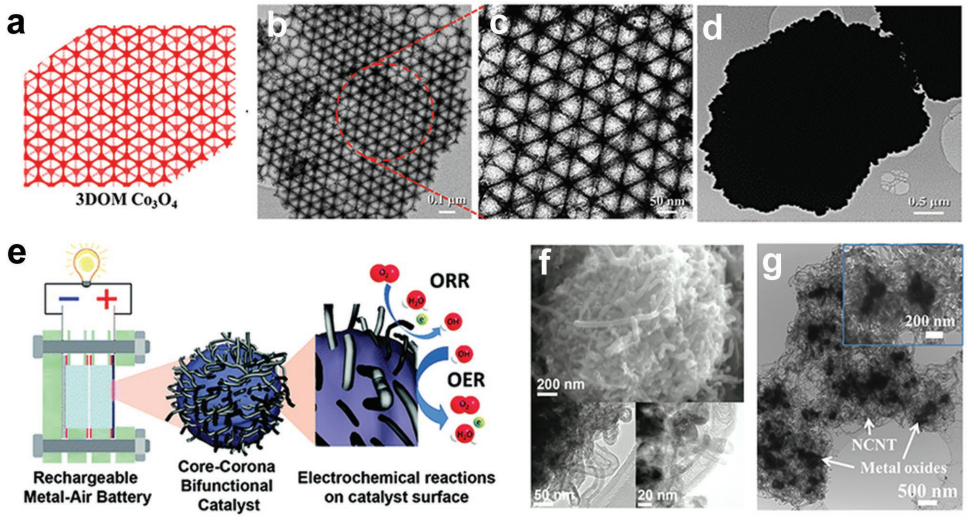

Figure 16. a–c) Schematic (a) and TEM images (b,c) of honeycomb-like 3D ordered mesoporous spinel Co_3O_4. d) TEM image of the bulk Co_3O_4. Reproduced with permission.[24] Copyright 2015, Wiley-VCH. e–g) Design and application of the core–corona-structured bifunctional catalyst (CCBC) for the rechargeable zinc–air battery. e) Schematic of the zinc–air battery using the CCBC at the air electrode. f,g) SEM (f) and TEM (g) images of the CCBC and intertwined-CCBC, respectively. f) Reproduced with permission.[204] Copyright 2012, American Chemical Society. g) Reproduced with permission.[125] Copyright 2014, American Chemical Society.

could be an efficient strategy to develop bifunctional electrocatalysts.[173,203] Chen et al.[204] synthesized a core–corona-structured bifunctional catalyst (CCBC) consisting of $LaNiO_3$ particles supporting nitrogen-doped carbon nanotubes (NCNTs) for zinc–air batteries (Figure 16e,f). In this synthesis, macrosized $LaNiO_3$ particles acted as the support and seed for the growth of NCNTs via a chemical vapor deposition (CVD) method. The importance of the core-and-corona morphology on the bifunctional electrocatalytic activity was highlighted as a means of combining advantages of the OER-active $LaNiO_3$ (core component) and the ORR-active NCNT (corona component), as well as enhanced charge-transport properties through the highly porous framework. The CCBC thus exhibited excellent ORR and OER catalytic activity similar to that of state-of-the-art Pt/C and $LaNiO_3$ catalysts, respectively, as well as sufficient stability. It was concluded that the synergistic effect between the two different materials and the stable catalyst structure arising from the unique core–corona configuration contributed significantly to the catalyst's bifunctional activity and selectivity. A zinc–air battery using the CCBC further demonstrated similar discharge and charge polarization compared to that of Pt/C and $LaNiO_3$, in good agreement with half-cell test results, while suffering much less degradation to battery performance upon cycling. To take full advantage of the core–corona morphology in the electrocatalytic activity, Lee et al.[125] presented an optimized core–corona morphology of the CCBC (referred to as IT-CCBC) stemming from size-controlled $LaNiO_3$ nanoparticles to promote prolific growth of intertwined NCNTs, knitting the clusters of the nanoparticles (Figure 16g). In this material, the highly tailored composite morphology enables an intimate interparticle interaction (enhanced synergistic effect) between the $LaNiO_3$ nanocores and the NCNT corona materials, and, accordingly, improved the diffusion of reactants and charge transfer of active species during the electrochemical oxygen reactions. Compared to the CCBC, the IT-CCBC displayed enhancement of both half-cell and zinc–air-battery performance, in terms of the bifunctional activity and electrochemical durability, due to the carefully engineered core–corona morphology. These results show the importance of morphology control in the preparation of composite materials as highly efficient bifunctional electrocatalysts.

6.2.3. Carbon Effects on Catalytic Activity, Selectivity, and Stability

Carbon materials with high surface areas are typically employed as supports to increase the number of active sites at the electrode/electrolyte interface. Particularly, graphitized carbons, such as carbon nanotubes (CNTs), carbon nanofibers (CNFs), carbon nanosheets, and graphene, are most commonly used owing to their relatively high anodic resistance to carbon corrosion in comparison to their low-crystallinity counterparts.[205] Aside from their utilization as support, carbon materials generally show a certain extent of catalytic activity toward the ORR in alkaline solutions.[174] Among these nanocarbons, CNTs and graphenes are two groups of carbon nanomaterials receiving extensive attention in heterogeneous catalysis, owing to their large surface area for extensive exposure of active sites, high electrical conductivity for rapid electron transfer, and high graphitic degree for enhanced electrochemical stability at high oxidation potentials.[205] Significantly, doping these nanocarbon materials with heteroatoms could significantly boost the ORR activity leading to a favorable formation of OH^- via the four-electron pathway; the ORR catalyzed by nitrogen- (N),[206] sulfur- (S),[207] phosphorous- (P),[208] boron- (B),[209] iodine- (I)[210] and dual-atom-doped[182,211] CNTs and/or graphene materials as metal-free electrocatalysts has been extensively studied. Despite the ORR enhancement, these carbon nanomaterials have yet to be readily employed as bifunctionally active catalysts

due mainly to their fairly low OER catalytic activity and the unavoidable carbon corrosion when exposed to the high oxidation potentials of the OER; the carbon corrosion could further aggravate the aggregation of the catalysts and block the active surface with formed carbonates (due to CO_2 evolution).[195] As mentioned above, CNTs and graphene exhibit relatively high oxidation stability, benefiting from their extensively conjugated graphitic structure; their stability could further be improved through selectively introducing heteroatom dopants.[212] Understanding the exact catalytic reaction mechanisms of the ORR and OER on heteroatom-doped nanocarbon is thereby of importance to finely tune the bifunctional activity and selectivity, as well as the improvement of the overall stability.

Recently, for the first time, Yang et al.[170] experimentally identified the bifunctionally active sites in N-doped graphene-nanoribbon materials; the electron-donating quaternary N sites were responsible for a four-electron ORR, whereas the electron-withdrawing pyridinic N species served as OER active sites. The zinc–air battery adopted with N-doped graphene-nanoribbon catalysts exhibited a peak power density of 65 mW cm^{-2}, as well as good cycling stability over 30 h at a current density of 20 mA cm^{-2}. The identification of bifunctionally active sites associated with different nitrogen species provides important implications for the development of carbon-based, metal-free bifunctional catalysts for practical zinc–air-battery applications. Qu et al.[182] developed N,S-co-doped mesoporous carbon nanosheets using S-modified polydopamine as a precursor. Benefiting from the multiple doping, this material exhibited excellent ORR/OER bifunctional activity and durability, even better than that of transition-metal and noble-metal catalysts.

Recently, metal–organic frameworks (MOFs)-derived nanocarbon composites with abundant functional groups have been investigated as promising bifunctional catalysts toward the ORR and the OER. Xia et al.[213] demonstrated a direct synthesis of hollow-structured, N-doped CNTs derived from zeolitic imidazolate framework (ZIF-67) particles (referred to as NCNTFs) as a promising bifunctionally active catalyst for zinc–air batteries (**Figure 17**). The ZIF-67 particles not only provided a carbon and nitrogen source for the growth of N-doped CNTs catalyzed by the in-situ-formed cobalt nanoparticles, but also acted as the template for the formation of the hollow structure. It is known that N-doped CNTs provide a good catalytic activity toward the ORR, but their OER activity is often unsatisfactory. The resultant NCNTFs exhibited enhanced catalytic activity toward the OER, as well as superior ORR activity, strongly comparable to that of commercial Pt/C catalysts. This enhancement was mainly related to the modified electronic structure and carbon defects of the CNTs, which were induced by chemical interaction of nitrogen with nearby cobalt and carbon atoms.

Some studies have shown that covalently hybridizing graphene and CNTs, as well as heteroatom doping, can be a promising strategy to enhance the bifunctional catalytic activity and stability.[214,215] This hybrid configuration not only inherits the advantages of both the CNTs and the graphene, such as high specific surface area and superior electronic conductivity, but also effectively extends the exposure of active sites through the 3D framework. Moreover, the intimate connection between graphene and CNTs through covalent C–C bonding enables fast electron and charge transfer as a whole. Tian et al.[214] prepared a 3D hybrid catalyst composed of interconnected N-doped graphene and CNTs by the CVD method. This catalyst demonstrated a high ORR and OER activity, strongly comparable to that of commercial 20 wt% Pt/C and 20 wt% IrO_2/C catalysts, respectively, as well as superior durability, thus establishing it as a high-performance, metal-free bifunctional catalyst.

Another type of carbon-based hybrid bifunctional catalyst typically consists of strongly coupled inorganic nanomaterials and functionalized carbons, synthesized by direct nucleation and growth of inorganics (e.g., transition metals, oxides, or sulfides) on the functional groups (e.g., oxygen, nitrogen,

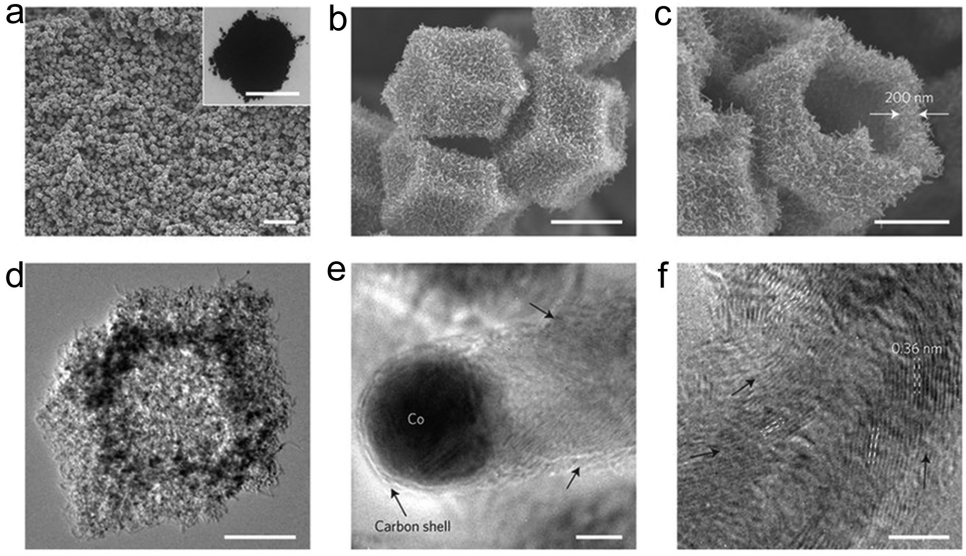

Figure 17. Morphology and structural characterization of NCNTFs obtained at 700 °C in the presence of H_2. a–c) FESEM images. d) TEM image. e,f) HRTEM images. In (f) 0.36 nm refers to the lattice spacing indicated by the white dashed lines, on the carbon (002) plane. The arrows in (e) and (f) indicate the direction of the graphitic layers. The inset of (a) is a digital photo, scale bar is 1 cm. Scale bars: a) 10 µm; b,c) 1 µm; d) 500 nm; e,f) 5 nm. Reproduced with permission.[213] Copyright 2016, Macmillan Publishers Limited.

or sulfur) of a nanocarbon support.[216] This approach affords strong chemical interactions and electrical coupling as a means of a synergistic effect between the two components, giving rise to the increased activity and durability for both the ORR and the OER, in comparison to those of individual components or their physical mixtures. Thippani et al.[195] synthesized a bifunctional catalyst comprising cobalt and N-doped CNTs (referred to as N-MWCNTs-Co) for rechargeable zinc–air batteries. Based on the electrochemical measurements, in addition to moderately high ORR activity, the N-MWCNTs-Co catalyst exhibited good OER selectivity and stability against carbon corrosion, as evident by the absence of the precipitation of carbonates (i.e., $CaCO_3$ for electrolytes containing $Ca(OH)_2$) on the electrode surface. The recognition of the synergistic effect between spinel-Co3O4 nanoparticles and N-doped graphene or mildly oxidized CNTs has also led to drastically improved bifunctional activity of those hybrid catalysts, as well as stability, compared to that of Co3O4.[217] Such a synergistic effect could be general to transition metals, oxides, hydroxides, sulfides, or phosphates coupling with heteroatom-doped graphene and CNTs.

6.3. Integration of Bifunctional Air Electrodes

Despite all the progress of bifunctional electrocatalysts, their practical performance in zinc–air batteries suffers from poor integration into the air electrode.[141] That is, a number of nanosized catalysts are buried during the air-electrode fabrication, leading to a lack of access to the electrolyte. Typically, the fabrication of the bifunctional air electrode involves physical incorporation of the bifunctional catalysts and ancillary additives into the GDL framework, through a variety of methods, such as drop-casting, screen-printing, and spray-coating. The ancillary materials are required in these approaches to construct a continuous, porous, and ionic/electronic conductive network in the air electrode, for the sake of electron and charge transfer, as well as mass diffusion. They generally include polymeric binders (e.g., Nafion perfluorinated, Tokuyama AS4 alkaline ionomers) and a conductive catalyst support (e.g., acetylene black). However, the use of these ancillary materials has a negative impact on the battery performance. For instance, acetylene black is readily corroded, especially when encountering highly oxidative electrochemical potentials during charging. The carbon corrosion aggravates aggregation/sintering or even leaching of catalysts, severely reducing the overall battery performance. Another issue is associated with the detachment of weakly bound catalysts from the electrode surface due to degradation of polymeric binders in a strong caustic and oxidizing environment.[141] This issue results in loss of active materials and large interfacial impedances, giving rise to high overpotentials for discharging and charging reactions. Thus, there exists a need for a novel integrative design of bifunctional air electrodes for rechargeable zinc–air batteries that overcomes the aforementioned deficiencies.[218] Approaches such as electrodeposition and CVD have been taken as methods of directly growing nanostructured catalysts on conductive and porous substrates, in order to make carbon-support-free and binder-free bifunctional air electrodes.[140,141,147,172,218–221] Without additional carbon support and binders, these advanced air electrodes also can provide a high accessibility of the catalytic sites and a low interfacial contact resistance. Additionally, such integrative bifunctional air electrodes as a whole are directly synthesized with the current collector (conductive substrates), and are free of the conventional complex preparation processes, which would be of great benefit to large-scale fabrication. To realize flexible integrative air electrodes, physically robust or bendable substrates (e.g., carbon cloth or metal meshes/foams) are strongly demanded.

Table 3 presents a summary of some of the recently reported integrative bifunctional air electrodes for electrically rechargeable zinc–air batteries. To access the overall air-electrode performance, the voltage gap between the discharge and charge, the power density, and the cycle stability are compared. As an example, we recently developed a free-standing bifunctional air electrode through morphological emulation of a human-hair array.[141] This air electrode assembly was constructed based on an array of hair-like bifunctional catalysts vertically grown on a stainless-steel mesh (**Figure 18**). Each individual hair-like catalyst of the array contained a nanoassembly of mesoporous Co_3O_4 nanopetals in nitrogen-doped multiwalled carbon nanotubes (NCNTs); the synergistic effect between the Co_3O_4 and the NCNTs was found to enhance bifunctional catalytic activity. Given that the stainless-steel mesh is highly conductive, a current collector at the air electrode is not necessary. This completely eliminates the voltage drop that reduces battery performance due to the interfacial resistance between the current collector and the air electrode. The morphological advantages of this electrode can be embodied by several aspects: facile accessibility of catalytic active sites, favorable interfacial properties and mass transfer, enhanced air-electrode stability against corrosion and aggregation of the catalysts/catalyst support, and superior mechanical integrity with robust flexibility. Using this air electrode, a flexible solid-state zinc–air battery was able to deliver a high energy density of 847.6 W h kg^{-1} and a power density of 160.7 mW cm^{-2}, as well as a remarkable cycling stability over 600 h of operation at a current density of 25 mA cm^{-2}.

7. Battery-Performance Evaluation

While the previous sections have focused on the characteristics and performance of the individual components in a zinc–air battery, it must also be realized that each component can have significant and complex influences on the others during operation. Therefore, it is important for novel components to be demonstrated within a complete zinc–air cell. This section provides an overview of the variety of experimental testing techniques that may be used to evaluate the performance of zinc–air batteries. Factors such as open-circuit voltage (OCV), operating voltage, energy efficiency, specific capacity, energy density, power density, and cyclic stability are essential parameters that should be evaluated in the investigation of novel zinc–air batteries. These parameters can be revealed with the galvanodynamic polarization (Section 7.1), galvanostatic cycling (Section 7.2), and galvanostatic full-discharge (Section 7.3) methods. In addition, individual resistance, capacitance, and electrode polarization values can aid in the understanding of

Table 3. Summary of recently reported binder-free, integrative bifunctional air electrodes.

Reference	Bifunctional air electrode	Synthesis method	Feature	Cell components	Δ(charge–discharge)[a] *E* [V] @ *j* [mA cm^{-2}]	Power density and durability
[141]	Co_3O_4–NCNT on stainless steel	CVD/ electrodeposition	Flexible	Zinc powder/cellulose film gelled with 6 M KOH/air	0.72[b] @ 25	167 mW cm^{-2} @ 253 mA cm^{-2}; ≈600 h @ 25 mA cm^{-2} for 20 min–10 h per cycle
[222]	N-doped carbon fiber film	Electrospinning/ pyrolysis	Flexible	Zinc plate/6 M KOH + 0.2 M zinc acetate/air	0.73 @ 10	185 mW cm^{-2} @ 300 mA cm^{-2}; ≈83 h @ 10 mA cm^{-2} for 20 min per cycle
[220]	Co_4N/intertwined carbon fibers on carbon cloth	Electrodeposition/ carbonization	Flexible	Zinc plate/6 M KOH/air	0.84 @ 10	174 mW cm^{-2} @ 260 mA cm^{-2}; ≈136 h @ 10 mA cm^{-2} for 30 min per cycle
[140]	Co_3O_4 on stainless steel	Hydrothermal	Flexible	Zinc plate/6 M KOH + 0.2 M zinc acetate/air	1.1[b] @ 17.4	40 mW cm^{-2} @ 65 mA cm^{-2}; ≈600 h @ 50 mA for 6 h per cycle
[147]	RuO_2 on CNT	Dip coating	Flexible	Zinc wire/gelled PVA & PEO alkaline electrolyte/air	0.82 @ 1[e]	NA; ≈30 h @ 1 A g^{-1} for 1 h per cycle
[219]	MnO_x on stainless steel	Electrodeposition	Flexible	NA[c]	NA[c]	27 mW cm^{-2} @ 58 mA cm^{-2}; NA
[221]	a-MnO_2 on carbon paper	Immersion process	Rigid	Zinc plate/6 M KOH + 20 g L^{-1} $ZnCl_2$/air	0.82 @ 15[d]	108 mW cm^{-2} @ 168 mA cm^{-2}; ≈125 h @ 15 mA cm^{-2} for 5 min–4 h per cycle[d]
[223]	Co_3O_4 on carbon nanofiber mat	Electrospinning/ pyrolysis	Rigid	Zinc plate/6 M KOH + 0.2 M $ZnCl_2$/air	0.85 @ 20	125 mW cm^{-2} @ 200 mA cm^{-2}; ≈55 h @ 20 mA cm^{-2} for 1 h per cycle
[224]	P–g-C_3N_4 carbon-fiber paper	Hydrothermal	Rigid	Zinc plate/6 M KOH/air	1.41 @ 20	NA; ≈8.3 h @ 20 mA cm^{-2} for 10 min per cycle
[218]	AgCu on nickel foam	Pulsed-laser deposition	Rigid	Zinc plate/6 M KOH + 0.1 M zinc acetate/air	1.04[b] @ 10	86.3 mW cm^{-2} @ 100 mA cm^{-2}; ≈50 h @ 20 mA cm^{-2} for 15 min per cycle
[228]	N-doped NiFe double-layered hydroxide/Ni foam	Chenical-bath deposition	Rigid	Zinc foil/3 M KOH + 0.2 M zinc acetate/oxygen	0.9[b] @ 5[f]	0.55 mW cm^{-2} @ 0.65 mA cm^{-2}; ≈166 min @ 5 mA cm^{-2} for 200 s per cycle[f]

[a]Current density represented by *j*; [b]The voltage gap was estimated based on the discharge–charge cycling measurements; [c]Not reported; [d]Measurements at a discharge current of 15 mA cm^{-2} for 5 min, followed by a charge current of 7.5 mA cm^{-2} for 10 min; [e]Unit of *j* is A g^{-1}; [f]Measurements at a charge current of 5 mA cm^{-2} for 200 s, followed by a discharge current of 0.5 mA cm^{-2} for 2000 s.

various phenomena. Electrochemical impedance spectroscopy (Section 7.4) and three-electrode testing (Section 7.5) may be employed to determine these values.

7.1. Galvanodynamic Polarization

The galvanodynamic polarization technique is used to evaluate the degree of departure of the battery's operating voltage from the OCV in response to discharging and charging currents. The technique is generally carried out by applying negative (discharging) or positive (charging) currents with progressively higher magnitudes to the battery electrodes. The potential responses are recorded as a function of current, yielding the discharge and charge polarization curves. **Figure 19**a shows a typical example of discharge and charge polarization plots (black and brown solid lines, respectively) of the rechargeable zinc–air battery obtained by the galvanodynamic polarization method. The difference between the operating voltage and the OCV (i.e., discharge or charge overpotential) directly represents the sum of the voltage losses associated with activation and mass-transfer polarization at each electrode, in addition to the Ohmic resistance of every component of the electrochemical circuit (refer to Figure S1, Supporting Information). Taking the discharge polarization curve as an example, the steep initial voltage drop is mostly caused by the energy barrier for the electron-transfer reactions occurring at the electrodes (referred to as activation polarization). The oxygen reactions at the air electrode constitute the majority of activation losses in zinc–air batteries. When the current is further increased, additional voltage losses are dominated by Ohmic polarization, and thus the voltage decreases almost linearly with the current density. In this Ohmic region, the voltage loss mostly comes from the internal resistance of the electrolyte to ionic flow and the interfacial resistances between the electrodes and the electrolyte; this is the desirable operating regime for the zinc–air battery. Both the activation (influenced mainly by catalyst activity) and Ohmic resistances (influenced mainly by the electrolyte properties) are key power performance drivers of zinc–air batteries. The sharp voltage drop at the end is associated with the limited mass transfer of reactants (i.e., oxygen or OH^-) to the electrodes, referred to as mass-transfer polarization. The power density (blue solid line) of the zinc–air battery can be plotted as a function of current density by multiplying the discharge voltage by the applied current density, allowing determination of the peak power density (and corresponding current density). In addition, the zinc–air battery's energy efficiency (red solid line) can also be determined at a certain current density by simply dividing the discharge voltage by the charge voltage. In this example, at the peak power output, the battery energy efficiency is 31.5%, indicating that almost 70% of the energy put into the battery is lost to the discharge and charge overpotentials (this assumes the battery is charged and discharged at the same current density).

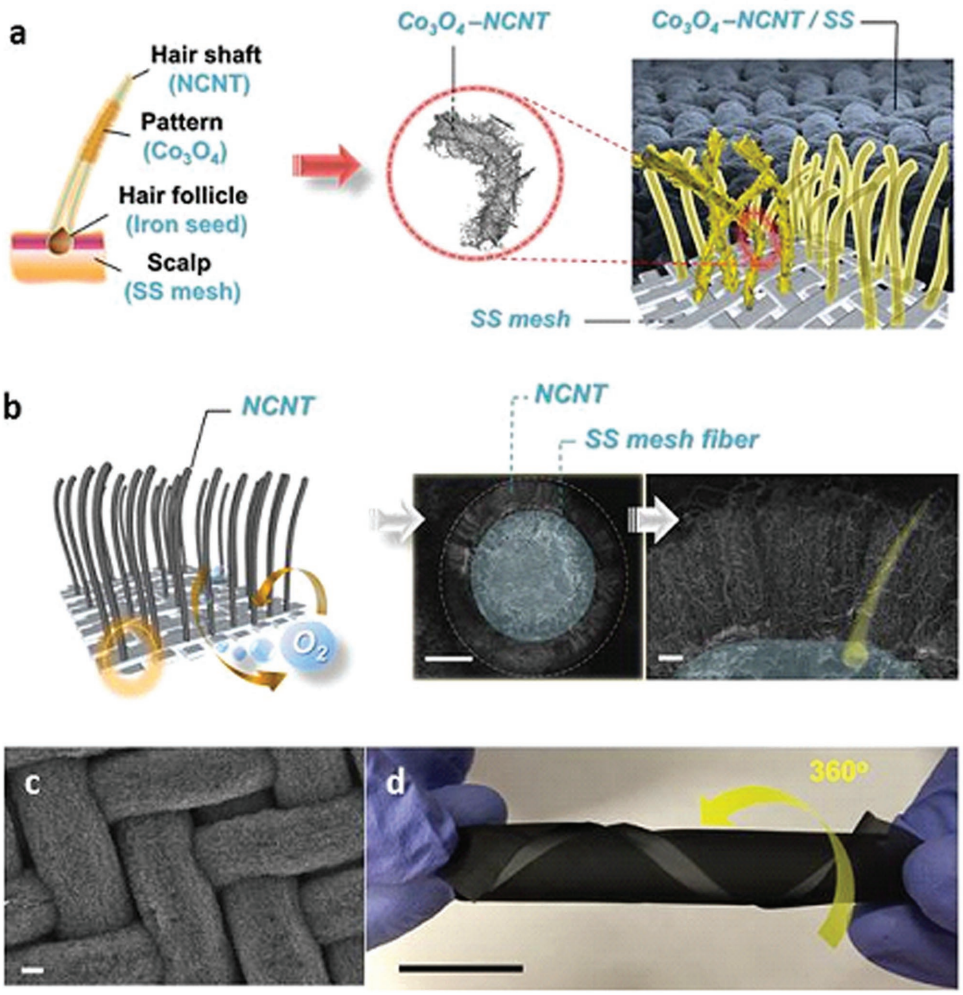

Figure 18. a) A schematic illustration of hair-like array of a Co_3O_4-NCNT/SS air electrode. b) Illustration and cross-sectional SEM images of vertically aligned NCNT framework directly grown on the surface of every individual SS mesh fibers. c) SEM image of the (Co_3O_4-NCNT/SS air electrode. d) Digital photo of the Co_3O_4-NCNT/SS electrode with twisting the electrode to 360°. Scale bars, 10 µm, 1 µm (b), 10 µm (c), 2 cm (d). Reproduced with permission.[141] Copyright 2016, Wiley-VCH.

7.2. Galvanostatic Cycling

Galvanostatic cycling is an accelerated testing technique for investigating the electrochemical durability of zinc–air batteries. The galvanostatic discharge/charge cycling test is performed by alternately applying fixed negative and positive currents while the corresponding discharge and charge voltages are recorded. A typical plot obtained from this test is presented in Figure 19b. The commercial Pt/C catalyst from this investigation displayed a higher discharge voltage than that of a nitrogen-doped carbon-nanofiber catalyst (NCNF-1000) at 10 mA cm^{-2} in the initial few cycles.[222] However, the discharge voltage of Pt/C was severely decreased from approximately 1.3 V to 0.8 V after hundreds of cycles, while the discharge voltage of NCNF-1000 only decreased from approximately 1.2 V to 1.05 V. The large loss of ORR activity for the Pt/C catalyst was likely caused by severe corrosion during the charging process, while the NCNF-1000 catalyst was comparatively more durable.

In comparison to galvanodynamic polarization testing, a galvanostatic cycling test involves the choice of more test conditions, including discharge/charge current density, the number of cycles, and the time length and/or cut-off voltage for each cycle; each of these parameters will affect the test results. Cycling tests for zinc–air batteries can be broadly divided into two different categories, the first of which uses a large number of cycles with short time lengths for each cycle (i.e., pulse cycling test). For example, in Figure S2a in the Supporting Information, the galvanostatic discharge and charge polarization performances were compared at different current densities with a short length of cycle (200 s per cycle). In this method, the cycling durability is most likely to be limited by the air electrode, since the zinc electrode is usually only discharged to a small fraction of its total capacity in each cycle. In contrast, the second category involves a shorter number of cycles with longer time lengths. For example, Figure S2b in the Supporting Information shows the length of a cycle is applied at 20 h with a total of 2 cycles. This testing method is more suitable for evaluating the real recharge capacity retention of the zinc–air battery rather than the pulse cycling method. This is because the time length of each cycle is typically long enough

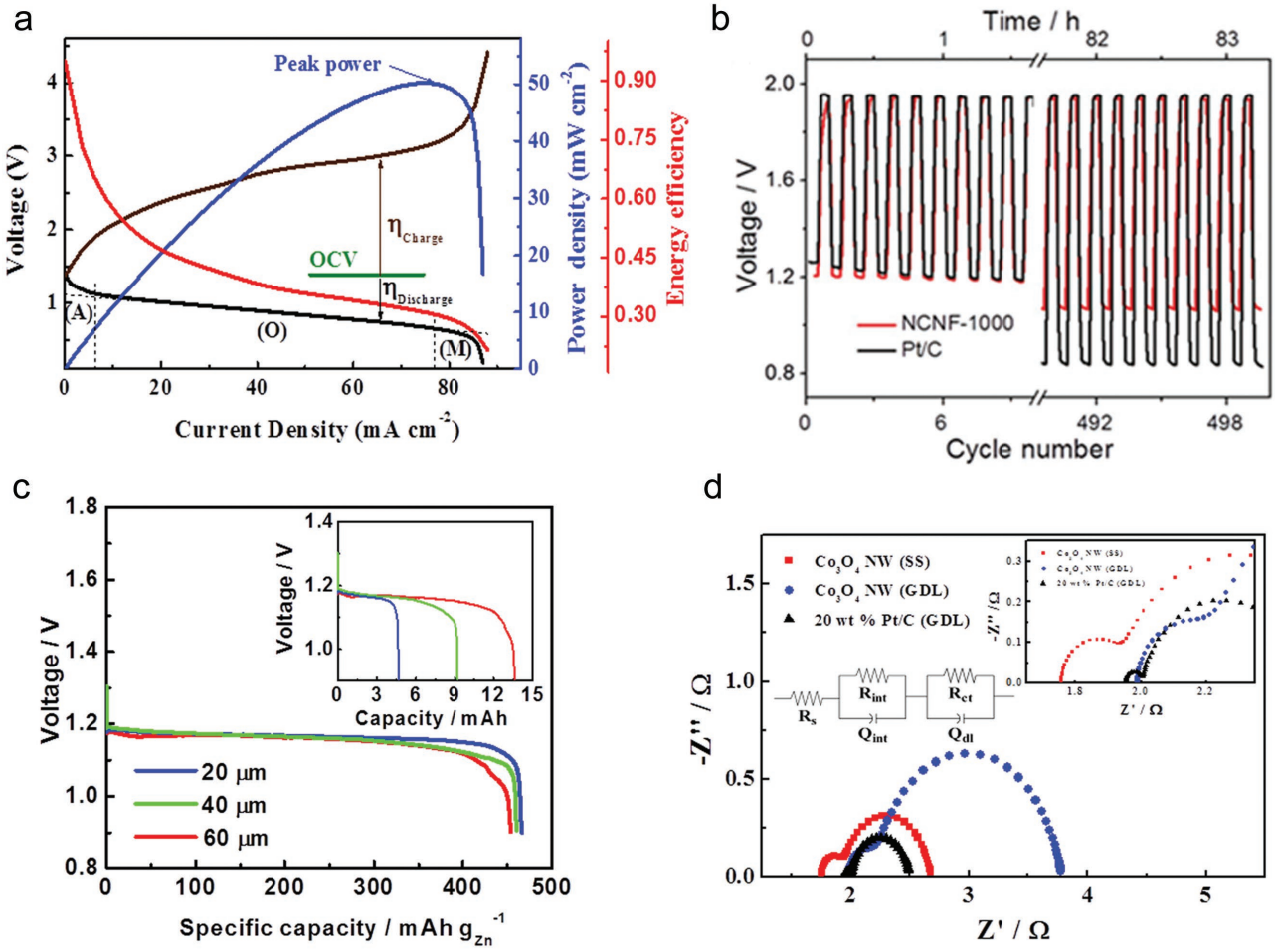

Figure 19. a) Typical discharge and charge polarization curves for the rechargeable zinc–air battery, as well as the power density and energy efficiency. The activation (A), Ohmic (O), and mass transfer (M) polarization regions are identified on the discharge curve by black dashed lines. b) Typical galvanostatic discharge/charge battery cycling test. Nonprecious (NCNF-1000) and precious catalysts (Pt/C) are tested. 10 mA cm^{-1} and 10 min are applied as the current density and length of a cycle, respectively. The battery voltage is recorded versus zinc. Reproduced with permission.[222] b) Copyright 2016, Wiley-VCH. c) Typical specific capacity curves of the battery with different thicknesses of zinc film at a current density of 250 A L^{-1} (50 A kg^{-1}) with an inset view of the corresponding capacities. The gravimetric energy density and specific capacity calculation are based on the mass of zinc electrode. Reproduced with permission.[146] Copyright 2015, Wiley-VCH. d) Nyquist plots obtained by EIS using air under ambient conditions of Co_3O_4 nanowires grown on a stainless-steel mesh (red squares), Co_3O_4 nanowires sprayed on GDL (blue circles), and Pt/C sprayed on GDL (black triangles). Inset: high frequency range of the Nyquist plot, and the equivalent circuit. Reproduced with permission.[140] Copyright 2013, Wiley-VCH.

to utilize a significant portion of the zinc electrode's capacity. Investigations focused on the zinc electrode performance often employ a cut-off voltage instead of a defined time length for each cycle;[62,65,82,88,91] this allows evaluation of the zinc-electrode capacity with respect to cycle number. Another advantage of using longer cycling times is that more realistic voltage values are likely to be obtained, as opposed to cycling times that are too short to allow the voltages to reach a stable value. However, since the two different cycling methods provide uniquely useful information, it is recommended to conduct both types of experiments in investigations of complete zinc–air batteries.

Unfortunately, no standard parameters have been established for the in-lab testing of zinc–air batteries. In Table S2 in the Supporting Information, rechargeable zinc–air-battery performances from three different categories of catalysts evaluated by galvanostatic discharge/charge cycling tests are listed. It can be seen that the respective studies utilize widely different testing parameters (current density, length of a cycle, and cycle number), which makes it difficult to compare the resultant performances. Therefore, it would be beneficial to determine a general standard for testing parameters based on different battery applications, including EVs, smart grids, and personal electronics. However, agreement on these standards is not likely to be reached in the short term. Therefore, zinc–air battery researchers should employ the same or similar testing parameters used by the prior investigations that are mostly closely aligned with their investigations (in terms of materials or applications).

7.3. Galvanostatic Full-Discharge

The galvanostatic full-discharge test determines the capacity of the zinc–air battery by applying a fixed discharge current until

a defined cut-off voltage is reached. Since a zinc–air battery's capacity is dictated by the zinc electrode, the capacity is often normalized by the mass of the zinc electrode or the mass of zinc within the zinc electrode; this enables a relative comparison to the theoretical specific zinc capacity of 820 mA h g^{-1}. In addition, a specific energy density normalized to the consumed mass of zinc (W h g^{-1}) can be obtained by simply multiplying the specific capacity and an average discharge voltage over the applied discharge period. Discharge curves for a flexible zinc–air battery are shown in Figure 19c. In this case, the discharge curves are extremely flat, meaning little Ohmic polarization of the battery. However, the specific capacity of the zinc electrode decreased as a function of thickness, which likely resulted from the non-uniform wetting by the solid-state electrolyte through the entire thickness of the electrode.[33] The working voltage of the battery as a function of discharge depth is also revealed by full-discharge experiments, and the relationship between the two can vary depending on the discharge current employed (for example, refer to Figure S3, Supporting Information). Typically, increasing the current density in a full discharge test results in a slightly lower attained capacity. This may be attributed to the increased rate of $Zn(OH)_4^{2-}$ ion production at the zinc-electrode surface. This results in a more severe $Zn(OH)_4^{2-}$ concentration gradient, causing earlier precipitation of ZnO at the electrode surface, and thus passivation at an earlier stage.

Interestingly, it has also been shown that the capacity extracted from the zinc electrode in a zinc–air battery can be affected by the efficiency of the catalyst in the air electrode (for example, refer to Figure S4, Supporting Information). The proposed explanation of this behavior involves the relative ability of different catalysts to provide and maintain the four-electron-pathway (Reaction (7)) instead of the two-electron-pathway (Reaction (8)) ORR. A poor or degraded catalyst will tend toward the two-electron pathway, and thus produce a greater concentration of peroxide ions in the electrolyte. The peroxide ions may travel alongside fully reduced hydroxide ions toward the zinc electrode during the discharge process and react directly with the zinc electrode, causing it to be self-discharged according to Reaction (9). Self-discharge processes occurring at the zinc electrode reduce the external capacity that it supplies, thus causing it to have a lower specific capacity. Researchers can elucidate this phenomenon by normalizing the measured capacity of the zinc–air battery by the mass of consumed zinc, since it reveals how much of the zinc's capacity was lost to self-discharge.[164,225]

$$Zn + HO_2^- \rightarrow ZnO + OH^- \quad (9)$$

7.4. Electrochemical Impedance Spectroscopy

Electrochemical impedance spectroscopy (EIS) can reveal individual resistances and capacitances within a zinc–air battery, enabling a better understanding of the major limiting factors. Typically, EIS in rechargeable zinc–air batteries is conducted with respect to the discharge and recharge processes at a fixed overpotential. The typical EIS spectra (i.e., Nyquist plots) of the battery using different catalysts, as well as the corresponding equivalent circuit, are shown in Figure 19d. The two semicircles in the Nyquist plot are modeled by the provided equivalent circuit including five elements: R_s, R_{int}, R_{ct}, Q_{int}, and Q_{dl}.[226,227] R_s and R_{int} signify the electrolyte resistance and the electrode–electrolyte interfacial resistance, respectively. R_{ct} represents the charge-transfer resistance of the air electrode during the electrochemical reaction, which is directly related to the electrocatalytic activity of the air electrode. The constant phase elements, Q_{int} and Q_{dl}, are characteristic capacitances from the interface between the electrode and electrolyte. In terms of general analysis of the results, a smaller charge-transfer resistance indicates higher ORR catalytic activities (the same trend is applied to OER activity on charging), leading to a higher discharge voltage.[227] In addition, smaller R_s and R_{int} imply lower internal resistances from the electrolyte and at the interfacial contacts, respectively, in the zinc–air battery. Interfacial resistance values are particularly important to quantify for solid-state electrolytes, due their relatively poor wetting characteristics compared to conventional aqueous electrolytes (refer to Section 5.2).

7.5. Three-Electrode Testing

For many of the tests described above, it can be beneficial to perform them in a three-electrode configuration rather than a two-electrode configuration (i.e., the usual zinc–air cell setup). In a three-electrode configuration, electrical current flows between a working electrode (WE) and counter electrode (CE), while the potential of the WE is measured against a reference electrode (RE). An example of a three-electrode apparatus employing the zinc electrode as the WE is shown schematically in **Figure 20**. This setup allows the potential of the zinc electrode or air electrode (whichever is employed as the WE) to be independently measured. This setup can be particularly useful when a polarization increase is observed during a galvanostatic cycling experiment, as it allows the experimenter to determine whether the air electrode or zinc electrode is the culprit, with complete confidence.

The three-electrode test setup is especially useful for studying the zinc electrode. The overpotential at the zinc electrode is difficult to detect if it is tested against an air electrode in a two-electrode setup, since the overpotential at the air electrode is typically much larger (resulting in the former being obfuscated by the latter). Therefore, it is recommended that investigators researching the zinc electrode in a zinc–air battery utilize a third electrode as a reference electrode. This allows for accurate detection of zinc-electrode overpotentials, which can be used to indicate processes such as nucleation and dendritic growth during charging or passivation during discharging.[63] An EIS experiment using a three-electrode setup can also provide the opportunity to perform equivalent-circuit modeling of the zinc electrode,[229] since the impedances in two-electrode EIS experiments are typically dominated by the air electrode in zinc–air batteries. Investigators may choose to employ a Hg/HgO reference electrode in three-electrode experiments, since this is the most widely used reference electrode in alkaline electrolytes.[56,72,92,116] Alternatively, a spare piece of zinc wire or zinc foil can be employed as the reference electrode to the zinc electrode under investigation.[20,230] While zinc is not a

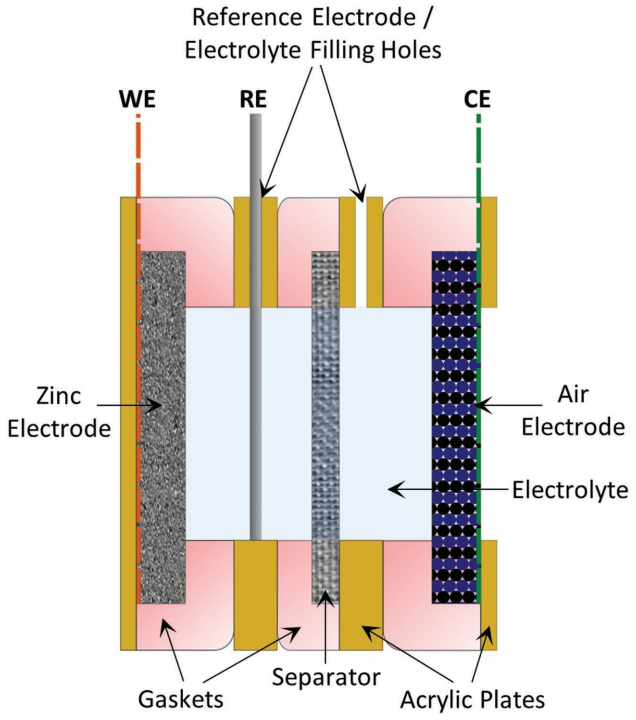

Figure 20. Schematic representation (side-view) of a three-electrode test setup employing the zinc electrode and air electrode as the WE and CE, respectively. The electrolyte chamber is formed by using acrylic plates and gaskets with circular holes, and is filled using the filling channels supplied at the tops of the plates.

conventional reference electrode, its low polarizability and general stability in alkaline electrolytes make it an acceptable substitute for a Hg/HgO reference electrode for this usage case.[231]

8. Conclusion and Outlook

Energy storage in densely populated urban environments, electric mobile applications, and flexible electronics require affordable batteries with low mass and space requirements. Electrically rechargeable zinc–air batteries are promising in this perspective; they can provide high energy density (gravimetrically 400–800 W h kg^{-1} or volumetrically 800–1400 W h L^{-1}) compared to other secondary batteries (e.g., 150–280 W h kg^{-1} or 600–700 W h L^{-1} for lithium-ion batteries) and can be manufactured at a very low cost (estimated from 135 US$ (kW h)$^{-1}$ to as low as 65 US$ (kW h)$^{-1}$).[38,232] Despite the intense research and improvements that were discussed, there is still much scope for further advancement of existing electrically rechargeable zinc–air batteries. Specific needs in materials science and engineering are as follows:

1) A reversible zinc electrode that i) has a high proportion of utilizable active material, ii) is capable of recharging with high efficiency, and iii) sustains its capacity over at least several hundred charge and discharge cycles. Structural modification through electrodeposition and advanced casting techniques, as well compositional modification by means of additives and/or chemical doping have been demonstrated to be feasible solutions for meeting all three of these requirements. The most promising additives are those that are effective in small quantities, since a larger proportion of additives reduces the overall zinc capacity.
2) New electrolyte technologies that allow long-lasting operation of zinc–air batteries. Up to now, aqueous alkaline electrolytes have been the most popular for zinc–air batteries, but issues associated with carbonate formation and electrolyte evaporation need to be addressed for long-term battery operation. In this case, ionic liquids are attractive because they limit aqueous electrolyte evaporation and exhibit resistance to hydrogen evolution and CO_2 poisoning, thereby improving battery efficiency and cycle life. However, their immediate application as high-performance electrolytes in zinc–air batteries faces other challenges, due to several shortcomings, such as high viscosity, low reaction kinetics for zinc and oxygen electrochemistry, and high cost. For flexible devices, "solidification" of the electrolytes is vital to maintain the structural integrity of the batteries under various deformations. Efforts toward improving the electrolyte–electrode interfacial properties must be emphasized when replacing the incumbent liquid electrolytes with versatile solid-state alternatives.
3) Novel, inexpensive bifunctional electrocatalysts that exhibit i) bifunctionality (requiring in-depth understanding of complex oxygen reduction and evolution processes in electrolytes), ii) versatility (requiring their function in a wide range of temperatures, voltages, and in both aqueous and non-aqueous electrolytes), and iii) scalability (ease of incorporation of catalysts into the air-electrode structure, enabling commercialization and widespread adoption). Moreover, to create a comparable link between laboratory results and commercial applications, the catalysts must be studied under practical test conditions. Often, catalysts that show high activities in analytical three-electrode cells do not perform well in commercially relevant devices that demand high current densities and operating temperatures with long lifetimes.
4) Advanced air-electrode design. The air electrode design currently adopted in many zinc–air batteries in the research phase is similar to that used in ordinary alkaline fuel cells, where the catalysts are supported mainly by carbon-based gas-diffusion electrodes. However, carbon materials can be readily corroded (oxidized) under the harsh conditions imposed by repetitive discharging and charging in alkaline electrolytes. In addition, the air-electrode preparation is often tedious and has an inherent disadvantage owing to the use of ancillary materials. New strategies to use either highly corrosion-resistant carbon materials or metallic meshes/foams, onto which the catalysts are directly grown, are suggested by researchers. Such approaches are free of the conventional complex preparation processes, which would be of great benefits to large-scale fabrication.
5) Optimal cell and stack design. Although simple designs are preferred, zinc–air batteries often require supplementary components; namely, the air electrode needs "organs" that facilitate the supply and purification of atmospheric air (e.g., CO_2 and particulate matter). The efficient stacking

of electrically rechargeable zinc–air cells in series is key to obtain high energy and power density by means of lowering weight, volume, and stack impedance. This performance success requires a smart design of electrically conductive air channels (e.g., bipolar plates), which connects the air electrode to the adjacent zinc electrode in the battery pack. The air channels should facilitate oxygen-gas flow through the stack during discharge and allow evaluated oxygen to easily escape during recharging.

Commercial developers have successfully introduced electrically rechargeable zinc–air flow batteries over the past few years, with their main advantage being their low cost and low environmental impact. Recently, confidence in grid-scale rechargeable zinc–air batteries was demonstrated when a Californian investor-owned electric utility announced the procurement of 13 MW of zinc–air-battery storage.[233] Zinc–air batteries are also excellent candidates to replace lead–acid batteries, which present hazards to the environment and human health,[234] in the residential storage market. With significant progress in the research areas discussed in this review, electrically rechargeable zinc–air batteries that are smaller, lighter, and ultimately more energy-dense with static electrolytes can also be realized. Success in these areas can render zinc–air batteries suitable for many more energy-storage applications, the most pressing of which is EVs. Thus far, the relatively high cost and limited energy density of lithium-ion batteries has caused the adoption of EVs to be largely reliant on government subsidies.[235] This problem can be alleviated with the implementation of zinc–air batteries, not only due to their lower cost and higher energy density, but also because of their inherent safety, allowing them to be employed with less protective equipment. Additionally, a high power performance with a rapid discharge capability of batteries is needed for bursts of energy, such as in vehicular acceleration. In this regard, dual energy-storage systems, which combine a high-power source for acceleration and regenerative braking with a high-energy-density source for baseload power, have also been proposed for EVs by Tesla and Mazda, among others.[236] The flat discharge curves exhibited by zinc–air batteries make them well-suited as the energy-dense component of these systems, since they can provide stable power outputs at almost any state of charge. A researcher has also demonstrated a novel hybrid air electrode, conducting both nickel–zinc and zinc–air reactions, on the rechargeable zinc–air battery, providing remarkably high power density and fast discharge capability for EV propulsion.[76] Meanwhile, the development of electronic devices with miniature sizes and adaptable shapes is currently limited by the rigidity and thick casing of current battery technology. Electrically rechargeable zinc–air batteries employing flexible solid-state electrolytes are increasingly being recognized as a viable solution for these applications. While their high specific and volumetric energy densities are a crucial reason for this, their safe operation also lowers the need for a thick casing, thereby further reducing their weight and space requirements.

While lithium–air batteries have thus far received the most attention in the academic literature on metal–air chemistries, zinc–air batteries have emerged as the most likely candidate to become a leading energy-storage solution. Existing manufacturing infrastructure for zinc electrodes in alkaline zinc-based batteries and the air-electrode design in primary metal–air batteries can be leveraged to quickly scale up the production and commercialization of electrically rechargeable zinc–air batteries. Overall, the promising combination of high energy density, safety, and low cost should allow electrically rechargeable zinc–air batteries to support the energy needs of an increasingly affluent, digital, and low-carbon global economy. Hence, accelerated research and development of this technology in the academic and industrial sectors is highly encouraged.

Supporting Information

Supporting Information is available from the Wiley Online Library or from the author.

Acknowledgements

J.F. and Z.P.C. contributed equally to this work. The authors wish to acknowledge the support provided by the Natural Sciences and Engineering Research Council of Canada (NSERC) and by the University of Waterloo and the Waterloo Institute for Nanotechnology. The authors also thank Dong Un Lee at the University of Waterloo for his valuable comments.
Note: The formatting of the header row of Table 2 was corrected on February 13, 2017.

Received: August 31, 2016
Revised: September 26, 2016
Published online: November 28, 2016

[1] a) C. Breyer, A. Gerlach, *Prog. Photovoltaics: Res. Appl.* **2013**, *21*, 121; b) L. A. H. Munoz, J. C. C. M. Huijben, B. Verhees, G. P. J. Verbong, *Technol. Forecasting Soc. Change* **2014**, *87*, 179.
[2] a) E. Shafiei, H. Thorkelsson, E. I. Ásgeirsson, B. Davidsdottir, M. Raberto, H. Stefansson, *Technol. Forecasting Soc. Change* **2012**, *79*, 1638; b) B. Propfe, D. Kreyenberg, J. Wind, S. Schmid, *Int. J. Hydrogen Energy* **2013**, *38*, 5201; c) O. Egbue, S. Long, *Energy Policy* **2012**, *48*, 717.
[3] M. A. Rahman, X. Wang, C. Wen, *J. Electrochem. Soc.* **2013**, *160*, A1759.
[4] a) S. R. Narayanan, G. K. S. Prakash, A. Manohar, B. Yang, S. Malkhandi, A. Kindler, *Solid State Ionics* **2012**, *216*, 105; b) X. Ren, Y. Wu, *J. Am. Chem. Soc.* **2013**, *135*, 2923; c) P. Hartmann, C. L. Bender, M. Vračar, A. K. Dürr, A. Garsuch, J. Janek, P. Adelhelm, *Nat. Mater.* **2013**, *12*, 228.
[5] J. S. Lee, S. Tai Kim, R. Cao, N.-S. Choi, M. Liu, K. T. Lee, J. Cho, *Adv. Energy Mater.* **2011**, *1*, 2.
[6] J. Muldoon, C. B. Bucur, T. Gregory, *Chem. Rev.* **2014**, *114*, 11683.
[7] T. Reddy, *Linden's Handbook of Batteries*, 4th Ed., McGraw-Hill Education, New York, NY, USA **2010**.
[8] a) A. J. Appleby, J. Jacquelin, J. P. Pompon, *SAE Tech. Pap.* **1977**, 770381; b) M. C. Cheiky, L. G. Danczyk, M. C. Wehrey, *SAE Tech. Pap.* **1990**, 901516; c) M. C. Cheiky, L. G. Danczyk, R. L. Scheffler, *SAE Tech. Pap.* **1991**, 910249.
[9] a) P. N. J. Ross, in *Proc. of the 21st Intersociety Energy Conversion Engineering Conf.*, Vol. 2, American Chemical Society, Washington, DC, USA **1986**, pp. 1066–1072; b) P. N. J. Ross (*The United States Of America As Represented By The United States Department Of Energy*), *US4842963 A*, **1989**.

[10] a) L. G. Danczyk, R. L. Scheffler, R. S. Hobbs, *SAE Tech. Pap.* **1991**, 911633; b) G. W. Merry, *SAE Tech. Pap.* **1991**, 911912; c) M. C. Cheiky, L. G. Danczyk, M. C. Wehrey, *SAE Tech. Pap.* **1992**, 920448; d) J. R. Goldstein, B. Koretz, *IEEE Aerosp. Electron. Syst. Mag.* **1993**, *8*, 34; e) J. F. Cooper, D. Fleming, D. Hargrove, R. Koopman, K. Peterman, *SAE Tech. Pap.* **1995**, 951948; f) D. Sieminski, in *Twelfth Annual Battery Conference on Applications and Advances, 1997.*, Ready Reproductions, Inc., Los Angeles, CA, USA **1997**, pp. 171–180; g) F. G. Will, in *The Thirteenth Annual Battery Conference on Applications and Advances, 1998*, Ready Reproductions, Inc., Los Angeles, CA, USA **1998**, pp. 1–6; h) J. Goldstein, I. Brown, B. Koretz, *J. Power Sources* **1999**, *80*, 171.

[11] a) M. C. Cheiky, L. G. Danczyk, M. C. Wehrey, *SAE Tech. Pap.* **1992**, 920448; b) P. N. Ross, in *Proc. Tenth Annual Battery Conference on Applications and Advances, 1995*, Long Beach, CA, USA **1995**, pp. 131–133.

[12] K. Tweed, Eos Energy Storage Closes $23M Funding Round for Cheap Grid Batteries, http://www.greentechmedia.com/articles/read/eos-energy-storage-closes-23m-funding-round (accessed: July 2016).

[13] E. Wesoff, Fluidic Energy Is the Biggest Zinc–air Battery Startup You Haven't Heard Of, http://www.greentechmedia.com/articles/read/Fluidic-Energy-is-the-Biggest-Zinc-air-Battery-Startup-You-Havent-Heard-Of (accessed: August 2016).

[14] N. R. C. Government of Canada, Archived – Government of Canada and SDTC Announce New Clean Technology Funding in British Columbia, http://news.gc.ca/web/article-en.do?nid=950589 (accessed: August 2016).

[15] B. Nykvist, M. Nilsson, *Nat. Clim. Change* **2015**, *5*, 329.

[16] P. A. Khan, B. Venkatesh, in *Smart City 360°*, (Eds: A. Leon-Garcia, R. Lenort, D. Holman, D. Staš, V. Krutilova, P. Wicher, D. Cagáňová, D. Špirková, J. Golej, K. Nguyen), Springer International Publishing, Cham, Switzerland **2016**, pp. 277–291.

[17] Y. Li, H. Dai, *Chem. Soc. Rev.* **2014**, *43*, 5257.

[18] a) V. Caramia, B. Bozzini, *Mater. Renew. Sustain. Energy* **2014**, *3*, 1; b) P. Pei, K. Wang, Z. Ma, *Appl. Energy* **2014**, *128*, 315.

[19] W. A. Garcia, H. F. Wilkins (ZAF Energy Systems, Inc.), US8871394 B1, **2014**.

[20] E. Deiss, F. Holzer, O. Haas, *Electrochim. Acta* **2002**, *47*, 3995.

[21] H. Ma, B. Wang, Y. Fan, W. Hong, *Energies* **2014**, *7*, 6549.

[22] W. Hong, H. Li, B. Wang, *Int. J. Electrochem. Sci.* **2016**, *11*, 3843.

[23] P.-C. Li, Y.-J. Chien, C.-C. Hu, *J. Power Sources* **2016**, *313*, 37.

[24] M. G. Park, D. U. Lee, M. H. Seo, Z. P. Cano, Z. Chen, *Small* **2016**, *12*, 2707.

[25] M. Skyllas-Kazacos, M. Chakrabarti, S. Hajimolana, F. Mjalli, M. Saleem, *J. Electrochem. Soc.* **2011**, *158*, R55.

[26] a) E. Farmer, A. Webb, *J. Appl. Electrochem.* **1972**, *2*, 123; b) C. D. Iacovangelo, F. G. Will, *J. Electrochem. Soc.* **1985**, *132*, 851; c) J. Cheng, L. Zhang, Y.-S. Yang, Y.-H. Wen, G.-P. Cao, X.-D. Wang, *Electrochem. Commun.* **2007**, *9*, 2639.

[27] a) P. Gouérec, L. Poletto, J. Denizot, E. Sanchez-Cortezon, J. Miners, *J. Power Sources* **2004**, *129*, 193; b) F. Bidault, D. Brett, P. Middleton, N. Brandon, *J. Power Sources* **2009**, *187*, 39.

[28] C. A. Friesen, R. Krishnan, G. Friesen (Fluidic, Inc.), *US8492052 B2*, **2013**.

[29] S. Amendola, M. Binder, P. J. Black, S. Sharp-Goldman, L. Johnson, M. Kunz, M. Oster, T. Chciuk, R. Johnson (Eos Energy Storage, Llc), *US20130115531 A1*, **2013**.

[30] D. Wolfe, C. A. Friesen, P. B. Johnson (Fluidic, Inc.), *US8741491 B2*, **2014**.

[31] a) M. Pinto, S. Smedley, J. A. Colborn (Metallic Power, Inc.), *US6296958 B1*, **2001**; b) M. Pinto, S. Smedley, G. Wu, *US20040251126 A1*, **2004**.

[32] a) A. M. Gaikwad, G. L. Whiting, D. A. Steingart, A. C. Arias, *Adv. Mater.* **2011**, *23*, 3251; b) X. Wang, X. Lu, B. Liu, D. Chen, Y. Tong, G. Shen, *Adv. Mater.* **2014**, *26*, 4763.

[33] J. Fu, D. U. Lee, F. M. Hassan, L. Yang, Z. Bai, M. G. Park, Z. Chen, *Adv. Mater.* **2015**, *27*, 5617.

[34] J. Fu, J. Zhang, X. Song, H. Zarrin, X. Tian, J. Qiao, L. Rasen, K. Li, Z. Chen, *Energy Environ. Sci.* **2016**, *9*, 663.

[35] Q. Liu, Y. Wang, L. Dai, J. Yao, *Adv. Mater.* **2016**, *28*, 3000.

[36] J. Park, M. Park, G. Nam, J. s. Lee, J. Cho, *Adv. Mater.* **2015**, *27*, 1396.

[37] S. Li, Z. P. Guo, C. Y. Wang, G. G. Wallace, H. K. Liu, *J. Mater. Chem. A* **2013**, *1*, 14300.

[38] O. Haas, F. Holzer, K. Müller, S. Müller, *Handbook of Fuel Cells*, John Wiley & Sons, Hoboken, NJ, USA, **2010**.

[39] K. Kordesch, V. Hacker, in *Handbook of Fuel Cells*, Vol. *4*, Part 4 (Eds: W. Vielstich, H. A. Gasteiger, A. Lamm), John Wiley & Sons, Hoboken, NJ, USA, **2003**, Ch. 56. pp. 765–773.

[40] J. Diggle, A. Despic, J. M. Bockris, *J. Electrochem. Soc.* **1969**, *116*, 1503.

[41] A. Despić, M. Purenović, *J. Electrochem. Soc.* **1974**, *121*, 329.

[42] M. Simičić, K. Popov, N. Krstajić, *J. Electroanal. Chem.* **2000**, *484*, 18.

[43] R. Wang, D. Kirk, G. Zhang, *J. Electrochem. Soc.* **2006**, *153*, C357.

[44] J. W. Diggle, A. R. Despic, J. O. M. Bockris, *J. Electrochem. Soc.* **1969**, *116*, 1503.

[45] R. Moshtev, P. Zlatilova, *J. Appl. Electrochem.* **1978**, *8*, 213.

[46] K. Popov, N. Krstajić, *J. Appl. Electrochem.* **1983**, *13*, 775.

[47] J. McBreen, *J. Electrochem. Soc.* **1972**, *119*, 1620.

[48] F. R. McLarnon, E. J. Cairns, *J. Electrochem. Soc.* **1991**, *138*, 645.

[49] Y. Shen, K. Kordesch, *J. Power Sources* **2000**, *87*, 162.

[50] a) K. W. Choi, D. N. Bennion, J. Newman, *J. Electrochem. Soc.* **1976**, *123*, 1616; b) K. W. Choi, D. Hamby, D. N. Bennion, J. Newman, *J. Electrochem. Soc.* **1976**, *123*, 1628; c) R. Einerhand, W. Visscher, J. De Goeij, E. Barendrecht, *J. Electrochem. Soc.* **1991**, *138*, 1; d) R. Einerhand, W. Visscher, J. De Goeij, E. Barendrecht, *J. Electrochem. Soc.* **1991**, *138*, 7.

[51] W. Sunu, D. Bennion, *J. Electrochem. Soc.* **1980**, *127*, 2007.

[52] T. Dirkse, N. Hampson, *Electrochim. Acta* **1972**, *17*, 383.

[53] a) X. G. Zhang, *Encyclopedia of Electrochemical Power Sources*, Elsevier, Amsterdam, The Netherlands **2009**; b) R. Gilliam, J. Graydon, D. Kirk, S. Thorpe, *Int. J. Hydrogen Energy* **2007**, *32*, 359.

[54] C. Y. Jung, T. H. Kim, W. J. Kim, S. C. Yi, *Energy* **2016**, *102*, 694.

[55] T. Chang, Y. Wang, C. Wan, *J. Power Sources* **1983**, *10*, 167.

[56] T. Adler, F. McLarnon, E. Cairns, *J. Electrochem. Soc.* **1993**, *140*, 289.

[57] X. G. Zhang, *J. Power Sources* **2006**, *163*, 591.

[58] E. G. Gagnon, Y. M. Wang, *J. Electrochem. Soc.* **1987**, *134*, 2091.

[59] T. Lee, *J. Electrochem. Soc.* **1971**, *118*, 1278.

[60] C. W. Lee, S. W. Eom, K. Sathiyanarayanan, M. S. Yun, *Electrochim. Acta* **2006**, *52*, 1588.

[61] J. F. Parker, C. N. Chervin, E. S. Nelson, D. R. Rolison, J. W. Long, *Energy Environ. Sci.* **2014**, *7*, 1117.

[62] Z. Yan, E. Wang, L. Jiang, G. Sun, *RSC Adv.* **2015**, *5*, 83781.

[63] S. Müller, F. Holzer, O. Haas, *J. Appl. Electrochem.* **1998**, *28*, 895.

[64] a) B. Bouwhuis, J. McCrea, G. Palumbo, G. Hibbard, *Acta Mater.* **2009**, *57*, 4046; b) A. Jung, M. R. Koblischka, E. Lach, S. Diebels, H. Natter, *Int. J. Mater. Sci.* **2012**.

[65] M. Chamoun, B. J. Hertzberg, T. Gupta, D. Davies, S. Bhadra, B. Van Tassell, C. Erdonmez, D. A. Steingart, *NPG Asia Mater.* **2015**, *7*, e178.

[66] P. Bonnick, J. Dahn, *J. Electrochem. Soc.* **2012**, *159*, A981.

[67] R. Othman, A. Yahaya, A. K. Arof, *J. Appl. Electrochem.* **2002**, *32*, 1347.

[68] M. Masri, A. Mohamad, *Corros. Sci.* **2009**, *51*, 3025.
[69] M. N. Masri, A. A. Mohamad, *J. Electrochem. Soc.* **2013**, *160*, A715.
[70] H. Li, C. Xu, C. Han, Y. Chen, C. Wei, B. Li, F. Kang, *J. Electrochem. Soc.* **2015**, *162*, A1439.
[71] K. Bass, P. Mitchell, G. Wilcox, J. Smith, *J. Power Sources* **1991**, *35*, 333.
[72] C. Biegler, R. Deutscher, S. Fletcher, S. Hua, R. Woods, *J. Electrochem. Soc.* **1983**, *130*, 2303.
[73] a) A. Mohamad, N. Mohamed, M. Yahya, R. Othman, S. Ramesh, Y. Alias, A. Arof, *Solid State Ionics* **2003**, *156*, 171; b) M. Hilder, B. Winther-Jensen, N. Clark, *J. Power Sources* **2009**, *194*, 1135; c) M. Hilder, B. Winther-Jensen, N. B. Clark, *Electrochim. Acta* **2012**, *69*, 308; d) D. Ozgit, P. Hiralal, G. A. Amaratunga, *ACS Appl. Mater. Interfaces* **2014**, *6*, 20752; e) J. Cheng, Z. F. Zhang, Y. Q. Zhao, W. L. Yu, H. Y. Hou, *Trans. Nonferrous Met. Soc. China* **2014**, *24*, 3551.
[74] Y. Yuan, Y. Li, S. Tao, F. Ye, J. Yang, S. Guo, J. Tu, *Electrochim. Acta* **2009**, *54*, 6617.
[75] R. Wang, Z. Yang, B. Yang, X. Fan, T. Wang, *J. Power Sources* **2014**, *246*, 313.
[76] D. U. Lee, J. Fu, M. G. Park, H. Liu, A. Ghorbani Kashkooli, Z. Chen, *Nano Lett.* **2016**, *16*, 1794.
[77] A. Himy, O. C. Wagner (The United States Of America As Represented By The Secretary Of The Navy), *US4327157 A*, **1982**.
[78] Y. Sato, M. Kanda, H. Niki, M. Ueno, K. Murata, T. Shirogami, T. Takamura, *J. Power Sources* **1983**, *9*, 147.
[79] J. McBreen, E. Gannon, *J. Electrochem. Soc.* **1983**, *130*, 1980.
[80] J. McBreen, E. Gannon, *J. Power Sources* **1985**, *15*, 169.
[81] C. Zhang, J. Wang, L. Zhang, J. Zhang, C. Cao, *J. Appl. Electrochem.* **2001**, *31*, 1049.
[82] Y. Yuan, L. Yu, H. Wu, J. Yang, Y. Chen, S. Guo, J. Tu, *Electrochim. Acta* **2011**, *56*, 4378.
[83] F. Moser, F. Fourgeot, R. Rouget, O. Crosnier, T. Brousse, *Electrochim. Acta* **2013**, *109*, 110.
[84] Z. Zhang, Z. Yang, J. Huang, Z. Feng, X. Xie, *Electrochim. Acta* **2015**, *155*, 61.
[85] A. Himy, O. C. Wagner (The United States Of America As Represented By The Secretary Of The Navy), *US4084047 A*, **1978**.
[86] J. McBreen, E. Gannon, *Electrochim. Acta* **1981**, *26*, 1439.
[87] S. Wang, Z. Yang, L. Zeng, *J. Electrochem. Soc.* **2009**, *156*, A18.
[88] D. Zeng, Z. Yang, S. Wang, X. Ni, D. Ai, Q. Zhang, *Electrochim. Acta* **2011**, *56*, 4075.
[89] X. Fan, Z. Yang, W. Long, Z. Zhao, B. Yang, *Electrochim. Acta* **2013**, *92*, 365.
[90] R. Wang, Z. Yang, *RSC Adv.* **2013**, *3*, 19924.
[91] R. Wang, Z. Yang, B. Yang, T. Wang, Z. Chu, *J. Power Sources* **2014**, *251*, 344.
[92] J. T. Nichols, F. R. McLarnon, E. J. Cairns, *Chem. Eng. Commun.* **1985**, *37*, 355.
[93] a) E. Gagnon, *J. Electrochem. Soc.* **1986**, *133*, 1989; b) E. Gagnon, *J. Electrochem. Soc.* **1991**, *138*, 3173.
[94] R. Jain, T. Adler, F. McLarnon, E. Cairns, *J. Appl. Electrochem.* **1992**, *22*, 1039.
[95] R. Shivkumar, G. P. Kalaignan, T. Vasudevan, *J. Power Sources* **1995**, *55*, 53.
[96] R. Shivkumar, G. P. Kalaignan, T. Vasudevan, *J. Power Sources* **1998**, *75*, 90.
[97] J.-S. Chen, L.-F. Wang, *J. Appl. Electrochem.* **1996**, *26*, 227.
[98] J. Yu, H. Yang, X. Ai, X. Zhu, *J. Power Sources* **2001**, *103*, 93.
[99] R. Renuka, L. Srinivasan, S. Ramamurthy, A. Veluchamy, N. Venkatakrishnan, *J. Appl. Electrochem.* **2001**, *31*, 655.
[100] S.-H. Lee, C.-W. Yi, K. Kim, *J. Chem. C* **2010**, *115*, 2572.
[101] Z. Luo, S. Sang, Q. Wu, S. Liu, *ECS Electrochem. Lett.* **2013**, *2*, A21.
[102] Y. Yuan, J. Tu, H. Wu, C. Zhang, S. Wang, X. Zhao, *J. Power Sources* **2007**, *165*, 905.
[103] a) Z. Feng, Z. Yang, J. Huang, X. Xie, Z. Zhang, *J. Electrochem. Soc.* **2014**, *161*, A1981; b) T. Wang, Z. Yang, B. Yang, R. Wang, J. Huang, *J. Power Sources* **2014**, *257*, 174; c) Z. Zhang, Z. Yang, R. Wang, Z. Feng, X. Xie, Q. Liao, *Electrochim. Acta* **2014**, *134*, 287.
[104] J. McBreen, M. Chu, G. Adzic, *J. Electrochem. Soc.* **1981**, *128*, 2287.
[105] a) M. Yano, S. Fujitani, K. Nishio, Y. Akai, M. Kurimura, *J. Power Sources* **1998**, *74*, 129; b) Y. Sato, M. Takahashi, H. Asakura, T. Yoshida, K. Tada, K. Kobayakawa, N. Chiba, K. Yoshida, *J. Power Sources* **1992**, *38*, 317.
[106] a) Y.-M. Wang, *J. Electrochem. Soc.* **1990**, *137*, 2800; b) D. Coates, E. Ferreira, A. Charkey, *J. Power Sources* **1997**, *65*, 109; c) X. Zhu, H. Yang, X. Ai, J. Yu, Y. Cao, *J. Appl. Electrochem.* **2003**, *33*, 607; d) Y. Yuan, J. Tu, H. Wu, Y. Li, D. Shi, X. Zhao, *J. Power Sources* **2006**, *159*, 357; e) C.-C. Yang, W.-C. Chien, P.-W. Chen, C.-Y. Wu, *J. Appl. Electrochem.* **2009**, *39*, 39; f) S. Wang, Z. Yang, L. Zeng, *Mater. Chem. Phys.* **2008**, *112*, 603.
[107] H. Yang, H. Zhang, X. Wang, J. Wang, X. Meng, Z. Zhou, *J. Electrochem. Soc.* **2004**, *151*, A2126.
[108] Y. M. Wang, G. Wainwright, *J. Electrochem. Soc.* **1986**, *133*, 1869.
[109] R. A. Sharma, *J. Electrochem. Soc.* **1986**, *133*, 2215.
[110] J. Huang, Z. Yang, R. Wang, Z. Zhang, Z. Feng, X. Xie, *J. Mater. Chem. A* **2015**, *3*, 7429.
[111] X. Fan, Z. Yang, R. Wen, B. Yang, W. Long, *J. Power Sources* **2013**, *224*, 80.
[112] V. R. Constantino, T. J. Pinnavaia, *Inorg. Chem.* **1995**, *34*, 883.
[113] R. F. Thornton, E. J. Carlson, *J. Electrochem. Soc.* **1980**, *127*, 1448.
[114] T. Dirkse, *J. Electrochem. Soc.* **1981**, *128*, 1412.
[115] J. F. Parker, I. R. Pala, C. N. Chervin, J. W. Long, D. R. Rolison, *J. Electrochem. Soc.* **2016**, *163*, A351.
[116] T. Adler, F. McLarnon, E. Cairns, *Ind. Eng. Chem. Res.* **1998**, *37*, 3237.
[117] J. Zhu, Y. Zhou, C. Gao, *J. Power Sources* **1998**, *72*, 231.
[118] C. W. Lee, K. Sathiyanarayanan, S. W. Eom, H. S. Kim, M. S. Yun, *J. Power Sources* **2006**, *159*, 1474.
[119] C. Lan, C. Lee, T. Chin, *Electrochim. Acta* **2007**, *52*, 5407.
[120] J. Zhu, Y. Zhou, *J. Power Sources* **1998**, *73*, 266.
[121] J. Vatsalarani, D. Trivedi, K. Ragavendran, P. Warrier, *J. Electrochem. Soc.* **2005**, *152*, A1974.
[122] H. Lee, M. Yanilmaz, O. Toprakci, K. Fu, X. Zhang, *Energy Environ. Sci.* **2014**, *7*, 3857.
[123] P. Arora, Z. Zhang, *Chem. Rev.* **2004**, *104*, 4419.
[124] H. J. Hwang, W. S. Chi, O. Kwon, J. G. Lee, J. H. Kim, Y. G. Shul, *ACS Appl. Mater. Interfaces* **2016**, *8*, 26298.
[125] D. U. Lee, H. W. Park, M. G. Park, V. Ismayilov, Z. Chen, *ACS Appl. Mater. Interfaces* **2015**, *7*, 902.
[126] H. W. Park, D. U. Lee, P. Zamani, M. H. Seo, L. F. Nazar, Z. Chen, *Nano Energy* **2014**, *10*, 192.
[127] E. L. Dewi, K. Oyaizu, H. Nishide, E. Tsuchida, *J. Power Sources* **2003**, *115*, 149.
[128] a) J. Qiao, J. Fu, L. Liu, J. Zhang, J. Xie, G. Li, *Solid State Ionics* **2012**, *214*, 6; b) J. Qiao, J. Fu, R. Lin, J. Liu, J. Ma, *ECS Trans.* **2010**, *33*, 1915; c) J. Qiao, J. Fu, L. Liu, Y. Liu, J. Sheng, *Int. J. Hydrogen Energy* **2012**, *37*, 4580; d) F. Jing, Z. Haiyan, Q. Jinli, M. Jianxin, *Acta Polym. Sin.* **2011**, 701; e) J. Qiao, J. Fu, R. Lin, J. Ma, J. Liu, *Polymer* **2010**, *51*, 4850; f) J. Fu, J. Qiao, H. Lv, J. Ma, X.-Z. Yuan, H. Wang, *ECS Trans.* **2010**, *25*, 15; g) J. Fu, J. Qiao, X. Wang, J. Ma, T. Okada, *Synth. Met.* **2010**, *160*, 193.
[129] Y. Kiros, *J. Power Sources* **1996**, *62*, 117.
[130] G. M. Wu, S. J. Lin, J. H. You, C. C. Yang, *Mater. Chem. Phys.* **2008**, *112*, 798.
[131] J.-S. Lee, S. Tai Kim, R. Cao, N.-S. Choi, M. Liu, K. T. Lee, J. Cho, *Adv. Energy Mater.* **2011**, *1*, 34.

[132] C. Chakkaravarthy, A. K. A. Waheed, H. V. K. Udupa, *J. Power Sources* **1981**, *6*, 203.
[133] D. M. See, R. E. White, *J. Chem. Eng. Data* **1997**, *42*, 1266.
[134] X. G. Zhang, *Encyclopedia of Electrochemical Power Sources*, Elsevier Science, Amsterdam, The Netherlands **2009**.
[135] J. F. Drillet, F. Holzer, T. Kallis, S. Muller, V. M. Schmidt, *Phys. Chem. Chem. Phys.* **2001**, *3*, 368.
[136] a) J. Goldstein, Y. Harats, Y. Sharon, N. Naimer (Electric Fuel (E.F.L.) Ltd.), *US5595949 A*, **1997**; b) H. H. Cheng, C. S. Tan, *J. Power Sources* **2006**, *162*, 1431.
[137] Z. Ma, P. Pei, K. Wang, X. Wang, H. Xu, Y. Liu, G. peng, *J. Power Sources* **2015**, *274*, 56.
[138] E. Malone, K. Rasa, D. Cohen, T. Isaacson, H. Lashley, H. Lipson, *Rapid Prototyping J.* **2004**, *10*, 58.
[139] Y. J. Wang, J. Qiao, R. Baker, J. Zhang, *Chem. Soc. Rev.* **2013**, *42*, 5768.
[140] D. U. Lee, J. Y. Choi, K. Feng, H. W. Park, Z. Chen, *Adv. Energy Mater.* **2014**, *4*, 1301389.
[141] J. Fu, F. M. Hassan, J. Li, D. U. Lee, A. R. Ghannoum, G. Lui, M. A. Hoque, Z. Chen, *Adv. Mater.* **2016**, *28*, 6421.
[142] a) C. C. Yang, S. J. Lin, *J. Power Sources* **2002**, *112*, 497; b) M. Hilder, B. W. Jensen, N. B. Clark, *J. Power Sources* **2009**, *194*, 1135; c) A. A. Mohamad, *J. Power Sources* **2006**, *159*, 752.
[143] G. M. Wu, S. J. Lin, C. C. Yang, *J. Membr. Sci.* **2006**, *280*, 802.
[144] Y. Wang, W. H. Zhong, *ChemElectroChem* **2015**, *2*, 22.
[145] J. Fu, J. Zhang, X. Song, H. Zarrin, X. Tian, J. Qiao, L. Rasen, K. Li, Z. Chen, *Energy Environ. Sci.* **2016**, *9*, 663.
[146] J. Fu, D. U. Lee, F. M. Hassan, L. Yang, Z. Bai, M. G. Park, Z. Chen, *Adv. Mater.* **2015**, *27*, 5617.
[147] Y. Xu, Y. Zhang, Z. Guo, J. Ren, Y. Wang, H. Peng, *Angew. Chem., Int. Ed.* **2015**, *54*, 15390.
[148] J. Zhang, J. Fu, X. Song, G. Jiang, H. Zarrin, P. Xu, K. Li, A. Yu, Z. Chen, *Adv. Energy Mater.* **2016**, *6*, 1600476.
[149] M. Armand, F. Endres, D. R. MacFarlane, H. Ohno, B. Scrosati, *Nat. Mater.* **2009**, *8*, 621.
[150] a) G. Girishkumar, B. McCloskey, A. C. Luntz, S. Swanson, W. Wilcke, *J. Phys. Chem. Lett.* **2010**, *1*, 2193; b) M. Balaish, A. Kraytsberg, Y. Ein-Eli, *Phys. Chem. Chem. Phys.* **2014**, *16*, 2801.
[151] M. Kar, T. J. Simons, M. Forsyth, D. R. MacFarlane, *Phys. Chem. Chem. Phys.* **2014**, *16*, 18658.
[152] a) M. J. Deng, P. Y. Chen, T. I. Leong, I. W. Sun, J. K. Chang, W. T. Tsai, *Electrochem. Commun.* **2008**, *10*, 213; b) M. J. Deng, P. C. Lin, J. K. Chang, J. M. Chen, K. T. Lu, *Electrochim. Acta* **2011**, *56*, 6071; c) T. J. Simons, P. C. Howlett, A. A. J. Torriero, D. R. MacFarlane, M. Forsyth, *J. Phys. Chem. C* **2013**, *117*, 2662; d) M. Xu, D. G. Ivey, Z. Xie, W. Qu, *Electrochim. Acta* **2013**, *89*, 756; e) M. Kar, B. W. Jensen, M. Forsyth, D. R. MacFarlane, *Phys. Chem. Chem. Phys.* **2013**, *15*, 7191.
[153] T. J. Simons, A. A. J. Torriero, P. C. Howlett, D. R. MacFarlane, M. Forsyth, *Electrochem.Commun.* **2012**, *18*, 119.
[154] C. Pozo-Gonzalo, C. Virgilio, Y. Yan, P. C. Howlett, N. Byrne, D. R. MacFarlane, M. Forsyth, *Electrochem. Commun.* **2014**, *38*, 24.
[155] C. A. Friesen, R. Krishnan, T. Tang, D. Wolfe, *US 8808929 B2*, **2014**.
[156] Y. Li, M. Gong, Y. Liang, J. Feng, J. E. Kim, H. Wang, G. Hong, B. Zhang, H. Dai, *Nat. Commun.* **2013**, *4*, 1805.
[157] a) H. Sadeghifar, N. Djilali, M. Bahrami, *J. Power Sources* **2014**, *248*, 632; b) E. Davari, A. D. Johnson, A. Mittal, M. Xiong, D. G. Ivey, *Electrochim. Acta* **2016**, *211*, 735.
[158] a) T. Burchardt, A. L. Becquet (Revolt Technology Ltd), *WO 2007144357 A1*, **2008**; b) S. Suren, S. Kheawhom, *J. Electrochem. Soc.* **2016**, *163*, A846.
[159] a) W. M. Yan, C. Y. Hsueh, C. Y. Soong, F. Chen, C. H. Cheng, S. C. Mei, *Int. J. Hydrogen Energy* **2007**, *32*, 4452; b) S. B. Park, Y. i. Park, *Int. J. Precis. Eng. Manuf.* **2012**, *13*, 1145.
[160] O. Haas, J. Van Wesemael, *Encyclopedia of Electrochemical Power Sources*, Elsevier Science, Amsterdam, The Netherlands **2009**.
[161] J. Park, H. Oh, T. Ha, Y. I. Lee, K. Min, *Appl. Energy* **2015**, *155*, 866.
[162] Z. Chen, D. U. Lee (University of Waterloo), *US 20150349325 A1*, **2015**.
[163] a) M. Bockelmann, U. Kunz, T. Turek, *Electrochem. Commun.* **2016**, *69*, 24; b) X. Li, D. Pletcher, A. E. Russell, F. C. Walsh, R. G. A. Wills, S. F. Gorman, S. W. T. Price, S. J. Thompson, *Electrochem. Commun.* **2013**, *34*, 228; c) S. W. T. Price, S. J. Thompson, X. Li, S. F. Gorman, D. Pletcher, A. E. Russell, F. C. Walsh, R. G. A. Wills, *J. Power Sources* **2014**, *259*, 43; d) F. Büker, D. Hertkorn, C. Müller, H. Reinecke, *ECS Trans.* **2014**, *58*, 69; e) F. Allebrod, C. Chatzichristodoulou, M. B. Mogensen, *ECS Trans.* **2014**, *64*, 1029.
[164] X. Liu, M. Park, M. G. Kim, S. Gupta, X. Wang, G. Wu, J. Cho, *Nano Energy* **2016**, *20*, 315.
[165] R. D. Brost, A. Weisenstein, K. M. Brost, H. F. Wilkins, R. M. Kosted, *US 8728671 B1*, **2014**.
[166] S. Guo, S. Zhang, S. Sun, *Angew. Chem., Int. Ed.* **2013**, *52*, 8526.
[167] L. Jörissen, *J. Power Sources* **2006**, *155*, 23.
[168] a) D. U. Lee, J. Scott, H. W. Park, S. Abureden, J.-Y. Choi, Z. Chen, *Electrochem. Commun.* **2014**, *43*, 109; b) Z. Chen, A. Yu, R. Ahmed, H. Wang, H. Li, Z. Chen, *Electrochim. Acta* **2012**, *69*, 295; c) D. U. Lee, B. J. Kim, Z. Chen, *J. Mater. Chem. A* **2013**, *1*, 4754.
[169] a) G. Li, X. Wang, J. Fu, J. Li, M. G. Park, Y. Zhang, G. Lui, Z. Chen, *Angew. Chem.* **2016**, *128*, 5061; b) D. U. Lee, M. G. Park, H. W. Park, M. H. Seo, X. Wang, Z. Chen, *ChemSusChem* **2015**, *8*, 3129; c) K. Qu, Y. Zheng, S. Dai, S. Z. Qiao, *Nano Energy* **2016**, *19*, 373.
[170] H. B. Yang, J. Miao, S. F. Hung, J. Chen, H. B. Tao, X. Wang, L. Zhang, R. Chen, J. Gao, H. M. Chen, L. Dai, B. Liu, *Sci. Adv.* **2016**, *2*.
[171] J. Zhang, Z. Zhao, Z. Xia, L. Dai, *Nat. Nanotechnol.* **2015**, *10*, 444.
[172] J. Zhang, L. Qu, G. Shi, J. Liu, J. Chen, L. Dai, *Angew. Chem., Int. Ed.* **2016**, *55*, 2230.
[173] a) D. U. Lee, P. Xu, Z. P. Cano, A. G. Kashkooli, M. G. Park, Z. Chen, *J. Mater. Chem. A* **2016**, *4*, 7107; b) J. Zhang, Z. Zhao, Z. Xia, L. Dai, *Nat. Nanotechnol.* **2015**, *10*, 444.
[174] C. Song, J. Zhang, in *PEM Fuel Cell Electrocatalysts and Catalyst Layers: Fundamentals and Applications*, (Ed: J. Zhang), Springer, London, UK **2008**, 89.
[175] R. Cao, J. S. Lee, M. Liu, J. Cho, *Adv. Energy Mater.* **2012**, *2*, 816.
[176] K. Kinoshita, *Electrochemical Oxygen Technology*, John Wiley & Sons, Hoboken, NJ, USA **1992**.
[177] X. Ge, A. Sumboja, D. Wuu, T. An, B. Li, F. W. T. Goh, T. S. A. Hor, Y. Zong, Z. Liu, *ACS Catal.* **2015**, *5*, 4643.
[178] S.-A. Park, E.-K. Lee, H. Song, Y.-T. Kim, *Sci. Rep.* **2015**, *5*, 13552.
[179] a) H. He, Y. Lei, C. Xiao, D. Chu, R. Chen, G. Wang, *J. Phys. Chem. C* **2012**, *116*, 16038; b) R. Cao, R. Thapa, H. Kim, X. Xu, M. Gyu Kim, Q. Li, N. Park, M. Liu, J. Cho, *Nat. Commun.* **2013**, *4*, 2076.
[180] a) J. Sunarso, A. A. J. Torriero, W. Zhou, P. C. Howlett, M. Forsyth, *J. Phys. Chem. C* **2012**, *116*, 5827; b) Y. Wang, H. P. Cheng, *J. Phys. Chem. C* **2013**, *117*, 2106.
[181] L. Qu, Y. Liu, J. B. Baek, L. Dai, *ACS Nano* **2010**, *4*, 1321.
[182] K. Qu, Y. Zheng, S. Dai, S. Z. Qiao, *Nano Energy* **2016**, *19*, 373.
[183] L. Trotochaud, S. W. Boettcher, *Scr. Mater.* **2014**, *74*, 25.
[184] T. Reier, M. Oezaslan, P. Strasser, *ACS Catal.* **2012**, *2*, 1765.
[185] M. S. Burke, L. J. Enman, A. S. Batchellor, S. Zou, S. W. Boettcher, *Chem. Mater.* **2015**, *27*, 7549.
[186] A. Tseung, S. Jasem, *Electrochim. Acta* **1977**, *22*, 31.
[187] a) X. Lu, C. Zhao, *J. Mater. Chem. A* **2013**, *1*, 12053; b) J. Rosen, G. S. Hutchings, F. Jiao, *J. Am. Chem. Soc.* **2013**, *135*, 4516;

c) H. Jin, J. Wang, D. Su, Z. Wei, Z. Pang, Y. Wang, *J. Am. Chem. Soc.* **2015**, *137*, 2688; d) G. S. Hutchings, Y. Zhang, J. Li, B. T. Yonemoto, X. Zhou, K. Zhu, F. Jiao, *J. Am. Chem. Soc.* **2015**, *137*, 4223.

[188] a) C. Zhu, D. Wen, S. Leubner, M. Oschatz, W. Liu, M. Holzschuh, F. Simon, S. Kaskel, A. Eychmuller, *Chem. Commun.* **2015**, *51*, 7851; b) G. Wu, N. Li, D.-R. Zhou, K. Mitsuo, B.-Q. Xu, *J. Solid State Chem.* **2004**, *177*, 3682; c) Y. Yang, H. Fei, G. Ruan, C. Xiang, J. M. Tour, *ACS Nano* **2014**, *8*, 9518.

[189] a) T. Otagawa, J. O. M. Bockris, *J. Electrochem. Soc.* **1982**, *129*, 2391; b) J. O. M. Bockris, T. Ottagawa (Texas A&M University), *US 4497698 A*, **1985**; c) S. Jung, C. C. McCrory, I. M. Ferrer, J. C. Peters, T. F. Jaramillo, *J. Mater. Chem. A* **2016**, *4*, 3068.

[190] Z. L. Wang, D. Xu, J. J. Xu, X. B. Zhang, *Chem. Soc. Rev.* **2014**, *43*, 7746.

[191] Y. Meng, W. Song, H. Huang, Z. Ren, S. Y. Chen, S. L. Suib, *J. Am. Chem. Soc.* **2014**, *136*, 11452.

[192] J. Suntivich, H. A. Gasteiger, N. Yabuuchi, H. Nakanishi, J. B. Goodenough, Y. Shao-Horn, *Nat. Chem.* **2011**, *3*, 546.

[193] Y. Jiao, Y. Zheng, M. Jaroniec, S. Z. Qiao, *J. Am. Chem. Soc.* **2014**, *136*, 4394.

[194] I. C. Man, H. Y. Su, F. Calle-Vallejo, H. A. Hansen, J. I. Martínez, N. G. Inoglu, J. Kitchin, T. F. Jaramillo, J. K. Nørskov, J. Rossmeisl, *ChemCatChem* **2011**, *3*, 1159.

[195] T. Thippani, S. Mandal, G. Wang, V. K. Ramani, R. Kothandaraman, *RSC Adv.* **2016**, *6*, 71122.

[196] T. Ling, D. Y. Yan, Y. Jiao, H. Wang, Y. Zheng, X. Zheng, J. Mao, X. W. Du, Z. Hu, M. Jaroniec, S. Z. Qiao, *Nat. Commun.* **2016**, *7*, 12876.

[197] Y. Tan, C. Wu, H. Lin, J. Li, B. Chi, J. Pu, L. Jian, *Electrochim. Acta* **2014**, *121*, 183.

[198] a) Y. Gorlin, T. F. Jaramillo, *J. Am. Chem. Soc.* **2010**, *132*, 13612; b) Y. Gorlin, B. Lassalle-Kaiser, J. D. Benck, S. Gul, S. M. Webb, V. K. Yachandra, J. Yano, T. F. Jaramillo, *J. Am. Chem. Soc.* **2013**, *135*, 8525.

[199] P. W. Menezes, A. Indra, N. R. Sahraie, A. Bergmann, P. Strasser, M. Driess, *ChemSusChem* **2015**, *8*, 164.

[200] M. R. Gao, Y. F. Xu, J. Jiang, S. H. Yu, *Chem. Soc. Rev.* **2013**, *42*, 2986.

[201] a) A. J. Esswein, M. J. McMurdo, P. N. Ross, A. T. Bell, T. D. Tilley, *J. Phys. Chem. C* **2009**, *113*, 15068; b) J. Liu, L. Jiang, B. Zhang, J. Jin, D. S. Su, S. Wang, G. Sun, *ACS Catal.* **2014**, *4*, 2998; c) T. Wang, M. Kaempgen, P. Nopphawan, G. Wee, S. Mhaisalkar, M. Srinivasan, *J. Power Sources* **2010**, *195*, 4350; d) L. Yuan, L. Jiang, J. Liu, Z. Xia, S. Wang, G. Sun, *Electrochim. Acta* **2014**, *135*, 168.

[202] B. Seo, Y. J. Sa, J. Woo, K. Kwon, J. Park, T. J. Shin, H. Y. Jeong, S. H. Joo, *ACS Catal.* **2016**, *6*, 4347.

[203] J. Qiao, *Meet. Abstr.* **2016**, *MA2016-01*, 181.

[204] Z. Chen, A. Yu, D. Higgins, H. Li, H. Wang, Z. Chen, *Nano Lett.* **2012**, *12*, 1946.

[205] Z. Chen, D. Higgins, A. Yu, L. Zhang, J. Zhang, *Energy Environ. Sci.* **2011**, *4*, 3167.

[206] a) D. Guo, R. Shibuya, C. Akiba, S. Saji, T. Kondo, J. Nakamura, *Science* **2016**, *351*, 361; b) R. Zhou, M. Jaroniec, S. Z. Qiao, *ChemCatChem* **2015**, *7*, 3808; c) K. Gong, F. Du, Z. Xia, M. Durstock, L. Dai, *Science* **2009**, *323*, 760.

[207] a) Z. Yang, Z. Yao, G. Li, G. Fang, H. Nie, Z. Liu, X. Zhou, X. Chen, S. Huang, *ACS Nano* **2012**, *6*, 205; b) L. Zhang, J. Niu, M. Li, Z. Xia, *J. Phys. Chem. C* **2014**, *118*, 3545; c) J. Park, Y. J. Jang, Y. J. Kim, M. Song, S. Yoon, D. H. Kim, S. Kim, *Phys. Chem. Chem. Phys.* **2014**, *16*, 103.

[208] a) C. Zhang, N. Mahmood, H. Yin, F. Liu, Y. Hou, *Adv. Mater.* **2013**, *25*, 4932; b) D. S. Yang, D. Bhattacharjya, S. Inamdar, J. Park, J. S. Yu, *J. Am. Chem. Soc.* **2012**, *134*, 16127.

[209] a) L. Yang, S. Jiang, Y. Zhao, L. Zhu, S. Chen, X. Wang, Q. Wu, J. Ma, Y. Ma, Z. Hu, *Angew. Chem., Int. Ed.* **2011**, *50*, 7132; b) Z. H. Sheng, H. L. Gao, W. J. Bao, F. B. Wang, X. H. Xia, *J. Mater. Chem.* **2012**, *22*, 390; c) S. Wang, L. Zhang, Z. Xia, A. Roy, D. W. Chang, J. B. Baek, L. Dai, *Angew. Chem., Int. Ed.* **2012**, *51*, 4209.

[210] a) Z. Yao, H. Nie, Z. Yang, X. Zhou, Z. Liu, S. Huang, *Chem. Commun.* **2012**, *48*, 1027; b) K. P. Singh, M. Y. Song, J. S. Yu, *J. Mater. Chem. A* **2014**, *2*, 18115.

[211] a) Y. Li, M. Li, L. Jiang, L. Lin, L. Cui, X. He, *Phys. Chem. Chem. Phys.* **2014**, *16*, 23196; b) D. C. Higgins, M. A. Hoque, F. Hassan, J. Y. Choi, B. Kim, Z. Chen, *ACS Catal.* **2014**, *4*, 2734; c) X. Qiao, S. Liao, C. You, R. Chen, *Catalysts* **2015**, *5*, 981; d) Y. Xue, D. Yu, L. Dai, R. Wang, D. Li, A. Roy, F. Lu, H. Chen, Y. Liu, J. Qu, *Phys. Chem. Chem. Phys.* **2013**, *15*, 12220; e) Y. Zhan, J. Huang, Z. Lin, X. Yu, D. Zeng, X. Zhang, F. Xie, W. Zhang, J. Chen, H. Meng, *Carbon* **2015**, *95*, 930.

[212] J. Duan, S. Chen, M. Jaroniec, S. Z. Qiao, *ACS Catal.* **2015**, *5*, 5207.

[213] B. Y. Xia, Y. Yan, N. Li, H. B. Wu, X. W. Lou, X. Wang, *Nat. Energy* **2016**, *1*, 15006.

[214] G. L. Tian, M. Q. Zhao, D. Yu, X.-Y. Kong, J. Q. Huang, Q. Zhang, F. Wei, *Small* **2014**, *10*, 2251.

[215] a) P. Chen, T. Y. Xiao, Y. H. Qian, S. S. Li, S. H. Yu, *Adv. Mater.* **2013**, *25*, 3192; b) T. Y. Ma, S. Dai, M. Jaroniec, S. Z. Qiao, *Angew. Chem., Int. Ed.* **2014**, *53*, 7281.

[216] H. Wang, H. Dai, *Chem. Soc. Rev.* **2013**, *42*, 3088.

[217] Y. Liang, Y. Li, H. Wang, J. Zhou, J. Wang, T. Regier, H. Dai, *Nat. Mater.* **2011**, *10*, 780.

[218] a) T. Y. Ma, S. Dai, S. Z. Qiao, *Mater. Today* **2016**, *19*, 265; b) T. Y. Ma, J. L. Cao, M. Jaroniec, S. Z. Qiao, *Angew. Chem., Int. Ed.* **2016**, *55*, 1138.

[219] a) X. Wu, F. Chen, Y. Jin, N. Zhang, R. L. Johnston, *ACS Appl. Mater. Interfaces* **2015**, *7*, 17782; b) J. W. D. Ng, M. Tang, T. F. Jaramillo, *Energy Environ. Sci.* **2014**, *7*, 2017.

[220] F. Meng, H. Zhong, D. Bao, J. Yan, X. Zhang, *J. Am. Chem. Soc.* **2016**.

[221] a) A. Sumboja, X. Ge, F. W. T. Goh, B. Li, D. Geng, T. S. A. Hor, Y. Zong, Z. Liu, *ChemPlusChem* **2015**, *80*, 1341; b) T. Y. Ma, S. Dai, M. Jaroniec, S. Z. Qiao, *J. Am. Chem. Soc.* **2014**, *136*, 13925.

[222] Q. Liu, Y. Wang, L. Dai, J. Yao, *Adv. Mater.* **2016**, *28*, 3000.

[223] B. Li, X. Ge, F. W. T. Goh, T. S. A. Hor, D. Geng, G. Du, Z. Liu, J. Zhang, X. Liu, Y. Zong, *Nanoscale* **2015**, *7*, 1830.

[224] T. Y. Ma, J. Ran, S. Dai, M. Jaroniec, S. Z. Qiao, *Angew. Chem., Int. Ed.* **2015**, *54*, 4646.

[225] a) X. Wang, P. Sebastian, M. A. Smit, H. Yang, S. Gamboa, *J. Power Sources* **2003**, *124*, 278; b) J. S. Lee, G. S. Park, H. I. Lee, S. T. Kim, R. Cao, M. Liu, J. Cho, *Nano Lett.* **2011**, *11*, 5362; c) G. Nam, J. Park, S. T. Kim, D. B. Shin, N. Park, Y. Kim, J. S. Lee, J. Cho, *Nano Lett.* **2014**, *14*, 1870; d) J. I. Jung, H. Y. Jeong, M. G. Kim, G. Nam, J. Park, J. Cho, *Adv. Mater.* **2015**, *27*, 266; e) X. Liu, M. Park, M. G. Kim, S. Gupta, G. Wu, J. Cho, *Angew. Chem., Int. Ed.* **2015**, *54*, 9654; f) X. Liu, W. Liu, M. Ko, M. Park, M. G. Kim, P. Oh, S. Chae, S. Park, A. Casimir, G. Wu, *Adv. Funct. Mater.* **2015**, *25*, 5799.

[226] a) D. U. Lee, H. W. Park, M. G. Park, V. Ismayilov, Z. Chen, *ACS Appl. Mater. Interfaces* **2014**, *7*, 902; b) D. U. Lee, M. G. Park, H. W. Park, M. H. Seo, X. Wang, Z. Chen, *ChemSusChem* **2015**, *8*, 3129.

[227] Z. Chen, A. Yu, D. Higgins, H. Li, H. Wang, Z. Chen, *Nano Lett.* **2012**, *12*, 1946.

[228] S. Chen, J. Duan, P. Bian, Y. Tang, R. Zheng, S. Z. Qiao, *Adv. Energy Mater.* **2015**, *5*, 1500936.

[229] a) J. Farr, N. Hampson, *Trans. Faraday Soc.* **1966**, *62*, 3493; b) H. J. Park, S. I. Mho, *Anal. Sci.* **1997**, *13*, 311; c) C. Tang, D. Zhou, S. Fang, L. Yang, *J. Electrochem. Soc.* **2012**, *159*, A1796.

[230] a) S. Müller, F. Holzer, O. Haas, C. Schlatter, C. Comninellis, *Chim. Int. J. Chem.* **1995**, *49*, 27; b) B. Koretz, Y. Harats, J. Goldstein, M. Korall, in *New Promising Electrochemical Systems for Rechargeable Batteries*, Vol. *6* (Eds: V. Barsukov, F. Beck), Springer Science & Business Media, Dordrecht, The Netherlands **2013**, Ch. 3.
[231] I. Epelboin, M. Ksouri, R. Wiart, *J. Electrochem. Soc.* **1975**, *122*, 1206.
[232] G. Toussaint, P. Stevens, R. Rouget, F. Fourgeot, *Meet. Abstr.* **2012**, *MA2012-02*, 1172.
[233] P. E. E. Communications, PG&E Presents Innovative Energy Storage Agreements, https://www.pge.com/en/about/newsroom/newsdetails/index.page?title=20151202_pge_presents_innovative_energy_storage_agreements_ (accessed August, 2016).
[234] J. Hoppmann, J. Volland, T. S. Schmidt, V. H. Hoffmann, *Renew. Sustain. Energy Rev.* **2014**, *39*, 1101.
[235] W. Sierzchula, S. Bakker, K. Maat, B. van Wee, *Energy Policy* **2014**, *68*, 183.
[236] a) S. G. Stewart, S. I. Kohn, K. R. Kelty, J. B. Straubel (Tesla Motors, Inc.), *US 20120041624 A1*, **2013**; b) R. Eckl, P. Burda, A. Foerg, H. Finke, M. Lienkamp, in *Conf. on Future Automotive Technology: Focus Electro Mobility*, Springer Fachmedien Wiesbaden, Wiesbaden, Germany **2013**, Ch. 3.